MICROCOPY RESOLUTION TEST CHART
NATIONAL BUREAU OF STANDARDS 1963-A

AD-A164 123

DEPARTMENT OF THE AIR FORCE

AIR UNIVERSITY

AIR FORCE INSTITUTE OF TECHNOLOGY

Wright-Patterson Air Force Base, Ohio

86 2 13 00

DTIC
SELECTE**D**
FEB 1 3 1986

D

THE APODISATION OF ABERRATED COHERENT

MULTIAPERTURE OPTICAL IMAGING SYSTEMS

THESIS

Arley J. Hugghins
Captain, USAF

AFIT/GEP/ENP/85D-6

AFIT/GEP/ENP/85D-6

THE APODISATION OF ABERRATED COHERENT

MULTIAPERTURE OPTICAL IMAGING SYSTEMS

THESIS

Presented to the Faculty of the School of Engineering

of the Air Force Institute of Technology

Air University

In Partial Fulfillment of the

Requirements for the Degree of

Master of Science in Engineering Physics

Arley J. Hugghins

Captain, USAF

December 1985

Accesion For		
NTIS CRA&I		☑
DTIC TAB		☐
Unannounced		☐
Justification		
By		
Distribution /		
Availability Codes		
Dist	Avail and / or Special	
A-1		

Approved for public release; distribution unlimited

AFIT/GEP/ENP/85D-6

THE APODISATION OF ABERRATED COHERENT

MULTIAPERTURE OPTICAL IMAGING SYSTEMS

THESIS

Presented to the Faculty of the School of Engineering

of the Air Force Institute of Technology

Air University

In Partial Fulfillment of the

Requirements for the Degree of

Master of Science in Engineering Physics

Arley J. Hugghins

Captain, USAF

December 1985

Preface

The purpose of this study was to conduct a computer investigation of imaging performance of an aberrated coherent multiaperture optical imaging system in which Gaussian apodisation was employed in an attempt to improve its imaging performance. Both a point source and an edge were chosen as objects of study. The study was motivated by a desire to support the Strategic Defense Initiative (SDI).

The investigation determined that Gaussian apodisation did not improve imaging performance. This was the case whether the object was a point source or an edge, whether the amount of spacing between subapertures was increased or held constant, or whether aberrations were present or not present. The most important implication of this was that the amount of spacing which a multiaperture optical imaging system could tolerate and still obtain acceptable imaging fell dramatically.

I am deeply indebted to my advisor, Maj J. Mills, for his good ideas and pleasant demeanor, to Lt K. Nufer and Frank Bakos for keeping the computer system up most of the time, and to my parents, who understood why they were not getting many letters.

<div align="right">Arley J. Hugghins</div>

Table of Contents

List of Figures

v

List of Tables

Abstract

This investigation determined that the application of a Gaussian apodiser did not improve the imaging performance through a coherent multiaperture optical imaging system. This was the case whether the object was a point source or an edge, whether the dilution was increased or held constant, or whether aberrations were present or not present. Further, the investigation determined that the amount of spacing between the subapertures which either an aberrated or unaberrated optical system could tolerate and still obtain acceptable imaging fell dramatically.

The analysis was accomplished with computer codes which made use of Fourier transform techniques to perform the imaging. The edge imaging results of this study can be applied without loss of generality to that of an imaging system with an annular exit pupil.

THE APODISATION OF ABERRATED COHERENT
MULTIAPERTURE OPTICAL IMAGING SYSTEMS

I.   Introduction

1.1 Goal of Study

The purpose of this thesis was to describe an
investigation of imaging performance of an aberrated
multiaperture coherent optical imaging system in which
apodisation was employed in an attempt to improve its
imaging performance. Both a point source and an edge were
chosen as objects of study. Depending on the application,
third order aberrations were applied to the system when
imaging a point source and first and third order aberrations
were added when imaging an edge. The investigation answered
among others two important questions. First, whether the
degree of array dilution could be increased through the use
of apodisers. Second, whether an apodiser was effective in
improving the imaging performance of a multiaperture optical
system. The answers to these questions are found in
Chapters IV and V. Two computer programs, one capable of
modeling the impulse response and the other the imaging of
an edge were developed to accomplish this goal. With a few
minor adjustments the program was in fact capable of
modeling the results of any random or symmetrical
multiaperture configuration of subapertures of various sizes

and shapes. However, this study was limited to a hexagonal configuration of circular pupils. The model variables in both programs included at the minimum: degree of array dilution and type of aberration(s). The degree of array dilution refers to the amount of spacing between the subapertures. The apodiser or amplitude filter used in this study was Gaussian.

It is well established that unapodised multiaperture systems of very low dilution show promise of providing greater angular resolution capabilities over that of single aperture systems (Goodman, 1970:3; Shack and others, 1971:257-259). Angular resolution refers to how well an optical system can resolve two closely spaced points. The Multiple Mirror Telescope (MMT) of the University of Arizona and several other MMT-type projects which are in the works now, point to the potential of the approach (Fender, 1984:7). However, the potential of these projects is bounded by the requirement that the dilution between the mirrors be held extremely low. In a related area it has been shown by several authors that apodisers improve imaging performance through single aperture coherent imaging systems (Mills, 1984:32). However, until this thesis effort, no one has investigated whether the use of apodisers improves the imaging performance of multiaperture coherent imaging systems. Previous work has also proven that apodisation significantly enhances the imaging

performance of single aperture coherent aberrated systems (Mills, 1984:1). But again, until this thesis effort, no one has investigated whether this benefit can be extended to dilute aperture systems. This study was motivated by the desire to support the Strategic Defense Initiative (SDI) program through demonstrating the potential of achieving greater angular resolution with multiaperture coherent optical systems and improving the imaging performance of such systems.

1.2 Introduction to the Multiaperture Concept

To appreciate this study, it is crucial to be aware of the potential advantage a multiaperture system has over a single aperture system. The most important limitation to the resolving power of an optical system is diffraction of light. That is, as the wavelength of incident light remains constant while the dimensions of the optical system increase, the effects of diffraction become less significant.

Often however, imperfections in the individual optical components of the optical system introduce wavefront aberrations which prevent this limitation from being reached. If the components are ground carefully enough, the aberrations can be minimized to the point that the diffraction limit is approached. But as optical elements become larger, aberration free components become more and more difficult and expensive to grind. Further, their

sheer size and weight make them awkward to use. Thus, there
is a practical limit of about eight meters
(Borrelle, 1985:8-9), on how big a single aperture optical
system can be made. This limit is smaller for space based
scenarios since the space shuttle can only lift optics of
less than 2 meters in diameter. It is therefore worth
considering alternative means of obtaining greater angular
resolution without the necessity of constructing ever larger
optical components. One way to do so is to approximate the
imaging results which would be obtained from a single large
aperture with configurations of smaller apertures with
spacing between them. Maximizing the spacing would yield
even greater benefits. The potential advantages to
successfully getting this idea to work include greater
angular resolution, less expense since it costs less to
construct several small optical components than a single
large one, and less payload due to the smaller optical
components if a dilute aperture system were taken into space.

1.3 Introduction to Effects of Apodisation, Aberrations, and Dilute Apertures

In order to gain a preliminary feel for the findings of
this study it is essential that one first understands what
effect apodisation, aberrations, and dilute subaperture
arrays each alone have on the imaging performance of an
optical system. The first two concepts are most easily
tackled when only single aperture systems are considered.

4

Hence, the ensuing explanation closely follows that of
James P. Mills, whose PhD dissertation dealt with the
effect of aberrations and apodisation on single aperture
coherent imaging systems (Mills, 1984:1-3). Apodisation is
the process whereby filters are added to an optical system
to deliberately modify the amplitude transmittance of the
system. As an illustrative example consider a centered,
circularly symmetric, aberration free, unapodised, coherent
optical system. The amplitude transmittance $A(x,y)$ of the
exit pupil of such a system can be denoted by the function

$$A(x,y) = cyl(r/d) \qquad\qquad (1.1)$$

where $r^2 = x^2 + y^2$, x and y are the coordinates of the
exit pupil, and d is the diameter of the exit pupil.
Cyl(r/d) represents a function which has the value
$A(x,y) = 1$ for $r \leq d/2$ and $A(x,y) = 0$ for $d/2 > 0$. The
modulus of the amplitude impulse response of a point source
through this system is shown in Fig. 1.1a. The outstanding
feature of the plot is the ringing which is present around
the base of the plot. When squared, it yields the
irradiance impulse response, which is an Airy diffraction
pattern, shown in Fig. 1.1c. The ringing is still there,
and this leads to undesirable effects when imaging
(Mills, 1984:38). If $A(x,y)$ is modified by a Gaussian
apodising function, the amplitude transmittance becomes

5
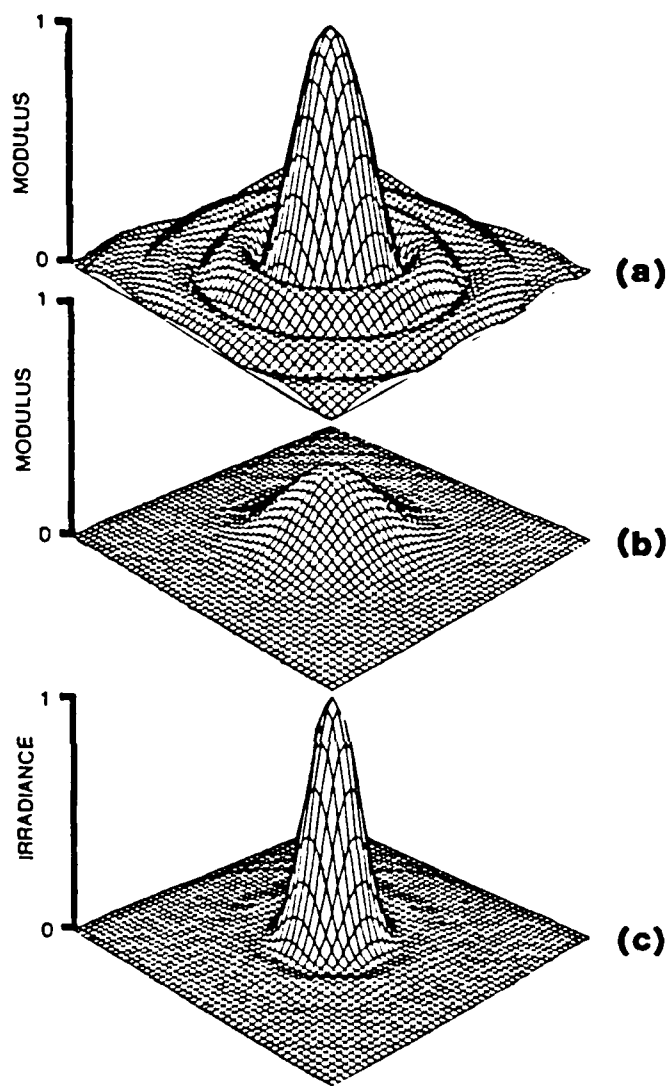
Fig. 1.1 The modulus of the amplitude impulse response
through a single aperture optical system with
(a) an unapodised aperture and (b) a Gaussian
apodiser in the aperture. The irradiance
impulse response with the unapodised aperture
is shown in (c). The vertical scales are in
relative units, with (a), (b), and (c) having
the same scale. The other axes of each plot
have units of relative distance, the scaling
of which is the same (Mills, 1984:3).

$$A(x,y) = cyl(r/d) \ exp[-(r/\beta)]^2 \qquad\qquad (1.2)$$

where β is the characteristic width of the Gaussian. The
Gaussian is only one of many possible apodising functions.
The modulus of the amplitude impulse response for this
system with β = .58 is shown in Fig. 1.1b (Mills, 1984:38).
The important thing to notice when comparing Figs. 1.1a and
1.1b is that the outer rings evident in Fig. 1.1a have been
totally suppressed in Fig.1.1b. It is apparent that the
term apodisation is appropriate since it is derived from the
Greek; a - meaning without, and pod - meaning foot. The
apodisation has indeed removed the feet of the amplitude
impulse response (Mills, 1984:1-3). This changed impulse
response has a profound impact on imaging.

It is also essential to understand what effect
aberrations in an optical system have on an image. Fig. 1.2
is useful in illustrating what an aberration is. The ideal
spherical reference wave S located at the exit pupil is the
result of a wave emanating from a point source object
travelling through an optical system free from aberrations.
It is converging toward the ideal image point P_i. Any
deviation from that reference wave, represented here by the
wavefront W is due to aberrations. The magnitude of the
segment QQ* corresponds to the amount of the aberration.
Thus, an aberration is a deviation in the phase
transmittance of an optical system.
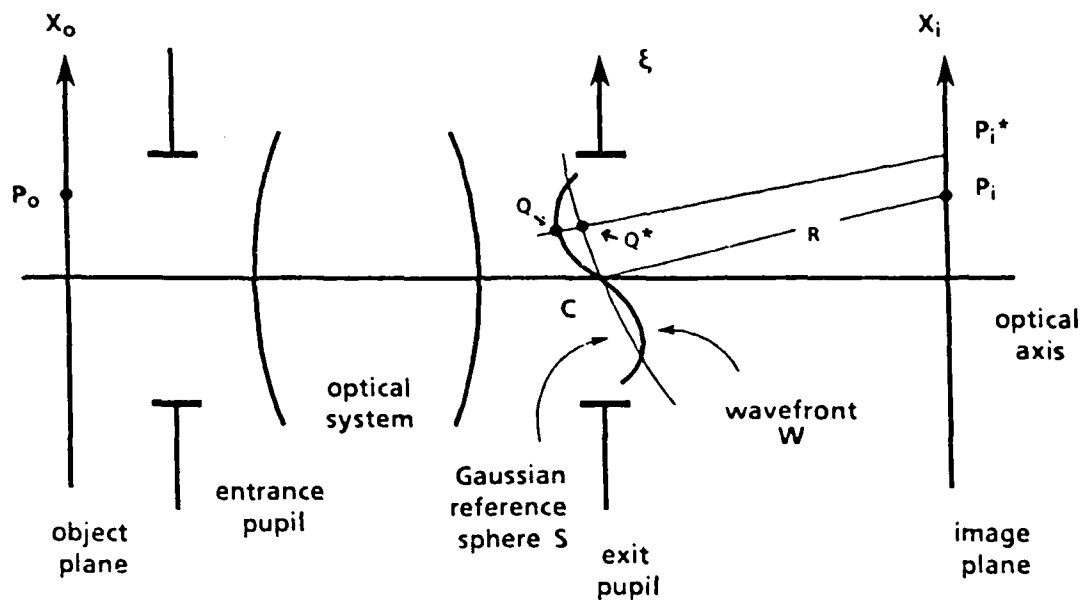
Fig. 1.2   The geometry of a centered optical system
           which gives rise to an aberrated wavefront W
           (Mills, 1984:15).

Aberrations are commonly expressed in terms of Zernike

polynomials. The Zernike polynomials are a complete set of

polynomials which are orthogonal over a unit circle. Hence,

when any two of the polynomials are multiplied together and

then integrated over a unit circle an answer of zero is

obtained. Table 1.1 contains a listing of the first and

third order aberrations. The first column of the table

lists the aberrations. The second column contains the

specific Zernike polynomial expressions for each aberration

8

Table 1.1

Tabulation of the First and Third Order Wavefront Aberrations (Malacara, 1978:493)

Aberration	Radial Zernike	Monomial Zernike
Third order spherical	$6\rho^4 - 6\rho^2 + 1$	$1-6y^2 - 6x^2 + 6y^4 + 12x^2y^2 + 6x^4$
Third order coma along x axis	$(3\rho^3 - 2\rho)\sin\theta$	$-2x + 3xy^2 + 3x^3$
Third order coma along y axis	$(3\rho^3 - 2\rho)\cos\theta$	$-2y + 3y^2 + 3x^2y$
Astigmatism with axis at $\pm 45°$	$\rho^2\sin2\theta$	$2xy$
Astigmatism with axis at 0 or 90°	$\rho^2\cos2\theta$	$y^2 - 2$
Focus Shift	$2\rho^2 - 1$	$-1 + 2y^2 + 2x^2$
x Tilt	$\rho\sin\theta$	x
y Tilt	$\rho\cos\theta$	y
Piston	1	1

9

in radial form. The third column lists the corresponding

aberrations when a conversion from the variables ρ and θ to

the rectangular variables x and y has been accomplished.

The monomial expressions of column three allow aberrations

to be modeled on a rectangular array. Rectangular arrays

were used to express the input waves used in the computer

simulations of this thesis. Hence, it is the monomial

forms which were essential. A more in depth discussion of

Zernike polynomials including their derivation and the

conversion process from the radial to monomial form can be

found in (Mills, 1984:28-30) and (Malacara, 1978:493).

Figs. 1.3 and 1.4 are depictions of all the aberrations

except piston listed in the table. Piston is a constant

term referring to uniform amounts of phase.

In Fig. 1.5 the effect of 0.5 wave of defocus on the

modulus of the amplitude impulse response due to a point

source imaged through a circularly symmetric aperture is

shown. Fig. 1.5a depicts the result when the aperture is

unapodised while Fig. 1.5b represents the result when a

Gaussian apodiser is applied to the aperture. The vertical

scales for the modulus plots are in units of relative

irradiance. The horizontal scales, represented by u and v,

are expressed in terms of normalized distance where u and v

can be quantified as follows

$$u = \frac{2\pi a}{\lambda d} x \quad , \quad v = \frac{2\pi a}{\lambda d} y \qquad (1.3)$$

10
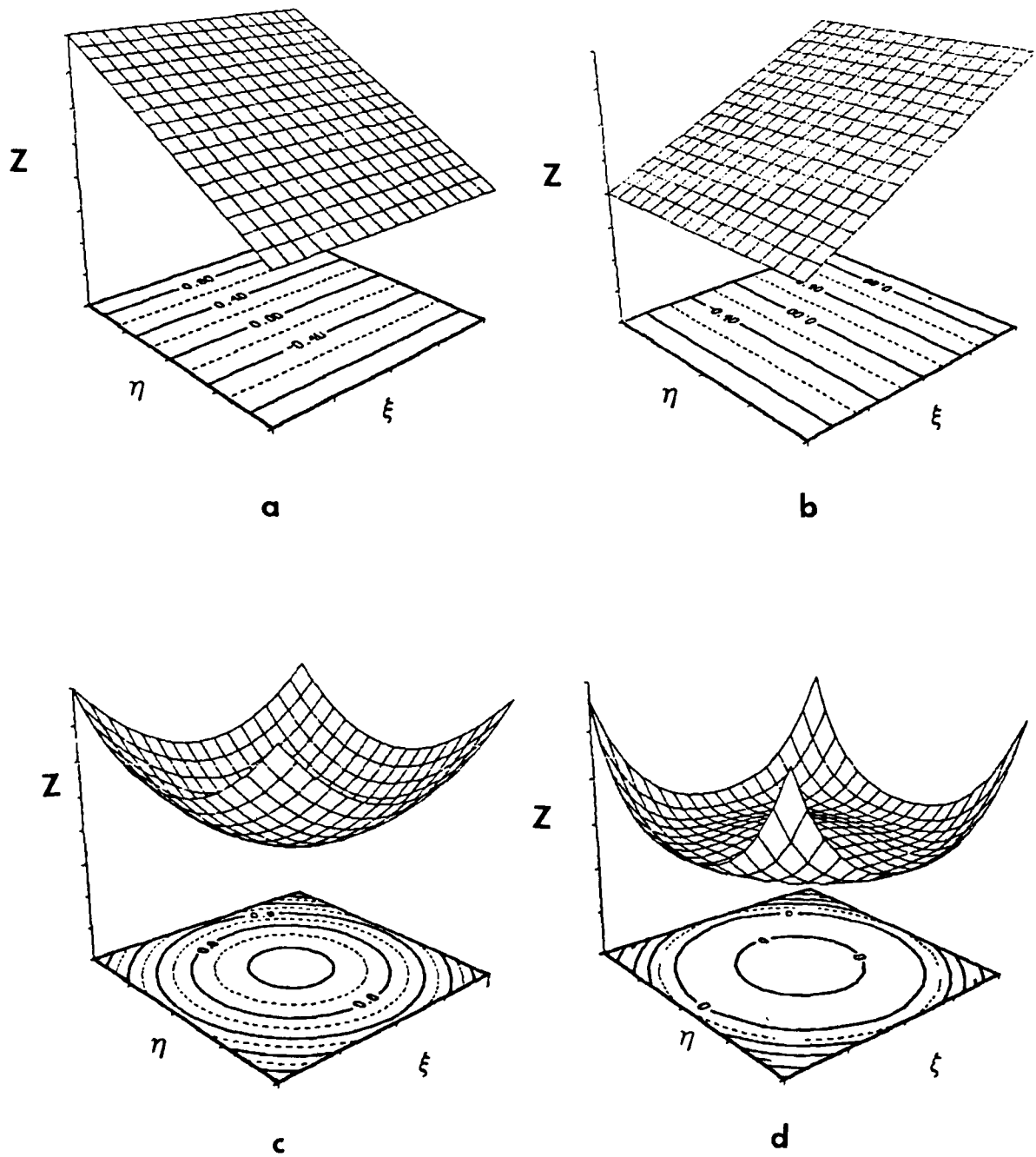
Fig. 1.3   Representation of (a) y tilt (b) x tilt
            (c) focus shift or defocus and (d) third
            order spherical (Kervin, 1982).

11
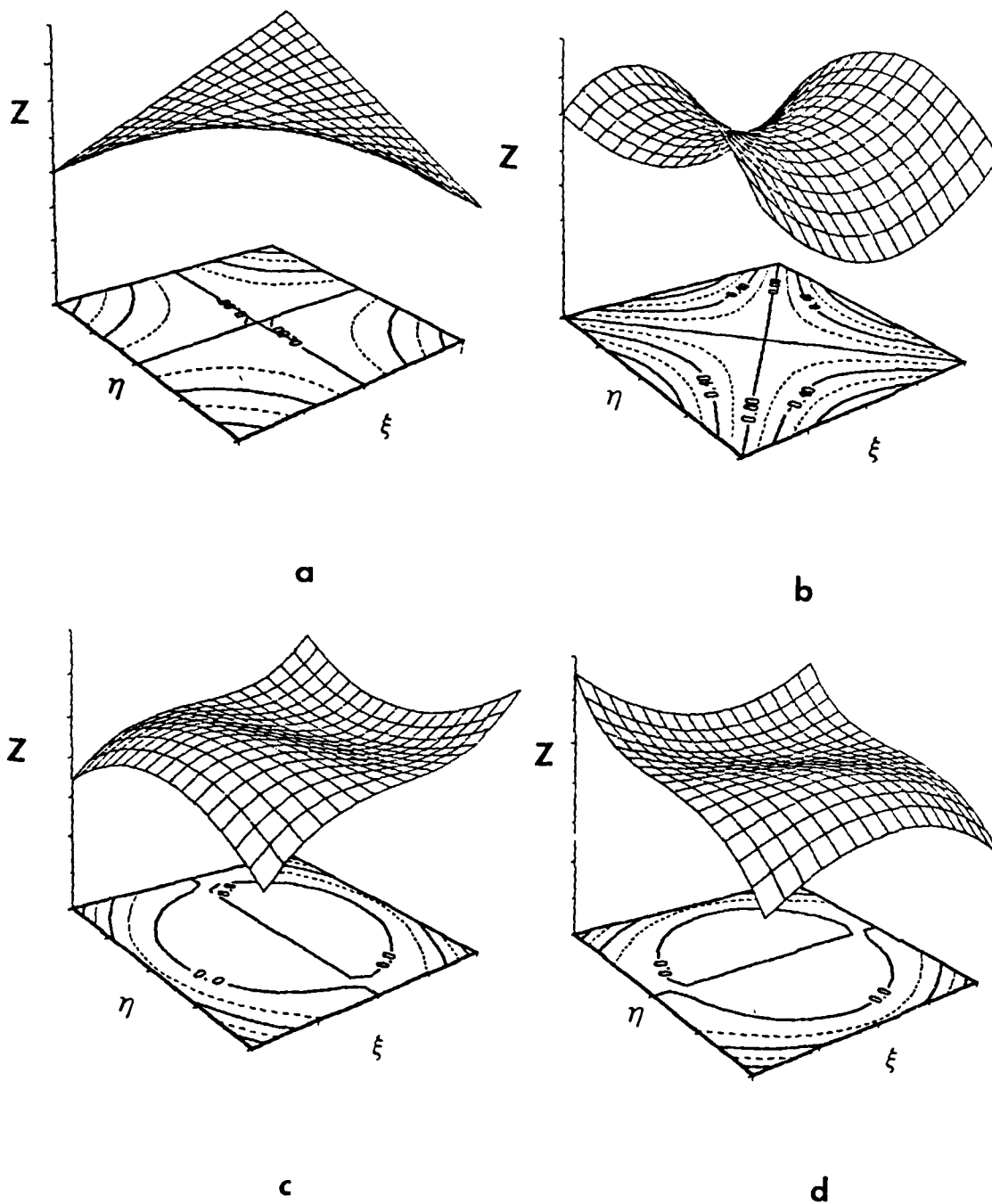
Fig. 1.4 Representation of (a) astigmatism with axis at ± 45°, (b) astigmatism with axis at 0° or 90°, (c) third order coma along y axis and (d) third order coma along x axis (Kervin, 1982).

12
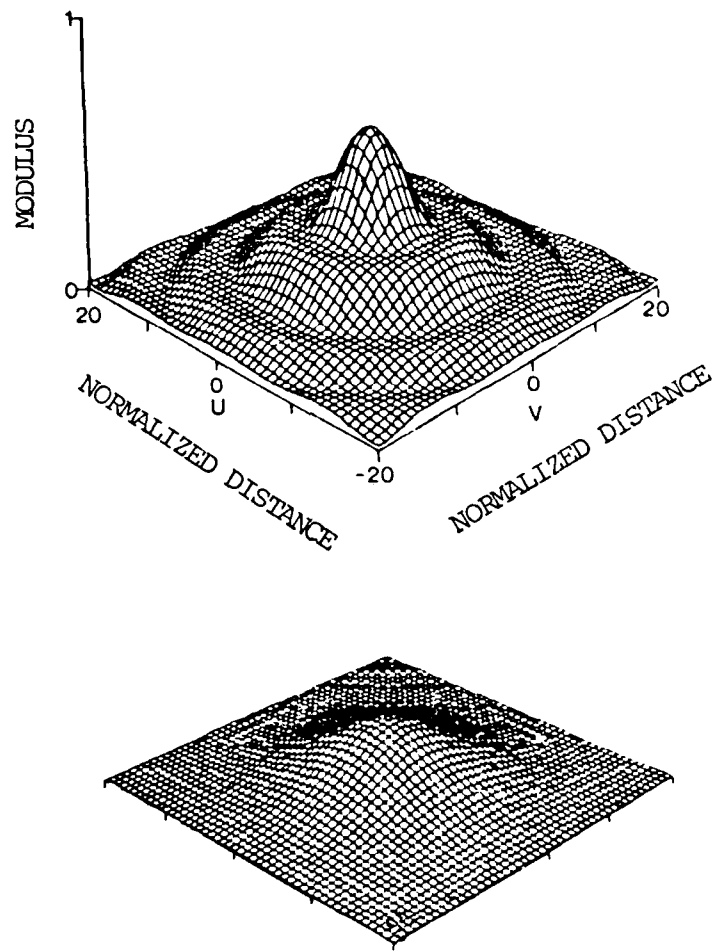
Fig. 1.5 The modulus of the amplitude impulse response
through a single aperture optical system in
the presence of 0.5λ defocus for the cases of an
unapodised and Gaussian apodised aperture. The
top plot represents the unapodised case while the
bottom plot represents the result when a
Gaussian apodiser is applied. The vertical
scale for both plots is indicated on the top plot
(Mills, 1984:51).

13

In equation 1.3, a refers to the single aperture radius (the exit pupil), λ to the mean wavelength of the illuminating laser, d to the distance between the exit pupil and image plane, and x and y to the horizontal and vertical coordinates, respectively, in the image plane (Mills, 1984:6). Again, the important thing to notice when comparing Figs. 1.5a and 1.5b is that the outer rings present in Fig. 1.5a have been totally suppressed in Fig. 1.5b.

To gain a concept of how a dilute aperture might effect imaging consider Fig. 1.6. Fig. 1.6a depicts the image of a point (the point spread function) through the coherent, aberration free, unapodised, nondilute, six-subaperture optical system shown to the right on the figure. The term nondilute means that there is not any space between adjacent subapertures, i.e. they are touching as the accompanying plot to the right in Fig. 1.6a shows. Fig. 1.6b depicts the result from the same optical imaging system which Fig. 1.6a depicts, except that the subapertures are dilute, or spread apart. As the dilution of the system is increased, the sidelobes of the point spread function increase in amplitude and get closer to the central lobe. The higher side lobes adversely effect imaging.

1.4 Reason for Research

This thesis is a logical extension of previous studies in the field of multiaperture coherent imaging. In recent years there have been a number of studies looking at

14
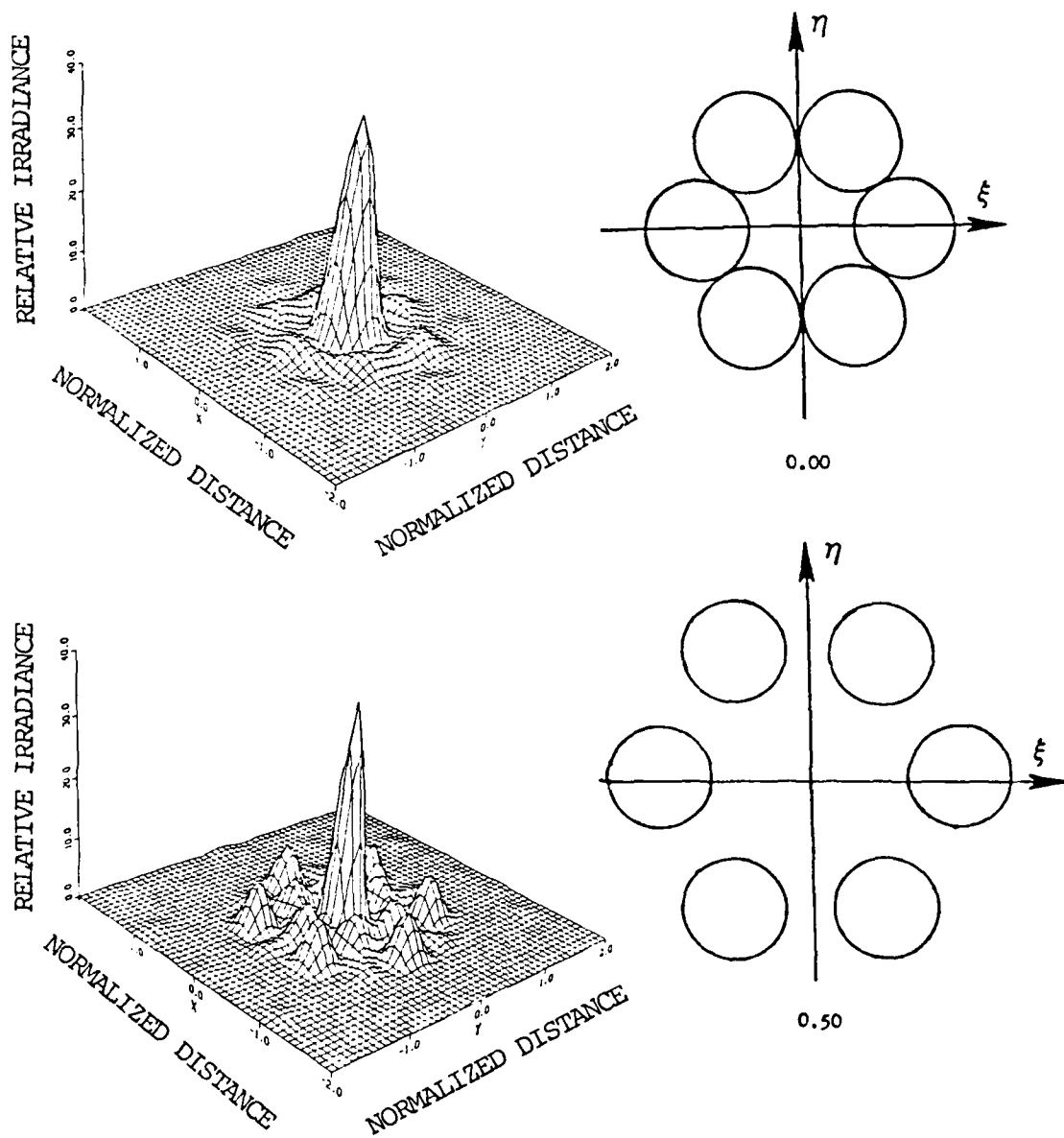
Fig. 1.6 Amplitude impulse response through a (a) nondilute case and (b) dilute case. The configuration of the subapertures which were used in the generation of each of the amplitude impulse responses are shown to the right of each impulse response. The vertical scale is expressed in relative units and represents irradiance. The horizontal scales represent relative units of distance.

apodisation in coherent single-aperture optical systems. But there have apparently been no studies investigating the effect of apodisation on multiaperture coherent optical systems. Also, there has only been one study which has analyzed the effect of apodisation on the performance of single aperture aberrated coherent optical systems (Mills, 1984:8). Again, there are no published studies which have analyzed the effect of apodisation on the performance of aberrated multiaperture coherent optical imaging systems.

The research embodied in this thesis has begun to investigate these two areas. The performance of coherent multiaperture optical systems have been theoretically analyzed under the following conditions: (1) no aberrations or apodisation, (2) apodisation but not aberrations, and (3) both aberrations and apodisation.

In Chapter II, the basic approach to generalized imaging through coherent, aberrated, dilute, aperture systems is developed, and previous research relating to this problem is reviewed. Chapter III describes the computer program used to arrive at the results. The results of the computer simulations are presented in Chapter IV, and finally, a summary of what has been determined composes Chapter V.

II. Theory

The investigations which were made during this study pertained to the quality of images generated by multiaperture coherent imaging systems. Accordingly, the first section of this chapter introduces the theory which explains the far field propagation of diffracted light. Next, a general approach to imaging is developed. After that, the general imaging approach is applied to the imaging of a point source and then the imaging of an edge through multiaperture systems. Finally, previous research relating to this thesis is reviewed.

2.1 Far Field Propagation of Diffracted Light

The first consideration which must be made when evaluating the quality of an imaging system is the effect of diffraction. Diffraction is the deviation from rectilinear propagation which occurs when light advances beyond an obstruction, which in the case of this thesis is an aperture. The task then is to arrive at an expression which accurately describes the behavior of light waves after they have travelled some distance from the aperture. Fig. 2.1 pictorially represents the task. The following development summarizes that of Goodman Chapter 3, sections 1-4, and Chapter 4, section 1, and Chapter 5, section 2 (Goodman, 1968:30-46,57-62,83-90).

17
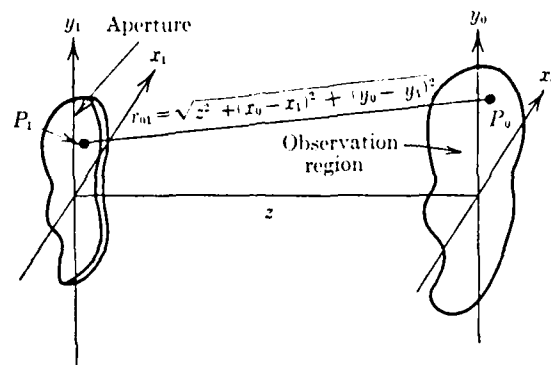
Fig. 2.1 Diffraction Geometry (Goodman, 1968:57).

Beginning with Maxwell's equations in free space

$$\nabla \cdot \underline{E} = 0$$

$$\nabla \cdot \underline{H} = 0$$

$$\nabla \times \underline{E} = -u_O \frac{J\underline{H}}{JT}$$

$$\nabla \times \underline{H} = \epsilon_O \frac{J\underline{E}}{JT} \tag{2.1}$$

an exact solution to the description of the electric field amplitude of the light wave at the point P_O in the observation plane is given by

$$\widetilde{U}(P_O) = (-1/2\pi) \iint\limits_{-\infty}^{\infty} \widetilde{U}(P_1) \ (\exp[ikr_{o1}]/r_{o1}) \ (ik - 1/r_{o1})$$

$$\cdot \cos(\bar{n}, \ \bar{r}_{o1})ds \tag{2.2}$$

where $k = 2\pi/\lambda$, r_{o1} is defined in the figure and $\cos(\bar{n}, \bar{r}_{o1})$ is the cosine of the angle between the line $\overline{P_1P_O}$ and the z axis (obliquity factor).

18

Eq (2.2) states that the field at the observation point P_O is proportional to an infinite summation of spherical waves; each originating from a different point within the aperture, and each weighted by the value of the aperture function at that point and by the obliquity factor for that point. This is Huygen's principle. Although infinite limits have been used on the integrals it is henceforth to be understood that the incident field and its partial space derivative is zero outside the aperture. Further, for now the incident field $\tilde{U}_i$ and its partial space derivative are considered to be the same across the aperture as it would be in the absence of the aperture. These are called the Kirchoff boundary conditions.

It is important to note that in order to reach this result the light wave has been treated as a scalar phenomenon. Thus only the scaler amplitude of the electric field vector of light has been considered. Experiments have shown, however that the scalar theory yields very accurate results if two conditions are met: (1) the diffracting aperture is large compared to the wavelength, and (2) the diffracted yields are not observed too close to the aperture (Silver, 1962:131). Both of these conditions are met throughout this thesis.

Several approximations can be made to further simplify Eq (2.2). First, the distance represented by r_{o1} in the figure is considered to be much larger than the

19

wavelength of the incident light, $r_{o1} >> $. Thus

$$(ik - \frac{1}{r_{o1}}) \approx ik \qquad (2.3)$$

Second, all observations are to be made in the paraxial region. Hence, the obliquity factor $\cos(\bar{n}, \bar{r}_{o1})$ is taken to be equal to one. Third, the distances represented by r_{o1} and z are considered to be approximately equal. Although this means that the r_{o1} term in the denominator can be expressed as z, the approximation is invalid in the exponent due to the fact that k is a large number. Substituting in the above approximations yields

$$\widetilde{U}(x_o, y_o) = (1/i \lambda z) \int\!\!\int_{-\infty}^{\infty} \widetilde{U}(x_1, y_1) \; \exp[ikr_{o1}]dx_1 dy_1 \qquad (2.4)$$

To simplify the exponent, the binomial expansion

$$\sqrt{1 + b} = 1 + b/2 + b^2/8 + \ldots. \qquad (2.5)$$

is used where $b = r_{o1}$ as defined in Fig. 2.1. The $b^2/8$ term and all terms which follow it are very small and are discarded. Eq (2.4) then becomes

$$\widetilde{U}(x_o, y_o) = (1/i \lambda z) \int\!\!\int_{-\infty}^{\infty} \widetilde{U}(x_1, y_1)$$

$$\cdot \exp[[ikz][1 + (1/2z)]$$

$$\cdot [(x_o - x_1)^2 + (y_o - y_1)^2]]d_{x1}d_{y1} \qquad (2.6)$$

Upon expanding the exponent

$$\widetilde{U}(x_O,y_O) = (1/i\lambda z) \exp[ikz] \exp[ik(x_o^2 + y_o^2)/2z]$$

$$\cdot \iint\limits_{-\infty}^{\infty} \widetilde{U}(x_1,y_1) \exp[ik(x_1^2 + y_1^2)/2z]$$

$$\cdot \exp[-i2\pi(x_O x_1 + y_O y_1)/\lambda z] \, dx_1 dy_1 \qquad (2.7)$$

Aside from the multiplicative factors preceding the integral, this integral states that the observed field amplitude $\widetilde{U}(x_O,y_O)$ may be found as a Fourier transform of the field amplitude of the input object plane $G(x_1,y_1)$. The transform is evaluated at the spatial frequencies $f_x = x_O/\lambda z$ and $f_y = y_O/\lambda z$. Eq (2.7) is normally used only to describe light propagating in the Fresnel or near zone. In the far-field or Fraunhofer region, one more approximation can be made. Since z is very large in the Fraunhofer region

$$\exp[ik(x_1^2 + y_1^2)/2z] \approx 1 \qquad (2.8)$$

and

$$\widetilde{U}(x_O,y_O) = \exp[ikz]/i\lambda z \, \exp[ik(x_O{}^2 + y_O{}^2)/2z] \iint\limits_{-\infty}^{\infty} \widetilde{U}(x_1,y_1)$$

$$\cdot \exp[(-i2\pi)(x_O x_1 + y_O y_1)/\lambda z] dx_1 dy_1 \qquad (2.9)$$

The integral of Eq (2.9) is an exact Fourier transform. If the input aperture happens to be a lens the

21

curvature of the incident wave is adjusted as in Eq (2.10)

$$U'_1(x_1,y_1) = U_1(x_1,y_1)\exp[-i\pi(x_o^2 + y_o^2)/\lambda f] \qquad (2.10)$$

However, if the observation plane is placed a distance f
away from the exit pupil then Eq (2.7), with the aid of the
Fresnel integral, reduces to

$$U_o(x_o,y_o) = \exp[i2\pi f/\lambda]/i\ f\ \exp[i\pi(x_1^2 + y_1^2)/\lambda f]\ U_1(x_1,y_1)$$

$$\cdot \exp[-[i2\pi](x_1x_o + y_1y_o)/\lambda f]dx_1dy_1 \qquad (2.11)$$

The phase curvature disappears for this special case and the
integral is again an exact Fourier transform.

This thesis is intended to support the Strategic Defense
Initiative (SDI). Thus, the imaging systems considered in
this thesis are governed by the approximations used to reach
Eqs (2.9) and (2.11). The exit pupil or subaperture plane
is always in the Fraunhofer region with respect to the
object plane, and the image plane is always a distance f
from the exit pupil plane.

The implication of these approximations is critical. It
makes it possible to analyze the imaging systems considered
in this thesis using exact Fourier transforms.

Fig. 2.2 depicts the imaging geometry which was pertinent to this thesis. Once again d_O is large and $d_i \approx f$ for these applications.
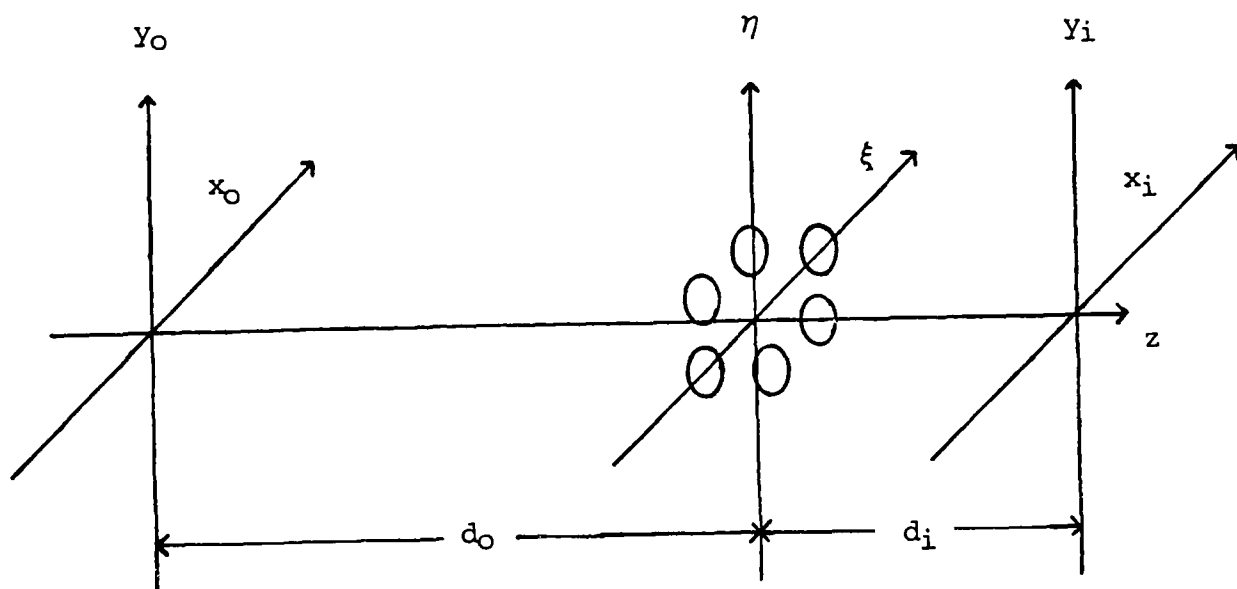
Fig. 2.2 Thesis Imaging Geometry

2.2 Imaging

2.2.1 Impulse Response. The symbol $h(x_i, y_i; x_o, y_o)$ denotes the response of an optical system at point (x_i, y_i) of the output image space to a δ function input at coordinates (x_o, y_o) of the input object space; that is,

$$h(x_i, y_i; x_o, y_o) = S\{ \delta (x_i - x_o, y_i - y_o) \} \qquad (2.12)$$

where $S\{ \}$ is a mathematical operator. The function h is called the impulse response of the system.

23

2.2.2 Imaging Using Fourier Transform Techniques. As
long as the paraxial restriction is maintained when
imaging, the form of the impulse response does not change
as the point input to the system moves about the input
plane. When this condition is met, the system is said to
be space-invariant or isoplanatic. In this region then,
Eq. 2.13

$$U_i(x_i,y_i) = U_O(x_O,y_O)*h(x_i - x_O,y_i - y_O) \qquad (2.13)$$

expresses the concept that the field amplitude in the image
plane can be thought of as the field amplitude in the
object plane convolved with the impulse response. Although
Eq (2.13) is useful from an intuitive standpoint, it does
not show directly how the imaging of any small object can
be accomplished through Fourier transform techniques.
Since it was established in section 2.1 that exact Fourier
transforms were appropriate to this thesis, it is
worthwhile to manipulate Eq (2.13) into a form which makes
use of Fourier transform techniques. The Fourier
transforms of $U_i(x_i,y_i)$, $U_O(x_O,y_O)$, and $h(x_O - x_i;y_O - y_i)$
are respectively

$$G_i(f_{x_i},g_{y_i}) = \iint\limits_{-\infty}^{\infty} U_i(x_i,y_i)$$

$$\cdot\exp[-i2\pi(f_{x_i}x_i + g_{y_i}y_i)]dx_idy_i, \qquad (2.14)$$

24

$$G_O(f_{x_o}, g_{y_o}) = \iint\limits_{-\infty}^{\infty} U_O(x_O, y_O)$$

$$\cdot \exp[-i2\pi(f_{x_o}x_i + g_{y_o}y_O)]dx_Ody_O, \qquad (2.15)$$

and

$$H(f_\xi, g_\eta) = \iint\limits_{-\infty}^{\infty} h(\xi, \eta) \exp[-i2\pi(f_\xi\xi + g_\eta\eta)d\xi d\eta \qquad (2.16)$$

G_i is the frequency spectrum in the image plane, G_O is the frequency spectrum in the object plane, and H is the Fourier transform of the impulse response, commonly referred to as the coherent transfer function. Upon taking the Fourier transform of each term and applying the convolution theorem Eq (2.13) becomes (Goodman, 1968:110-111)

$$G_i(\xi/\lambda f, \eta/\lambda f) = G_O(\xi/\lambda d_o, \eta/\lambda d_o) \; H(\xi, \eta) \qquad (2.17)$$

Taking the inverse Fourier transform represented by $F^{-1}\{\;\}$, of each term then yields

$$F^{-1}\{G_i(\xi/\lambda f, \eta/\lambda f)\} = F^{-1}\{H(\xi, \eta) \; G_O(\xi/\lambda d_o, \eta/\lambda d_o)\} \qquad (2.18)$$

Eq (2.18) reduces, where $F\{\;\}$ denotes the Fourier transform to

$$U_i(x_i, y_i) = F\{F^{-1}\{U_O(x_O, y_O)\}p(\xi, \eta)\} \qquad (2.19)$$

25

With Eq (2.19) the calculation of the image of any small
object can be realized using Fourier transform techniques.

2.3 Imaging of a Point

2.3.1 Impulse Response Through Single Aperture. When
a point source is the object Eq (2.19) simplifies further.
The inverse Fourier transform of a δ function is a
constant, which in two dimensions is a plane wave. Thus,
the impulse response (point source image) simply is
proportional to the Fourier transform of the (exit) pupil
function.

$$h(x_i - x_o; y_o - y_i) = F\{(const)(p(\xi,\eta)\} \qquad (2.20)$$

Henceforth, the constant will be understood to exist, but
will be dropped from the notation. The Fourier transform
of a circular, unapodised, unaberrated aperture yields a
Bessel function of the first kind over the argument of the
Bessel function (Parrent and Thompson, 1969:5). However,
for the purposes of this study the pupil function must take
into account apodisation, aberrations, and the
multiaperture nature of the problem.

2.3.2 Characterization of Pupil Function. Since the
pupil function always affects the image plane field
amplitude, its proper characterization is critical. To
begin, the pupil function accounts for the finite extent of
the aperture and in its unapodised, unaberrated form is

26

defined by (Goodman, 1968:83)

$$p(\xi,\eta) = \begin{cases} 1 \text{ inside the aperture} \\ 0 \text{ otherwise} \end{cases} \qquad (2.21)$$

An apodised aperture will still have a value of 1 in the center of the pupil, but elsewhere in the pupil it will decline to a smaller value as one approaches the edge.

The Gaussian apodiser was the only type of apodiser considered in this research. The Gaussian apodiser was also the only type considered in the single aperture research of Mills. Sticking with the same apodiser made it possible to compare the results of this study with his.

The reasons he chose a Gaussian apodiser are worth summarizing here. His study may be consulted for further justification. First, a Gaussian apodiser produces a real and positive amplitude impulse response. One of the undesirable effects of coherent imaging, edge ringing, occurs because the amplitude impulse response has negative regions. Hence, an apodiser which yields a real and positive amplitude impulse response is an appropriate countermeasure. The application of a Gaussian apodiser to an exit pupil produces an amplitude impulse response which is real and positive. The second reason Mills chose a Gaussian apodiser is that it does not vary significantly from other apodisation functions considered for use in

coherent optical systems. The final reason that a Gaussian apodiser was chosen is that it has a pair of intuitively pleasing effects when used in an optical system. The first is that the Fourier transform of a Gaussian is a Gaussian. The other is that when a Gaussian is used, the imaging system has some similarities to a laser propagation system. Both effects aid the intuitive process when thinking about the effects of the apodiser on the system.

The Gaussian apodiser used in this thesis had the form $A(r) = e^{-3r^2}$ where r is the radius and $r^2 = \xi^2 + \eta^2$. Fig. 2.3 is a plot of the amplitude transmittance of the Gaussian apodiser represented above versus the unapodised amplitude transmittance of the exit pupil. The function had a value of only 0.05 at the edge of the aperture. This low transmittance at the edge allowed a separation of the effects of aberrations from that of the hard aperture.

The presence of aberrations in an optical system leads to the introduction of phase variations across the system's exit pupil. Specifically, when wavefront errors exist, one can imagine that the exit pupil is illuminated by an ideal spherical wave, but that a phase-shifting plate exists within the aperture, thus deforming the wavefront that leaves the aperture. If the phase error at the point (ξ, η) in the exit pupil is represented by $kW(\xi, \eta)$ where $k = 2\pi/\lambda$ and W is the effective path length error, then the complex transmittance of the phase-shifting plate is given by $\exp[ikW(\xi, \eta)]$

28
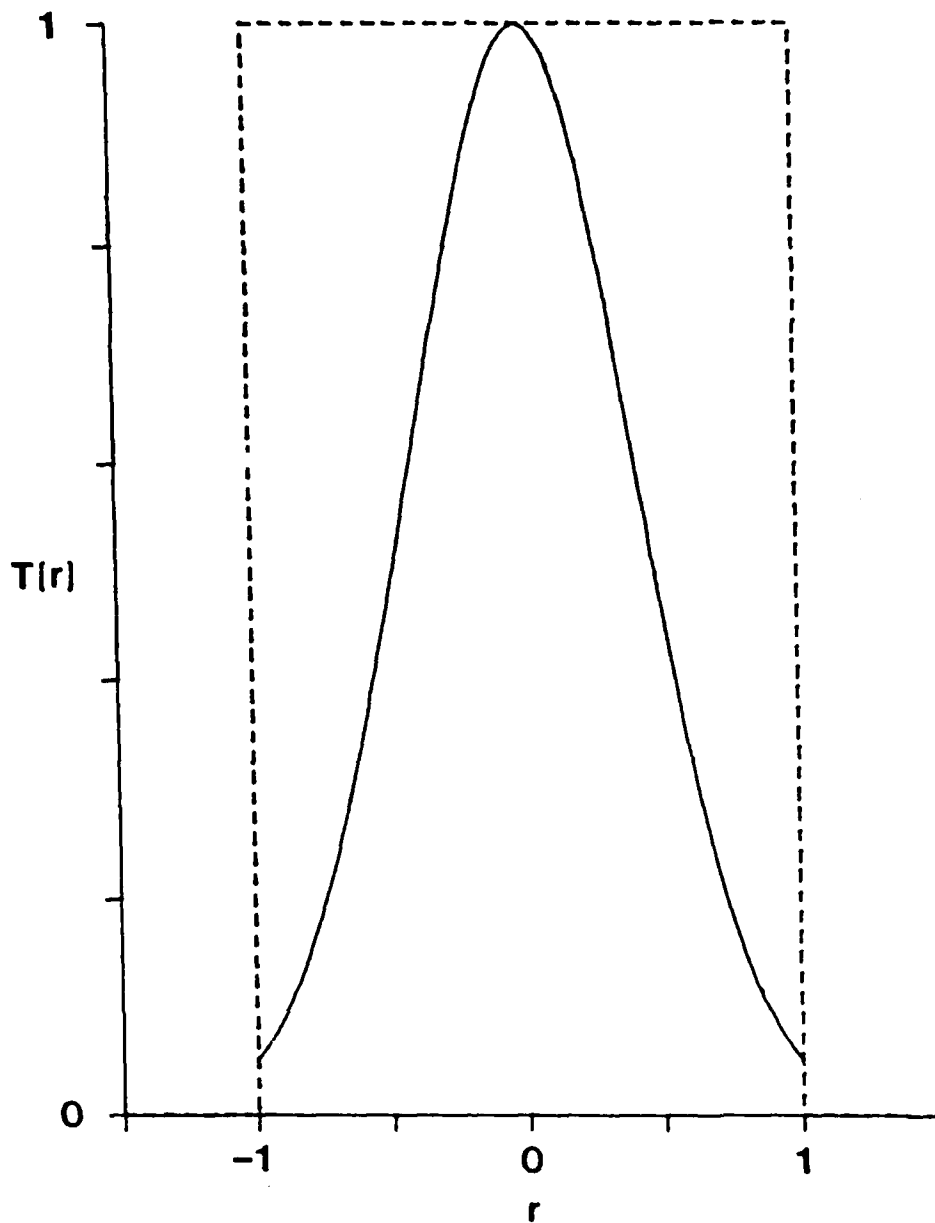
Fig. 2.3   The amplitude of the Gaussian filter used
in this study (solid line) is shown
relative to the unapodised amplitude
transmittance of the exit pupil (dashed
line) (Mills, 1984:44).

29

(Goodman: 1968:121). The pupil function then becomes

$$p(\xi,\eta) = \beta(\xi,\eta) \exp[ikW(\xi,\eta)] A(\xi,\eta) \qquad (2.22)$$

where $\beta(\xi,\eta)$ represents the finite size of the pupil and $A(\xi,\eta)$ represents the apodiser.

2.3.3 Multiaperture Pupil Function.

The development of the multiaperture pupil function in this section and the analysis of the impulse response through a multiaperature pupil function in the next section has been done before by both Brian Hooker and Janet Fender (Hooker, 1974:14-19; Fender, 1984:2-7) and thus follows closely their development. The pupil function of a multiaperture imaging system is the sum of the individual subaperture pupil functions. It follows then that in Cartesian coordinates, the pupil function for N elements each centered at (ξ_n,η_n) is

$$p(\xi,\eta) = \sum_{n=1}^{N} p_n(\xi - \xi_n, \eta - \eta_n) \exp[ikW(\xi - \xi_n, \eta - \eta_n)]$$
$$\cdot A(\xi - \xi_n, \eta - \eta_n) \qquad (2.23)$$

The $p_n(\xi - \xi_n, \eta - \eta_n)$ terms describe the finite extent of the subapertures, the $\exp[ikW(\xi - \xi_n, \eta - \eta_n)]$ terms describe the wave aberration functions over each subaperture, and the $A(\xi - \xi_n, \eta - \eta_n)$ terms describe the amplitude transmittance of the subapertures. For aberrations which extend across the full multiaperture

30

system, such as those generated by atmospheric turbulence, the pupil function is multiplied by an additional term $\exp[ikW'(\xi,\eta)]$. The pupil function then becomes

$$p'(\xi,\eta) = p(\xi,\eta) \exp[ikW'(\xi,\eta)] \qquad (2.24)$$

2.3.4 Impulse Response Through a Multiaperture System.

As stated in Section 2.3.1 the impulse response of a multiaperture imaging system is determined by the Fourier transform of the pupil function:

$$p(f_\xi,f_\eta) = F\{p(\xi,\eta)\}\Big|_{f_\xi = \xi/\lambda f,\; f_\eta = \eta/\lambda f} \qquad (2.25)$$

$$= \sum_{n=1}^{N} F\{p_n(\xi - \xi_n, \eta - \eta_n)$$

$$\cdot \exp[ikW_n(\xi - \xi_n, \eta - \eta_n)]$$

$$\cdot A(\xi - \xi_n, \eta - \eta_n)\}\Big|_{f_\xi = \xi/\lambda f,\; f_\eta = \eta/\lambda f}$$

The spatial frequency coordinates are f_ξ and f_η evaluated in the far field at $f_\xi = \xi/\lambda f$ and $f_\eta = \eta/\lambda f$, with f being the distance to the image plane. Noting that the shift theorem

$$F\{p_n(\xi - \xi_n, \eta - \eta_n)\} = P(f_\xi,f_\eta) \exp[i2\pi(f_\xi \xi_n + f_\eta \eta_n) \qquad (2.26)$$

can be expressed

$$F\{p_n(\xi - \xi_n, \eta - \eta_n)\} = F\{p_n(\xi,\eta)\}$$

$$\cdot \exp[i2\pi(f_\xi \xi_n + f_\eta \eta_n)] \qquad (2.27)$$

31

and that upon change of variable $\xi = \xi - \xi_n, \eta = \eta - \eta_n$

$$p_n(\xi - \xi_n, \eta - \eta_n) \exp[ikW_n(\xi - \xi_n, \eta - \eta_n)] A(\xi - \xi_n, \eta - \eta_n)$$
$$= p_n(\xi, \eta) \exp[ikW_n(\xi, \eta)] \quad A(\xi, \eta) \qquad (2.28)$$

the shift theorem may be used to convert Eq (2.27) to

$$F\{p_n(\xi, \eta) = F\{p_n(\xi, \eta)\} \exp[ikW_n(\xi, \eta)] \quad A(\xi, \eta)$$
$$\cdot \exp[-i2\pi(f_\xi \xi_n + f_\eta \eta_n)] \qquad (2.29)$$

Recalling what the spatial frequency coordinates are allows the impulse response to be of the form

$$P(\xi, \eta) = \sum_{n=1}^{N} \exp[-ik(\xi \xi_n/f + \eta \eta_n/f)] \qquad (2.30)$$
$$\cdot F(p_n(\xi, \eta) \exp[ikW_n(\xi, \eta)]$$
$$\cdot A(\xi, \eta)\} \Big|_{f_\xi = \xi/\lambda f, \; f_\eta = \eta/\lambda f}$$

The impulse response equation can be expressed in polar coordinates by substituting

$$\xi = r\sin\theta \qquad \xi_n = \rho_n \sin\theta_n$$
$$\eta = r\cos\theta \qquad \eta_n = \rho_n \cos\theta_n \qquad (2.31)$$

where ρ_n is the radius of the circle the subapertures are centered on and θ is the angular orientation in the subaperture plane. And the equation for $P(\xi,\eta)$ becomes

$$P(r,\theta) = \sum_{n=1}^{N} \exp[(-ikr\rho_n)/f] [[(\sin\theta\sin\theta_n) + (\cos\theta\cos\theta_n)]]$$

$$\cdot F\{P_n(\rho,\theta) \exp[ikW_n(\rho,\theta)] A(\rho,\theta)\} \qquad (2.32)$$

Or in more convenient notation

$$P(r,\theta) = \sum_{n=1}^{N} A_n(r,\theta) U_n(r,\theta) \qquad (2.33)$$

where

$$A_n(r,\theta) = \exp[(-ikr\rho_n/f) [(\sin\theta\sin\theta_n) + (\cos\theta\cos\theta_n)]]$$

$$U_n(r,\theta) = F\{P_n(\rho,\theta) \exp[ikW_n(\rho,\theta)] A(\rho,\theta)\}$$

Hence, the impulse response of an N-element multiaperture system is represented by the contribution from each of the N subapertures. Each subaperture contribution is the product of the Fourier transform of its pupil function, $U_n(r,\theta)$, times a phase factor $A_n(r,\theta)$ that depends on the position of the subaperture element within the multiaperture array.

The evaluation of $U_n(r,\theta)$ is extremely involved except when all of the subapertures are unaberrated and unapodised. Thus, for aberrated and apodised multi-

33

aperture systems analysis is best left to a computer.
However, if all the subapertures are identical, unaberrated
and unapodised, the Fourier transform of each pupil
function is the same. In the case of circular apertures
once again this is the Bessel function of the first kind
over the argument of the Bessel function given by
(Born and Wolf, 1965:395):

$$U(r,\theta) = (i2\pi a^2/\lambda f)\ J_1[(ka/f)r]/[(ka/f)r] \qquad (2.34)$$

where a = radius of the subapertures

$k = 2\pi/\lambda$

f = distance between imaging and exit pupil planes

r = distance on the image plane away from the point
     where the optical axis intersects the image plane
     (the origin)

The phase factor, $A_n(r,\theta)$, can be easily evaluated
once the array is specified. For a multiaperture system
composed of N subapertures positioned on a circle of
radius ρ_n, the impulse response is given by Eq (2.34)
where $\theta = n(2\pi/N)$. With N=6, then $\theta_n = \pi n/3$ and
$A_n(r,\theta)$ becomes

$$A_n(r,\theta) = \sum_{n=1}^{N} \exp[(-ikr\rho_n/f)[(r\sin\theta\sin(\pi n/3))$$

$$+\ (\cos\theta\cos(\pi n/3))]] \qquad (2.35)$$

34

Combining Eqs (2.34) and (2.35) after the expansion of (2.35) yields

$$P(r,\theta) = -i2\pi a^2/\lambda f \; J_1[(ka/f)r]/[(ka/f)r]$$

$$+ \{\exp[(-ikr\rho_n/f)(\sqrt{3}/2 \sin\theta + 1/2 \cos\theta)]$$

$$+ \exp[(ikr\rho_n/f)(\sqrt{3}/2 \sin\theta - 1/2 \cos\theta)] \qquad (2.36)$$

$$+ \exp[(-ikr\rho_n/f)(-\sqrt{3}/2 \sin\theta - 1/2 \cos\theta)]$$

$$+ \exp[(-ikr\rho_n/f)(\cos\theta)] + \exp[(-ikr\rho_n/f)(\cos\theta)]\}$$

Making use of the relationship $2\cos\theta = \exp[i\theta] + \exp[-i\theta]$, Eq (2.36) reduces to:

$$P(r,\theta) = -i2\pi a^2/\lambda f \; J_1[(ka/f)r]/[(ka/f)r]\{2\cos[(kr\rho_n/f)\cos\theta]$$

$$+ 2\cos[(kr\rho_n/f)(\sqrt{3}/2 \sin\theta - 1/2 \cos\theta)]$$

$$+ 2\cos[(kr\rho_n/f)(\sqrt{3}/2 \sin\theta + 1/2 \cos\theta)]\} \qquad (2.37)$$

The irradiance or modulus squared is

$$I(r,\theta) = |P(r,\theta)|^2$$

$$= 4\pi^2 a^4/\lambda^2 f^2 \; \{J_1[(ka/f)r]/[(ka/f)r]\}$$

$$\cdot \; \{6 + 2\cos[(2kr\rho_n/f)\cos\theta]$$

$$+ 2\cos[(kr\rho_n/f)(\sqrt{3}\sin\theta + \cos\theta)]$$

$$+ 2\cos[(kr\rho_n/f)(\sqrt{3}\sin\theta - \cos\theta)]$$

$$+ 4\cos[(kr\rho_n/f)(\sqrt{3}/2 \sin\theta + 3/2 \cos\theta)]$$

$$+ 4\cos[(kr\rho_n/f)(\sqrt{3}/2 \sin\theta - 1/2 \cos\theta)]$$

$$+ 4\cos[(kr\rho_n/f)(\sqrt{3}/2 \sin\theta + 1/2 \cos\theta)]$$

$$+ 4\cos[(kr\rho_n/f)(\sqrt{3}/2 \sin\theta - 3/2 \cos\theta)]$$

$$+ 4\cos[(kr\rho_n/f)(\sqrt{3}\sin\theta)]$$

$$+ 4\cos[(kr\rho_n/f)\cos\theta]\} \qquad (2.38)$$

Eq (2.38) represents an Airy pattern modulated by nine
cosine fringe fields. When the fringe fields are added
together they form a series of peaks modulated by the Airy
diffraction envelope. As ρ_n is increased, which
increases the degree of dilution, the width of the central
peak decreases while the magnitude of the fringe peaks
increase. The peak amplitude of the central peak is
proportional to the square of the number of subapertures
(Fender, 1984:6). Thus, the peak irradiance is
proportional to the square of the number of subapertures.

2.4 Imaging of an Edge

2.4.1 Field Amplitude of Edge at Pupil Function. The
approach to imaging an edge through an optical system is
the same as the approach taken in imaging the impulse
response through the system. Hence, under the conditions
detailed in section 2.2.2 the field amplitude in the image
plane $U_i(x_i,y_i)$ is related to the object field
amplitude $U_o(x_o,y_o)$ by Eq (2.19)

$$U_i(x_i,y_i) = F\{F^{-1}\{U_o(x_o,y_o)\}p(\xi,\eta)\} \qquad (2.19)$$

where F represents the forward Fourier transform, F^{-1}
represents the inverse Fourier transform, and $p(\xi,\eta)$ is the
pupil function represented in Eq (2.22).

An edge in the object (x_o,y_o) plane can be
described by

$$e(x_O, y_O) = step(-x_O) = 1 \text{ if } x \leq 0$$
$$0 \text{ otherwise} \qquad (2.39)$$

where the edge has been aligned to be coincident with the y_O axis. Noting that $step(-x_O) = 1/2 + sgn(-x_O)$, the inverse Fourier transform of Eq (2.39) is given by (Gaskill, 1978:195,205-6)

$$F^{-1}\{e(x_O, y_O)\} = 1/2[\delta(g) + (1/i\pi g)]\delta(f) \qquad (2.40)$$

where δ is the Dirac delta function and f and g are spatial frequency coordinates in the exit pupil plane:

$$g = \frac{\xi}{\lambda d_O} \qquad \text{and} \qquad f = \frac{\eta}{\lambda do} \qquad (2.41)$$

The coordinates (ξ, η) refer to the space coordinates in the exit pupil plane and d_O is the distance from the object plane to the pupil plane. Since $\delta(f)$ is also a delta function, the problem reduces to one dimension. Thus, the electric field amplitude is located entirely along the axis. It is real at the origin and imaginary everywhere else. Hence Eq (2.40) can be written

$$U_i(x_i, y_i) = F\{(1/2)[\delta(\xi/\lambda d_O) + \lambda d_O/i\pi\xi]p(\xi)\} \qquad (2.42)$$

37

The pupil function is given by

$$p(\xi) = B(\xi) \exp[ikW(\xi)]A(\xi) \tag{2.43}$$

where $B(\xi)$ represents the finite extent of the pupil, $\exp[ikW(\xi)]$ represents the phase transmittance and thus characterizes any aberrations present, and $A(\xi)$ the apodisation. The amplitude transmittance of the apodiser function is the same as the one introduced earlier in the chapter, except that $A(\xi) = e^{-3(\xi \pm \eta)}$ is expressed in one dimension. The result of imaging an edge through an unapodised, unaberrated single aperture is shown in Fig. 2.4.

   2.4.2 Edge Through a Multiaperture System. Imaging the edge through a multiaperture system is only slightly more complicated. Fig. 2.5 represents the field amplitude at the pupil plane passing through a multiaperture system. In the figure a represents the radius of the individual subapertures while R is a constant. The product Ra is the radius of the circle the subapertures are centered upon. The change which has occurred over the single aperture case is in the finite extent of the pupil function. The only part of the field amplitude which passes through the pupil plane is the imaginary part along ξ which gets through the top and bottom subapertures. The field amplitude never

38
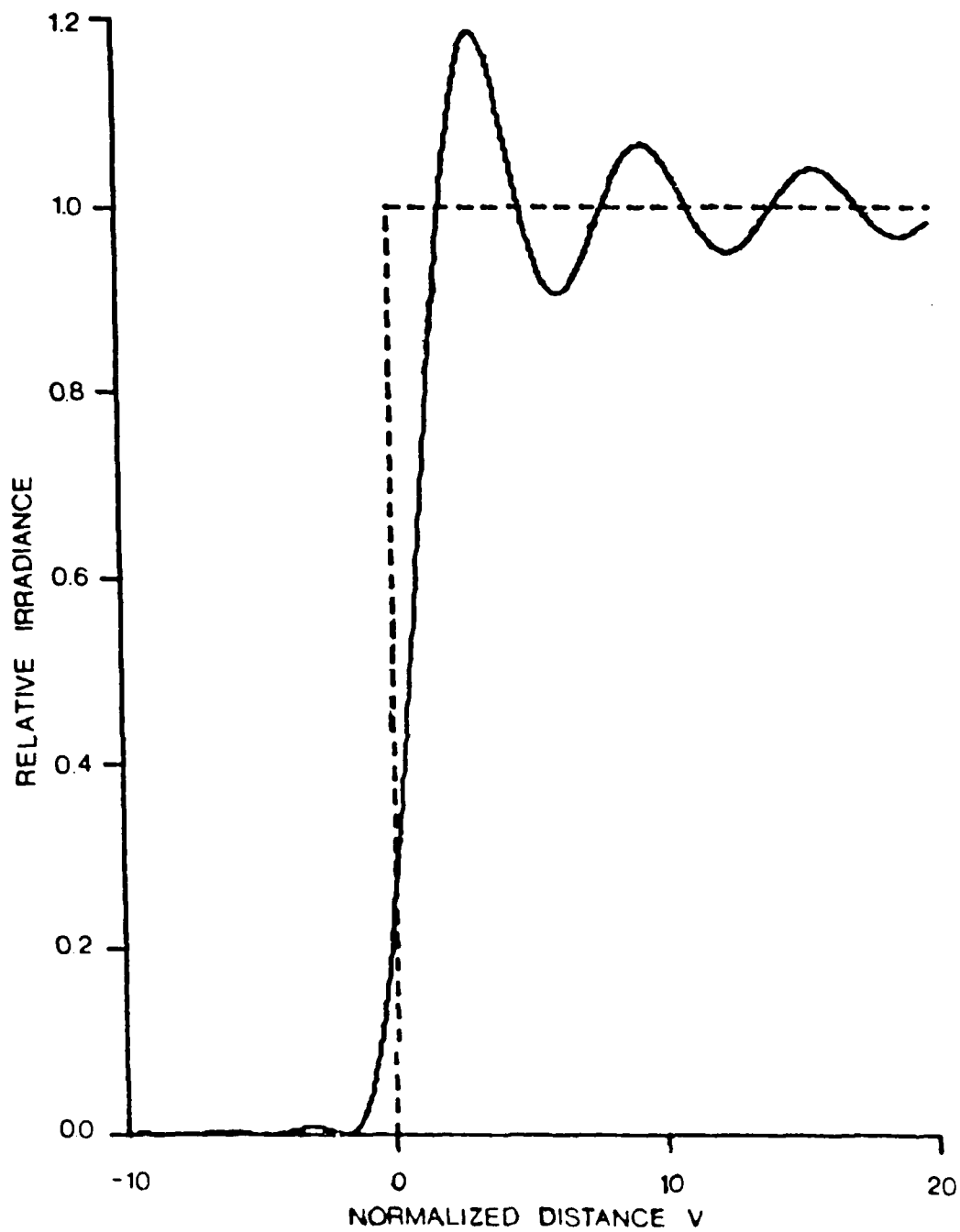
Fig. 2.4   Coherent image through a single aperture of
an edge plotted relative to the geometrical
image of an edge (Mills, 1984:5).

39
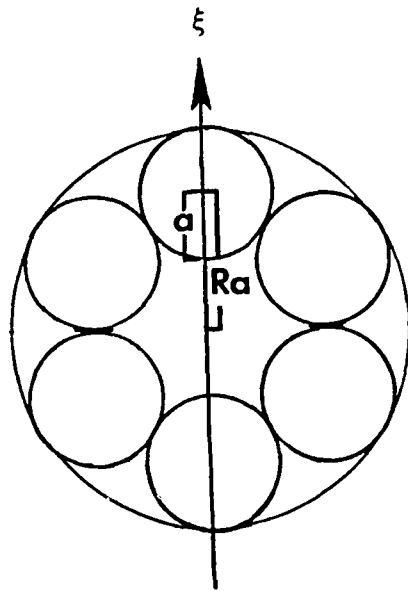
Fig. 2.5   Field amplitude at multiaperture pupil plane.

passes through the subapertures on either side and can thus

be discarded from the pupil function representation.   It's

worth noting that in the subaperture configuration

represented in Fig. 2.6 there is no overlap between the

field amplitude and subapertures.   Hence there is no

transmittance.   In view of this, an annular ring would be a

better edge imaging system.   The results of this thesis can

be applied to an annular system without loss of generality.
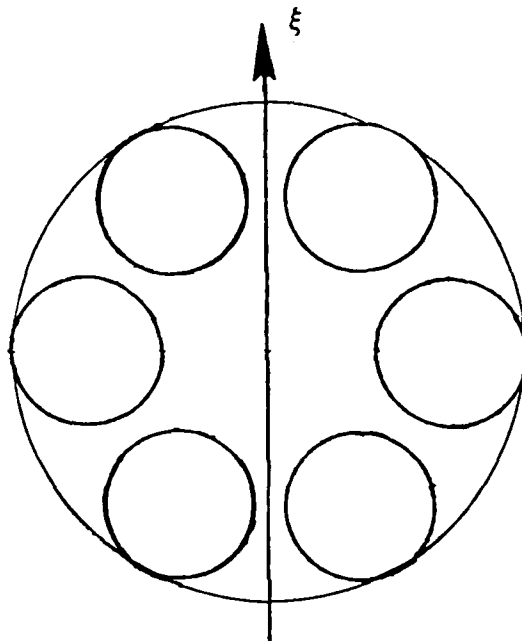
Fig. 2.6 Field amplitude at rotated
multiaperture pupil plane.

Under the conditions represented by Fig. 2.5 the field
amplitude just after the exit pupil plane can be expressed

$$U'(\xi,\eta) = 1/2[\delta(\xi/\lambda d_o) + (\lambda d_o/i\pi\xi)] \delta(\eta/\lambda d)$$

$$\cdot \frac{cyl[(\xi + Ra)^2 + \eta^2]^{1/2}}{2a} + \frac{cyl[(\xi - Ra)^2 + \eta^2]^{1/2}}{2a} \qquad (2.44)$$

Using one of the properties of delta functions in a product
(Gaskill, 1978:57)

$$f(\eta) \delta(\eta - \eta_o) = f(\eta_o) (\eta - \eta_o) \qquad (2.45)$$

41

where all the operations occur along the line $\eta = 0$ so that $\eta_O = 0$ in this case, Eq (2.44) can be reduced and combined with Eq (2.42) to yield

$$U_i(x_i,y_i) = F\{1/2[cyl(\xi + Ra) + cyl(\xi - Ra)][\delta(\xi/\lambda d_O) + \lambda d_O/i\pi\xi] \qquad (2.46)$$

Again the $\delta(f)$ term has disappeared due to the one-dimensional nature of the problem.

2.5 Previous Research

There are two main areas which contain research pertinent to this thesis. The first is the field of multiaperture optical imaging, which is still quite new. Much of the research to this point has been concentrated on incoherent imaging systems. Nevertheless, there are several works which have been done which are relevant to this study. The second main area is the application of apodisation techniques to improve the imaging properties of optical systems. Here too, past investigations have dealt primarily with incoherent illumination. However, recently an investigation was completed which analyzed the effect of apodisation on single aperture aberrated coherent imaging systems. It was in fact that study which spawned this thesis. Hence, the conclusions which it reached are also important to the work here.

42

2.5.1 Studies of Multiaperture Systems. The previous

research in this area which is of interest to this thesis

includes a theoretical investigation of dilution, a

theoretical and experimental investigation of aberrations, and

an experimental and theoretical analysis of coherent imaging

systems.

One of the initial questions raised by the advent of

multiaperture optical systems was how much dilution could be

tolerated between the individual subapertures. Accordingly,

in 1971 a team from the Optical Sciences Center, University of

Arizona, performed a study with a computer program written by

Robert R. Shannon of Itek Corp., which modeled the incoherent

impulse response of a symmetric hexagonal array of circular

subapertures at various degrees of dilution. The study

arbitrarilly concluded from the general appearance of the

optical transfer functions that pictures taken out to spacings

between the subapertures of about four tenths the unit

subapertures' diameter would be of acceptable quality. If the

dilution were increased any further, zeros would occur between

the single element transfer function and spatial information

at certain frequencies and azimuthal angles would be lost from

the recorded image (Shack and others, 1971:257-9). It was

this spacing which was actually used for the Mt. Hopkins MMT,

where practical engineering problems and maximization of

system resolution were jointly considered

(Sanger and others, 1972:161-70). Dilution of this amount

43

results in an increase in resolving power of 3.6 times as great as that of a single element.

Another early question that needed answering about multiaperture optical systems was what effect did the various aberrations have on imaging. This subject was explored by Brian Hooker in his PhD dissertation when he investigated the effects of several aberrations on one subaperture within an array. His study was limited to the incoherent impulse response. He concluded that piston error was easily the most significant aberration, with serious alterations in the PSF occuring in the range $0.1\lambda - 0.25\lambda$. Tilt, defocus, and system defocus were next, with a maximum tolerable magnitude of 0.35λ. The least significant aberrations were astigmatism, coma, and spherical aberration. The tolerable magnitudes for them lay in the 0.5λ to 1.0λ range (Hooker, 1974:155-56).

Both of the studies cited above dealt exclusively with incoherent imaging. The only multiaperture coherent imaging study related to this thesis is a project completed in 1983 by another team from the Optical Sciences Center, University of Arizona (Meinel and others, 1983:149-201). The Arizona team created a photographic atlas of the impulse responses generated by various configurations of subapertures. The light source was the green line of an Argon laser. They also created a series of two-dimensional slices of the impulse responses of a few key configurations

44

they were studying. Among those configurations was the
configuration studied in this thesis. The usefulness of
their work lay in the fact that the results generated by the
present study were identical to the results they obtained.
This was also the case when in the course of developing the
computer progam for this thesis several more of the Arizona
team's photographic impulse responses for other
configurations were verified quantitatively. Their work
endeavored to determine whether a four square, eight square,
eight square plus a central subaperture, eight circular, six
circular plus a central subaperture, or a six circular
subaperture configuration was best for multiaperture
imaging. They determined that there was little advantage in
choosing one configuration over another as long as each
system had about the same angular resolution. However, if a
faint object were being imaged, a configuration with a
central subaperture with close spacing was best due to the
boost those configurations gave to the central maximum
(Meinel and others, 1983:149-201).

    2.5.2 <u>Apodisation of Coherent Imaging Systems</u>. Most
of the studies which have evaluated the utility of apodisers
in improving the performance of coherent imaging systems
have concentrated almost entirely on the impulse response.
It was not until last year, with the publication of the PhD
dissertation by Mills, that the issue of generalized imaging
through an aberrated, apodised, coherent optical system was

addressed. His thesis was an investigation of the effects of third order aberrations on imaging for both unapodised and apodised single aperture systems. He determined that apodisation was indeed effective in improving the performance of these aberrated systems. It was the success of his work that prompted this thesis. One of the two main questions answered by this thesis is whether apodisation is also effective in improving the imaging performance of multiaperture systems.

III. The Computer Program

3.1 Single Aperture Impulse Response Program

The impetus for the research embodied in this thesis arose from the results of James P. Mills in his PhD dissertation. His work proved that apodisation sharply curtailed the effects of aberrations on a single aperture, coherent imaging system. Hence, it became a worthwhile pursuit to extend his results to multiaperture systems. Accordingly, the approach that was taken was to modify his computer program, which dealt of course with only a single aperture, to deal with multiaperture systems. This chapter describes the important modifications which were necessary to make that jump.

The single aperture program was run on a VAX 11/750 computer and was written in Fortran-77. It calculated the modulus, phase, and irradiance of the point spread function (PSF) through a single circular aperture. The inputs to the program were the size of the array representing the exit pupil field, the third order aberrations in terms of the monomial Zernike coefficients, and the radial width factor of the Gaussian apodiser. The exit pupil itself, which was the circular aperture, was constructed early in the programm, and required no adjustment. The point spread function was found by performing a fast Fourier transform of the exit pupil array (Mills, 1984:16,43). The Fourier

47

transform was accomplished using a fast-Fourier transform
subroutine from the VAX IMSL package.

3.2 Modifications to Single Aperture PSF Program

The process of modifying the Mills program involved
chiefly three tasks. The first was to incorporate the far
field response that corresponded to a particular
configuration of subapertures into the program. The second
was to develop the most efficient means of passing the
contribution to the total impulse response from a
subaperture or set of subapertures during subsequent runs
of the program. The third was to increase the resolution
of the resultant impulse response.

Returning to the first task, it is useful to recall
Eq (2.33) from Chapter 2:

$$P(r,\theta) = \sum_{n=1}^{N} A_n(r,\theta) U_n(r,\theta) \tag{3.1}$$

where $A_n(r,\theta) = \exp[(-ikr\rho_n/f)(\sin\theta\sin\theta_n) + (\cos\theta\cos\theta_n)]$

$U_n(r,\theta) = F\{P_n(\rho,\theta) \exp[ikW_n(\rho,\theta)]\}$

As stated earlier, the far field performance of an
N-element multiaperture system is represented by the
contribution from each of the N subapertures. Each
subaperture contribution is the product of the Fourier
transform of its pupil function, $U_n(r,\theta)$, times a phase
factor $A_n(r,\theta)$ that depends on the position of the

48

subaperture element within the multiaperture array. Mill's program calculated $U_n(r,\theta)$ for single circular apertures and hence was a perfect core to any program which computed the far field response of multiaperture configurations of circular apertures. If one desired to model a system of square, rectangular, or other shape of subaperture the pupil function in the beginning of the program would have to be adjusted, but the approach would still be the same.

As noted in Eq (2.34) of Chapter 2, the impulse response of a point source through a circular, unaberrated, unapodised aperture is a Bessel function of the first kind over the argument of the Bessel function. Thus, the far field performance of any configuration of circular subapertures is represented by the summation of the $J_1(x)/x$ functions associated with the particular subapertures (which vary with the subapertures' size) times the phase factor associated with the various subapertures' positions in the exit pupil plane. Hence

$$P(r,\theta) = \sum_{n=1}^{N} (-i2\pi a^2/\lambda f) \ J_1[(ka/f)r]/[(ka/f)r]$$

$$\cdot \ exp[(-ikr\rho_n/f)(\sin\theta\sin\theta_n + \cos\theta\cos\theta_n)] \qquad (3.2)$$

For this reason the phase contribution to the impulse response was computed directly after the $J_1(x)/x$ function was calculated and then multiplied times it. The next thing

which was necessary to properly characterize the far field
performance of multiaperture systems was to effect a
transfer from the coordinate system of the subaperture-exit
pupil plane to the coordinate system of the image plane.
For example, the coordinate system of a symmetric set of
hexagonal equally sized circular subapertures is represented
in Fig. 3.1.
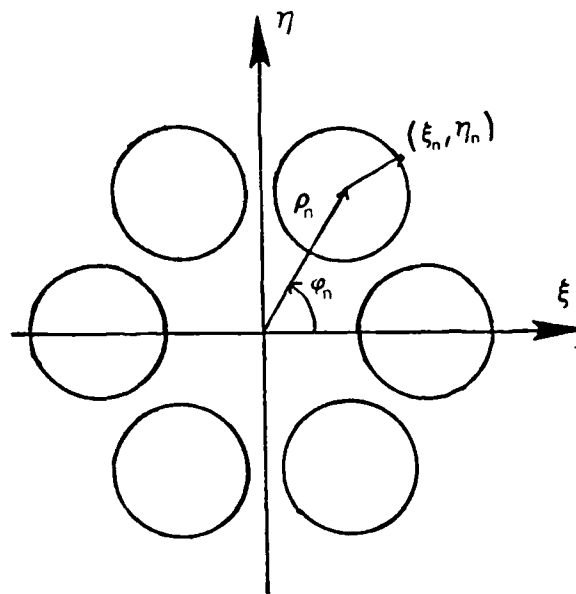
Fig. 3.1 Coordinates of subaperture plane.

They had to be transferred to the coordinate system of the
image plane which is represented in Fig. 3.2.
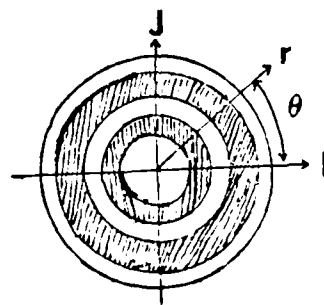
Fig. 3.2 Coordinates of image plane.

50

It turned out that the dimensions of the $J_1(x)/x$ function in the output array generated by a single aperture could be used to make the transfer. The expression for the $J_1(x)/x$ function in the radial coordinates of the image plane was

$$J_1[(2\pi ar/\lambda f)/(2\pi ar/\lambda f)] \qquad (3.3)$$

which in Cartesian coordinates became

$$J_1\{[(2\pi a/\lambda f)(\sqrt{\xi^2 + \eta^2})/(2\pi a/\lambda f)(\sqrt{\xi^2 + \eta^2}) \qquad (3.4)$$

And upon making the substitutions

$$u = 2\pi a\xi/\lambda f \qquad\qquad v = 2\pi a\eta/\lambda f \qquad (3.5)$$

the expression took the form

$$J_1(\sqrt{u^2 + v^2}) / (\sqrt{u^2 + v^2}) \qquad (3.6)$$

The coordinates of the $J_1(x)/x$ function were then represented by Fig. 3.3:
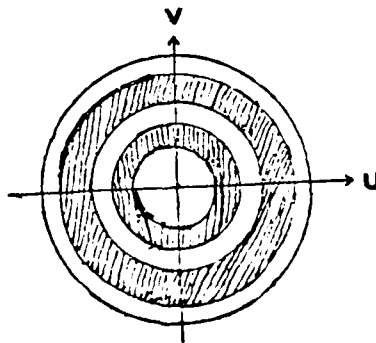
Fig. 3.3 Modified coordinates of image plane.

51

A plot of the $J_1(x)/x$ function (squared) shows how it was possible to relate the second minimum of the $J_1(x)/x$ function to the computer output array dimensions in terms of I and J:

RELATIVE IRRADIANCE

NORMALIZED DISTANCE
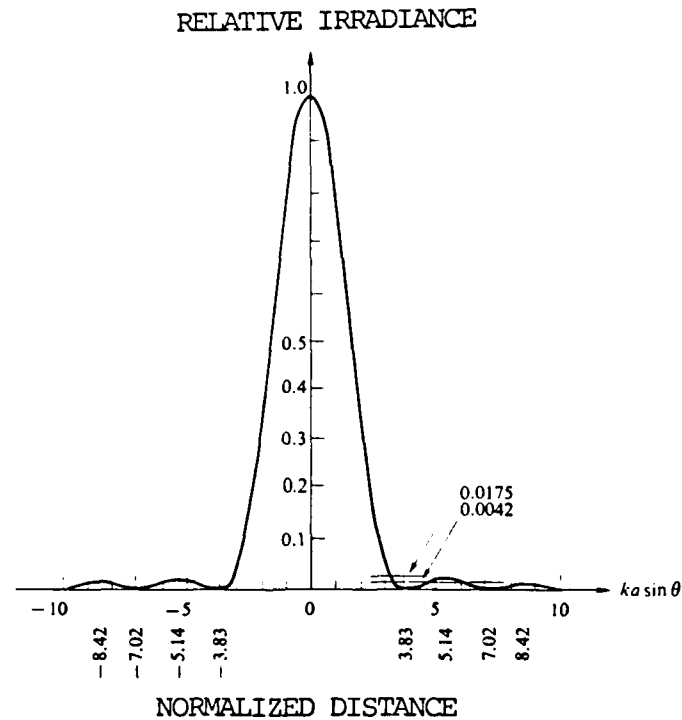
Fig. 3.4   Plot of Irradiance vs. Position for the function $J_1(x)/x$ (Hecht & Zajac, 1974:352). The vertical scale is the normalized irradiance while the horizontal a scale is in relative units of distance.

The second dark ring was chosen to relate I (and J in the other direction) to a specific known value. The second dark ring was chosen to increase accuracy and to increase the number of true zeros which were used to compute the values of I and J. When u = 7.016, I averaged 16.848. Thus

$$u = I(7.016)/16.848 \qquad v = J(7.016)/16.848 \qquad (3.7)$$

52

These substitutions removed the focal length and dependence of Eq (3.4) and made it possible to express the $J_1(x)/x$ function in terms of the dimensions of the computer output array. All that remained was to get the phase factor for the far field performance expressed in terms of known quantities

$$P(r,\theta) = -i2\pi a^2/\lambda f \; J_1[(kar/f)/(kar/f)]$$

$$\cdot \; \exp[(-ikr\rho_n/f)\sin\theta\sin\theta_n + \cos\theta\cos\theta_n)] \qquad (3.8)$$

The radial coordinate in the exit pupil plane, ϕ_n, could be expressed $\phi_n = 2n\pi/N$, with N = total number of subapertures in the array, and n = position of the individual subaperture in the array. The term outside the summation is simply the Airy pattern. Multiplying the phase factor by a/a and upon converting to Cartesian coordinates one arrived at

$$A_n \; (r,\theta) = \sum_{n=1}^{N} \exp[(-i2\pi a/\lambda f)(\sqrt{\xi^2 + \eta^2})\rho_n/a$$

$$\cdot \; (\sin\theta\sin\phi_n + \cos\theta\cos\phi_n)] \qquad (3.9)$$

which recalling the earlier substitutions for u and v equaled

53

$$A_n(r,\theta) = \exp[(-i\rho_n/a)(\sqrt{u^2+v^2})(\sin\theta\sin\phi_n + \cos\theta\cos\phi_n) \quad (3.10)$$

where

$$\phi = \tan^{-1}(\eta/\xi) \quad (3.11)$$

The inputs to the angle   were represented by

$$\xi = J - 24.0 \qquad \eta = I + (24.0 - 2I) \quad (3.12)$$

Hence, the only variables in the expression were θ, ρ_n, and a, and all but a could be varied in the inputs to the program. The diameter of the aperture a, however, had to be varied indirectly. It was varied by changing the size of the input array describing the exit pupil. For example, if the size of the array was doubled in both directions while the diameter of the aperture was kept constant, the size of the aperture was effectively halved, which resulted in a doubling of the spread of the Airy pattern.

The second important task involved in converting the Mills single aperture program to a viable multiaperture program was to develop an efficient means of passing on the contribution to the total impulse response from each respective subaperture. A quick look at Eqs (3.2) and (3.10) make it clear that it makes no difference whether the $J_1(x)/x$ function is inside or outside the summation. Hence, as long as each circular aperture was the same size,

54

had the same aberrations applied across it, and had the same radial width on its Gaussian apodiser, the same function would be generated. Thus, when all the apertures were the same, the function corresponding to them only needed to be generated once. It was only necessary to sum the displacement phase contributions. It followed then that if the same aberration were applied to six identical subapertures, the program only needed to run once, rather than six times, which saved much computer time. If however, one or more of the subapertures were different, the function generated by each deviant subaperture was different, which necessitated that the program be run separately from the others. The best place to write and store the input from the deviant aperture was directly after the far field contribution, due to the subaperture had been calculated but before the modulus, irradiance, and phase had been calculated. That way only one file needed to be stored and consequently read in again when the program was run for another aperture. The results from the old data file were then added to the newly generated array and the modulus, phase, and irradiance were determined. When the subapertures were varied in size or shape the only requirement was that the storage data files were the same size as the arrays just generated.

The last important task in converting Mill's program into a multiaperture routine was to increase the resolution

of the generated impulse response. Multiaperture systems

create cosine fringes which are much sharper than the

diffraction patterns associated with single apertures.

Thus, it was important to increase the resolution of the far

field pattern being computed. It was explained earlier that

increasing the input array of the exit pupil while keeping

the aperture itself constant simulated a smaller aperture

and hence a more spread out point spread pattern. In

Mills's single aperture program a 256 x 256 input array

provided all the resolution which was needed. But for a

multiaperture system consisting of six subapertures a 256 x

256 input array was clearly inadequate. The tip off was

that the value of the narrow zeros located between the sharp

cosine fringes varied widely, and in the test cases which

were run were as large as 1/25 of the peak irradiance of the

central fringe. When the position of the sparse output

array happened to coincide with a precise zero, the fraction

of that zero to the peak irradiance was then much smaller.

Similarly, the resolution of the generated output array was

such that it was largely a matter of luck whether the

maximum irradiance of any particular cosine fringe was

accurately depicted. Further, even if luck allowed an

accurate depiction of the peak irradiance of one particular

fringe, that had no bearing on whether the next fringe's

peak irradiance was accurately calculated, which yielded the

possibility for a very inaccurate comparison between the

intensities of the fringes. Also, the sparse resolution made the cosine fringes appear much sharper than they really were.

Upon increasing the size of the input array of the exit pupil to 512 x 512 the improvement in the accuracy of the generated output array was substantial. To start, the narrow zeros in the test cases which were run never exceeded 1/125 of the peak irradiance, and usually the zeros were somewhat smaller. But more importantly, the cosine fringes themselves were depicted with better precision. In fact, the highest possible increase in the accuracy of the maximum irradiance of the cosine fringes, which was or was not fully realized depending on how much luck one had in the 256 x 256 case, averaged 25% for the test cases run. Hence, at least a 512 x 512 input array characterizing the exit pupil was necessary to provide enough output resolution for a six subaperture system.

A further increase to a 1024 x 1024 input array yielded an average highest possible increase in the accuracy of the maximum irradiance of the cosine fringes of 3.4% for the test cases run. Also the zeros between the fringes were never larger than 1/300 of the peak irradiance. But since the zeros for the 512 x 512 case were already only tiny fractions of the peak irradiance and thus quite satisfactory for three-dimensional plots, it was judged that the further modest increases in the accuracy of the cosine fringe

depictions were not worth the considerable increase in computer time needed to run the program with a 1024 x 1024 input array. Also, the apodiser had a smoothing influence on the output which made the extra fine resolution resulting from the 1024 x 1024 input array less necessary. Thus, the study was run with the input array of the exit pupil at 512 x 512. Incidentally, it was also determined that even a 1024 x 1024 input array was no longer adequate for multiaperture configurations of 27 subapertures or more.

In sum, there were three additional inputs to the program used in this thesis to those used in the single aperture program. They were the radius of the circle the particular subaperture was centered on, which allowed the user to control the distance of the subaperture from the optical axis of the system, the position of the subaperture in the array, which gave the user a way to control the angular position of the subaperture, and the number of elements in the array which incidentally could be used to help control the angular position of the subaperture. Finally, the shape of the pupil itself could be adjusted if one were willing to change the pupil function early in the main body of the program. The multiaperture program was run on a VAX 11/750 operating system. The outputs were expressed in terms of the modulus, phase, and irradiance of the point source.

3.3 Single Aperture Edge Program

The single aperture edge program of Mills was derived from his single aperture impulse response program. The program was written in Fortran-77, ran on a VAX 11/750, and employed a FFT routine from the VAX IMSL library. It evaluated Eq (2.42) of Chapter II. The inputs to the program included the one dimensional size of the array representing the exit pupil, the third order aberrations in terms of Zernike coefficients, and the radial width factor of the Gaussiaᴎ apodiser. The output of the program was expressed in terms of the irradiance of the image (Mills, 1984: 74,160).

3.4 Modifications to Single Aperture Edge Program

In Chapter II, Eq (2.42), which described the process of imaging on edge through a single aperture optical system was developed. For the multiaperture case, it had to be modified to reflect the multiaperture nature of the problem. Specifically, the change in the finite extent of the pupil function had to be incorporated into the imaging equation. The eventual result of that task was Eq (2.46), which completely describes the imaging of an edge through a multiaperture system. The chief modification to the single aperture program of Mills then was the incorporation of an algorithm which made the appropriate adjustments to the new pupil function. The algorithm was flexible enough to allow the circle the subapertures were centered upon to be

varied with an input parameter. For the purposes of this study, the effective aperture of the system was kept constant.

Two other minor modifications were made to the single aperture program. First, the first order aberrations, piston and tilt were added as input parameters. Second the resolution of the output array was doubled. This resulted in a small increase of 0.5% in the peak irradiance of the central peaks the program generated. It also yielded an exact mi..imum of zero halfway between the two peaks.

The name of the multiaperture edge imaging program was LED.FOR. It was also run on a VAX 11/750 system. The output was expressed in terms of the irradiance of the edge.

IV. Results

The goal of this investigation was to perform a
generalized imaging analysis of apodised, aberrated,
coherent, multiaperture optical systems. Accordingly, both
a point source and an edge were chosen as objects of
study. The configuration chosen for imaging was a
symmetric hexagonal array of circular subapertures. This
chapter is broken into two main sections. The first is a
discussion of the results obtained with the impulse
response. The second is a discussion of the results
obtained from the imaging of an edge.

4.1 Analysis of the Impulse Response

The parameters which were used to evaluate the changes
in the impulse response in this study were the Strehl ratio
and the central peak ratio.

The Strehl ratio is formed by the ratio of the peak
irradiance in the impulse response of an aberrated and/or
apodised optical system compared to the peak irradiance in
the impulse response of an unaberrated, unapodised optical
system. The central peak ratio is formed by the ratio of
the peak irradiance of the central peak of the impulse
response to the peak irradiance of the next highest peak or
set of peaks.

The introductory paragraph of Chapter I specifies two
principle issues which were resolved by this thesis. The

61

first was whether Gaussian apodisation used alone in unaberrated, coherent multiaperture imaging systems allows one to increase the dilution between subapertures without degrading the imaging performance. But since all real optical systems have aberrations, the answer to the first issue was only for a very special case. So the second issue was whether once aberrations are present, does Gaussian apodisation improve the imaging performance of such systems? Only third order aberrations were added to the impulse response studies.

Three separate approaches were useful in resolving these issues. In the first approach the dilution between the subapertures was increased for both the unapodised and apodised cases. Figure 4.1 is a three-dimensional representation of both cases. The scales of the vertical axes of each plot are in relative units of irradiance where a magnitude of 1.0 is equal to the peak irradiance obtained from the Airy distribution due to a single circular aperture. For the unapodised cases the peak irradiance of 36 was what was predicted by theory (see end of section 2.3.4). The peak irradiance of the central peak resulting from the apodised systems was 3.602 units. Thus, the Gaussian apodiser cut the peak irradiance by a factor of 10. Nevertheless, this was still more than the peak irradiance which would have resulted from any one of the single subapertures and thus is not necessarily a major

62
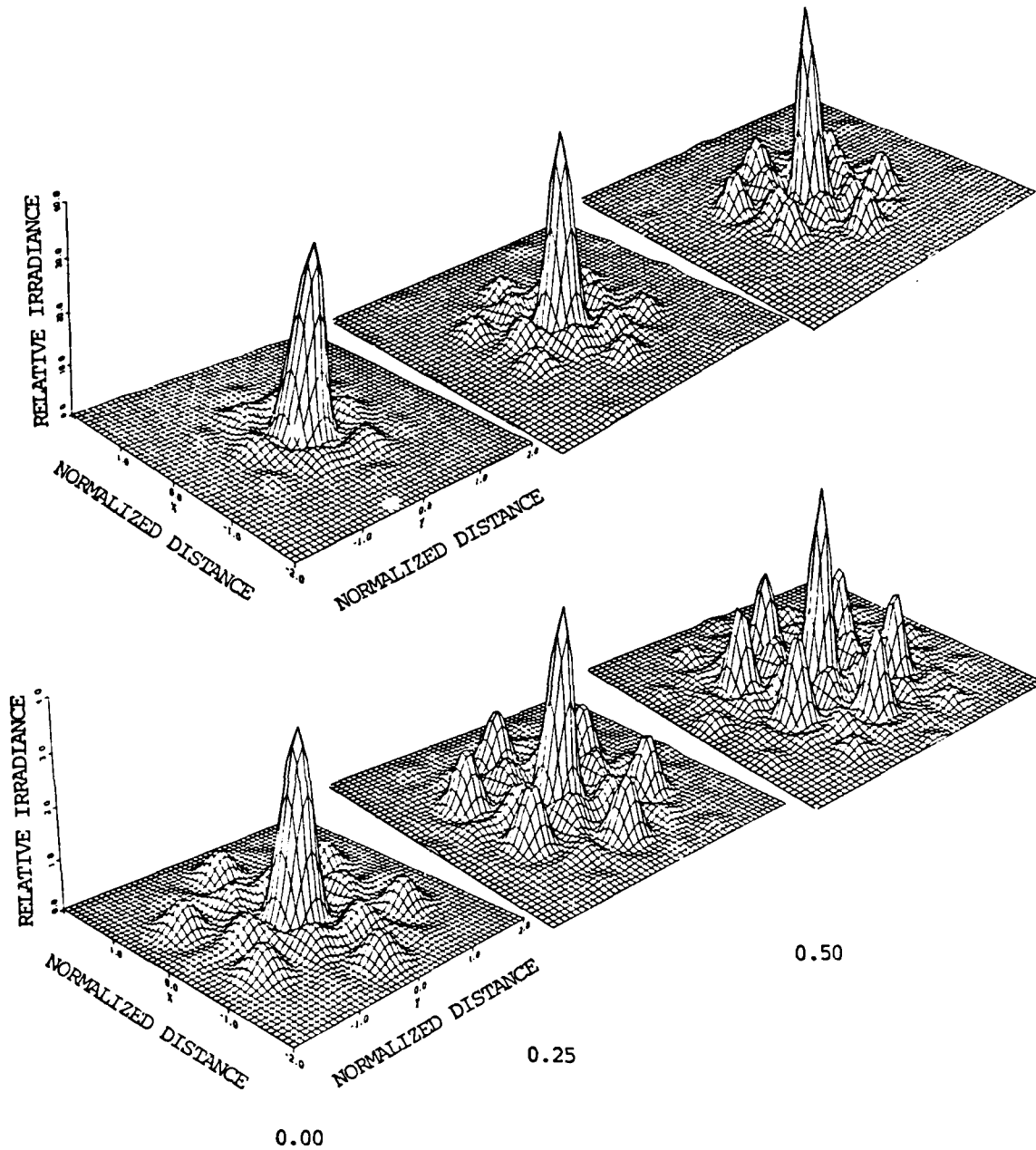
Fig. 4.1   Impulse responses in the absence of aberrations
for unapodised (top row) and apodised (bottom
row) cases. The degree of dilution is indicated
underneath each column. The scaling for each
row is represented by the plots in the left hand
column.

63

concern. The scales along the other axes are in relative units of distance and are equal in magnitude. Each point plotted represents the relative irradiance at a specific position located in a 48 x 48 input array. Located underneath each column is the degree of dilution scale. A dilution of 0.0 means that the subapertures were touching. A dilution of 0.25 means that the spacing between the subapertures was equal to one quarter of the diameter of the unit subapertures. A dilution of 0.50 corresponded to a spacing of one half the diameter of the unit subapertures. Fig. 4.2 aids in interpreting the degree of dilution scale.

Returning to Fig. 4.1, the growth of the sidelobes as the dilution was increased in the unapodised row was an expected result (see end of section 2.3.4). As the position of the peaks moved inward towards the central lobe, they intersected the single aperture diffraction envelope at ever higher positions, and thus grew taller. The apodised row also exhibited similar growth as the dilution was increased. But the most important result was the larger relative growth of the sidelobes which occurred when the subapertures were apodised as opposed to when they were unapodised.

This was not surprising either, once one considers what the effect of the apodiser will be using Fourier transform techniques. In one dimension the Gaussian function is defined to be (Gaskill, 1978:47)

$$\exp[-\pi((\xi - \xi_0/b))^2] = \text{Gaus}\,((\xi - \xi_0/b)) \qquad (4.1)$$
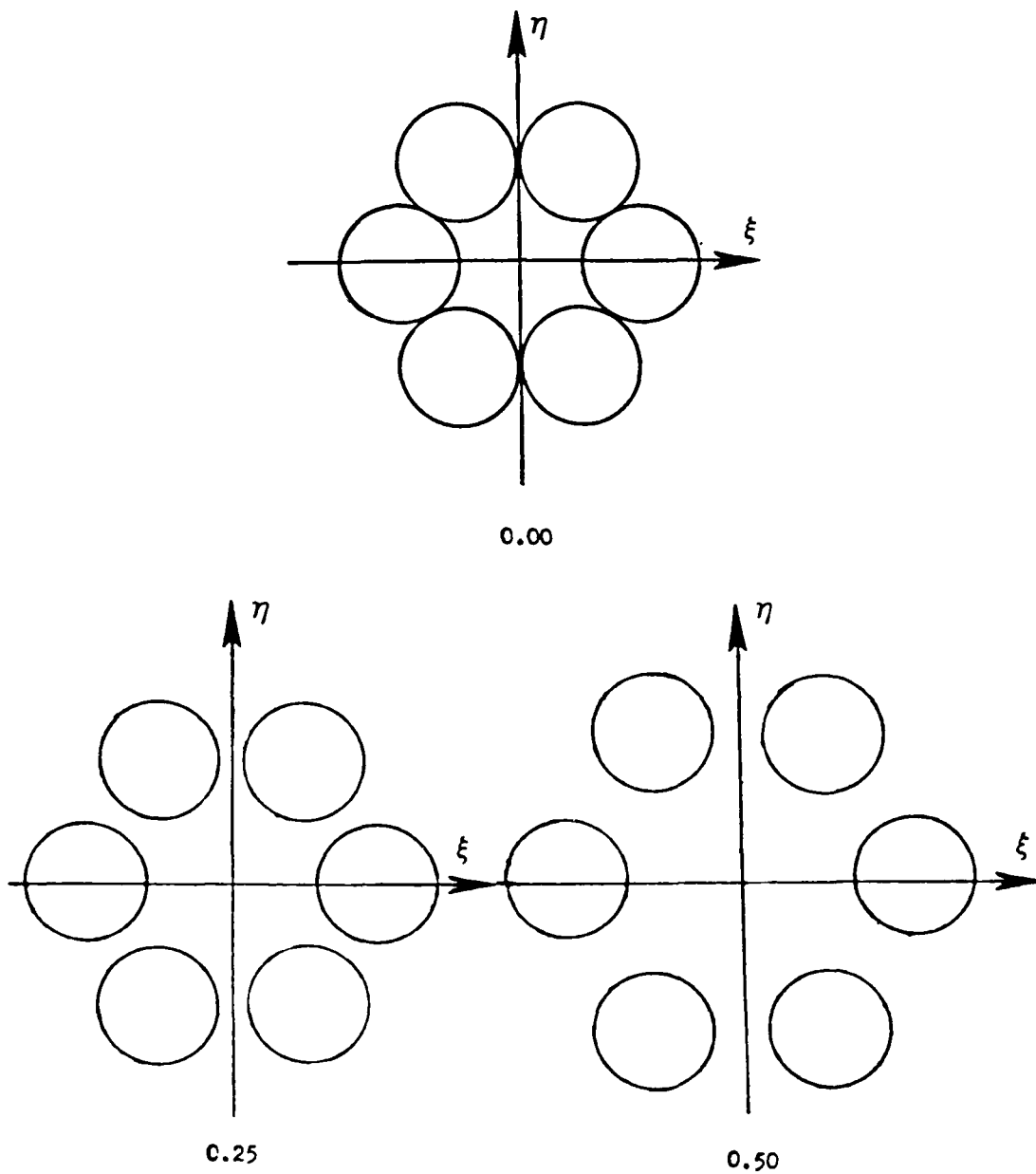
Figure 4.2   Depiction of subapertures at various degrees
of dilution.

where the Gaussian function has a height of unity and its area is equal to $|b|$. In this study each of the Gaussian apodisers were centered in their respective subapertures. Hence the apodiser could be expressed $Gaus(\xi/b)$. Upon taking the Fourier transform of $Gaus(\xi/b)$ one obtained (Gaskill, 1978:194,214)

$$F\{Gaus(\xi/b)\} = b \; Gaus(b\xi) \qquad (4.2)$$

When b was less than unity, (see fig. 2.5) as in the case of this thesis, the Fourier transform became shorter and wider. Hence the slope of the envelope of the Fourier transform was gentle and less than the slope of the diffraction envelope. Thus, the secondary lobes were limited at relatively higher values. Fig. 4.3 is a plot of the central peak ratio for both the unapodised and apodised cases as dilution was increased. The large drop in the ratio corresponded to a big loss of energy to the surrounding secondary maximas. The effect on imaging was a considerable reduction in contrast and a tendency towards the creation of periodic artifacts. The slashed line in the figure corresponds to the arbitrarily chosen approximate lower limit required to insure acceptable imaging.

Whether an image is of acceptable quality is a matter of judgement. Accordingly, no study to date has attempted
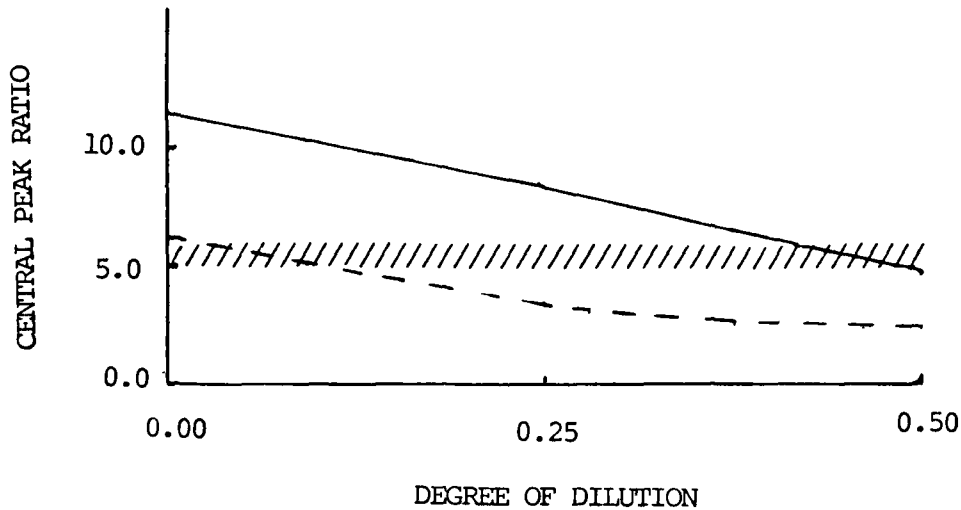
Figure 4.3 Plot of the central peak ratio vs. increasing dilution for unaberrated subapertures. The solid line (___) represents the unapodised case, while the dashedline (---) represents the apodised case. The wavy line (///) represents the approximate lower limit for acceptable imaging.

to establish rigorous guidelines linking dilution to image quality. Nevertheless, the two University of Arizona studies summarized earlier, and in particular the first one, have dealt somewhat with the subject. The second study, which was performed in 1983 by Meinel and others, has been the only one which has dealt with coherent imaging performance. That study arbitrarily placed the maximum allowable spacing to be between 0.4 (which corresponds to the spacing between the telescopes of the MMT) and 0.5 (Meinel and others, 1983:152). The first study, performed in 1971 by Shack and others, considered only incoherent imaging. It also established 0.5 as the maximum allowable

dilution although it noted that images formed from subapertures at that dilution would be of marginal quality (Shack and others, 1971:257-59). In this study the central peak ratio of the impulse response formed with a dilution of 0.4 was 6.67:1 while the central peak ratio of the impulse response formed with the subapertures at a dilution of 0.5 was 4.83:1. Hence, a central peak ratio in the range of 5:1 to 6:1 would be neccesary to insure acceptable imaging. Anything below that would result in images of questionable quality. Using that criteria, it can be seen from the figure that Gaussian apodisation actually cut the amount of spacing which can be allowed to obtain acceptable imaging from a dilution of around 0.5 to about 0.1. This decline in tolerable dilution was important in at least two respects. First, the effective aperture of the imaging system was cut by about 20%. But even more critically, current engineering constraints require a spacing of at least 0.2 when constructing a large Multiple Aperture Telescope (MAT) (Meinel and others, 1983:152,200; Sanger and others, 1972:161-170). Since a Gaussian apodised system would have to be built with a dilution below that limit, its construction would pose engineering problems which have not yet been resolved. Hence, the first principle issue which this thesis considered was resolved. The technique of apodisation alone, at least with a Gaussian apodiser, did not allow one to increase the

dilution between subapertures, relative to the criteria above.

Figure 4.4 is the result for a two subaperture system separated by a distance equal to their diameters. This positioning is analogous to the array in upper left hand corner of Fig. 4.2, except that only subapertures 1 and 4 were present. Again, the sidelobes grew upon apodisation. The central peak ratio fell to 1.42:1 in the apodised case from 1.84:1 in the unapodised case. As in the six subaperture systems, the peak irradiance of the central peak of the apodised system was cut by a factor of 10 when compared to the unapodised case.

Two approaches were used in resolving whether apodisation improved imaging performance once aberrations were present. In one approach the amount of a particular aberration which was present in the imaging system was increased while the dilution of the system was held constant. In the other, the dilution of the imaging system was increased while the amount of a particular aberration was held constant. Aberrations were always applied to all of the subapertures simultaneously. Figs. 4.5-4.8 depict the changes which the impulse response underwent as various amounts of the aberrations were introduced to each subaperture equally in the optical system while dilution was held constant at 0.0 (no spacing between the subapertures). Whether unapodised or apodised

69
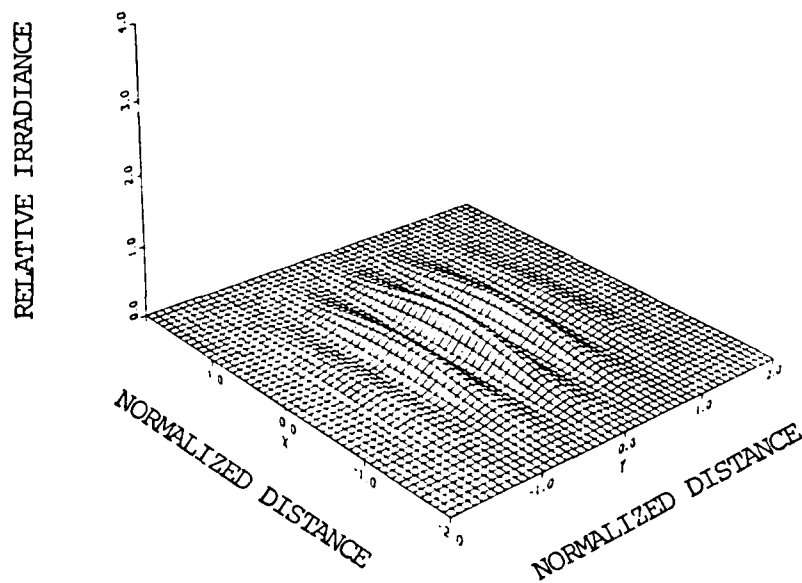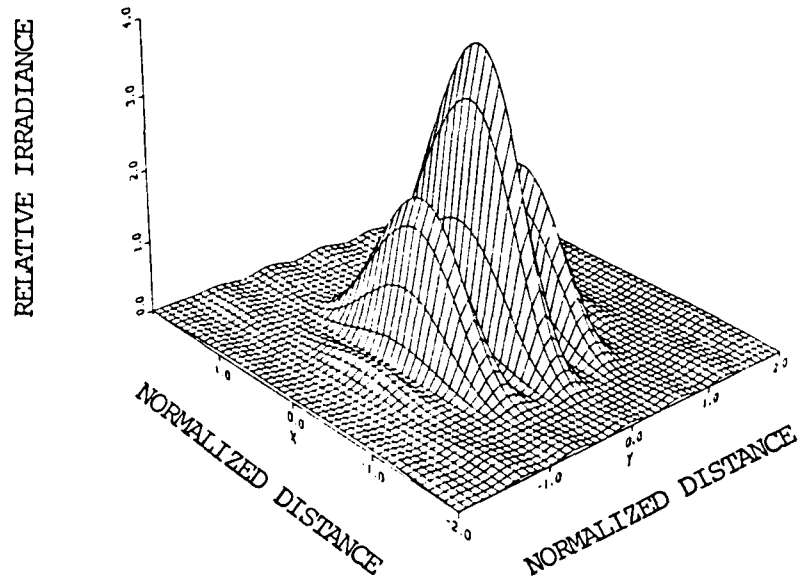
Figure 4.4   Unaberrated impulse response generated from
             two unapodised subapertures (top) and two
             apodised subapertures (bottom). The vertical
             axes are expressed in relative units of
             irradiance while the other axes denote
             relative units of distance.

70

the peak irradiance of the central lobe trended downward. The measure of this activity is called the Strehl ratio, which was defined earlier. Fig. 4.9 depicts the variations in the Strehl ratio which occur. Notice that the peak irradiance occurred when there were no aberrations and no apodiser was applied.

The Strehl ratios for both the apodised and unapodised cases matched precisely, as was expected, the results generated by Mills in his single aperture study (Mills, 1984:50-68). Added to the agreement referred to in section 2.5.1 with the University of Arizona team's results, these results lent further credibility to both the theoretical development of this thesis, and the computer program which was built and utilized based upon that development.

The Strehl ratios in the apodised cases were as expected much smaller. Nevertheless, even the smallest central peak irradiance maximums were greater than the peak irradiance reached by the Airy distribution generated by a single element of the subaperture array.

The central peak ratio plots of Fig. 4.10 were useful in determining how much of a particular aberration could be tolerated. In the unapodised imaging systems 45° astigmatism degraded first, followed by defocus and x coma. In the case of large amounts of 45° astigmatism and defocus the central peak ratio declined to under one.
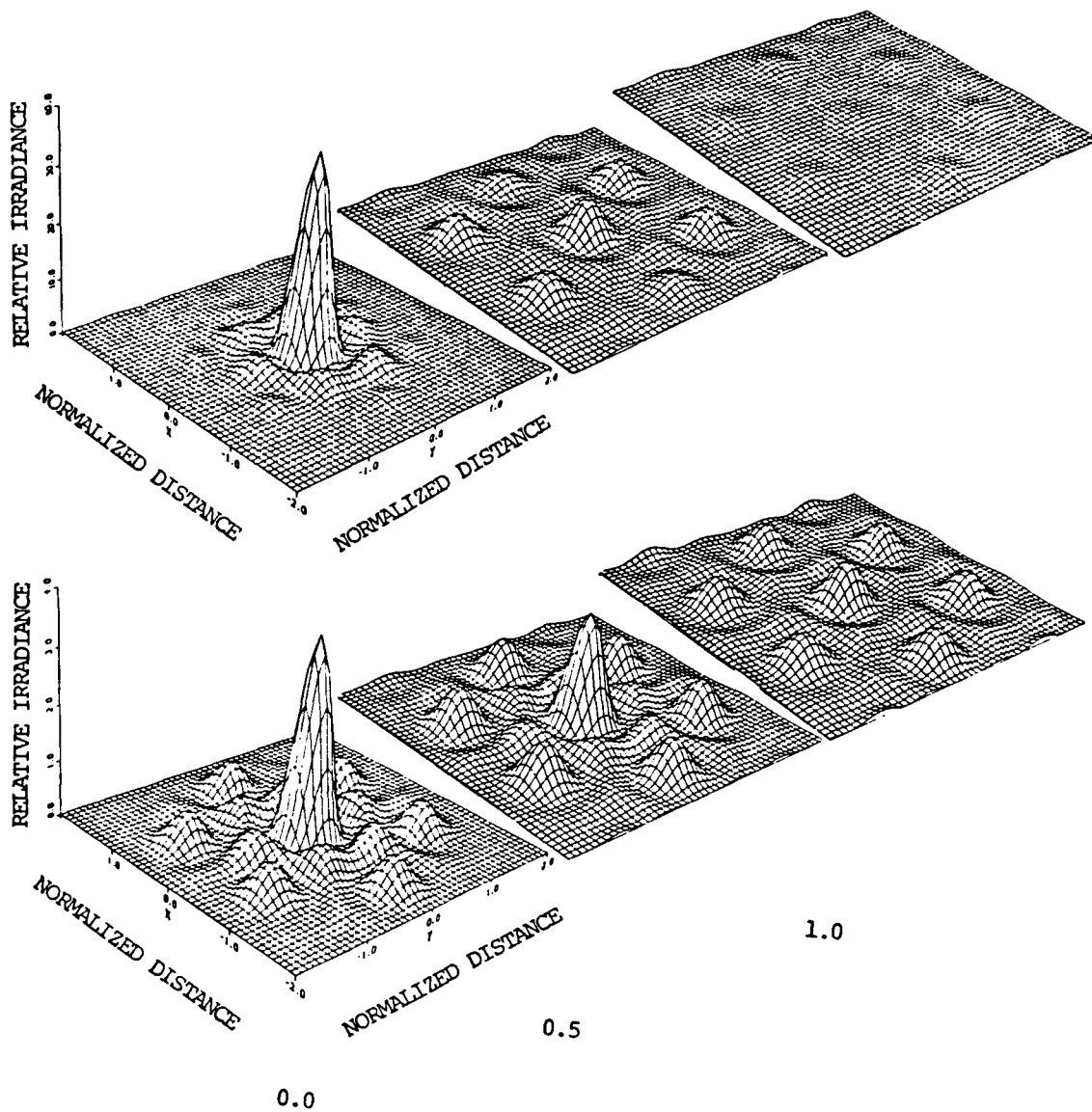
Figure 4.5   Impulse responses as 45° astigmatism is
             increased at constant dilution for unapodised
             (top row) and apodised (bottom row) cases.
             The amount of 45° astigmatism present is
             indicated underneath each column. The scaling
             for each row is represented by the plots in
             the left hand column and is the same as that
             used in Fig. 4.1.

72
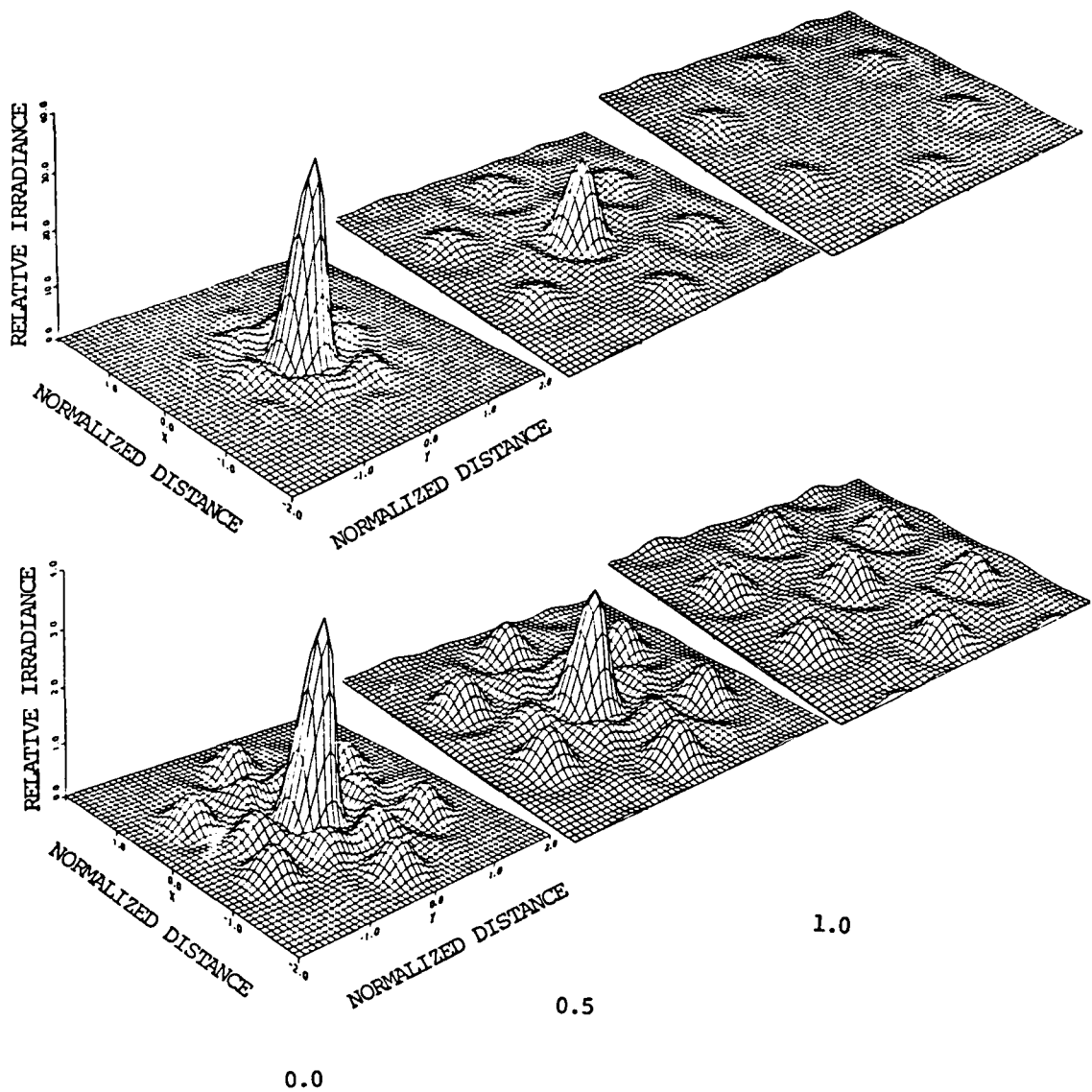
Figure 4.6   Impulse responses as defocus is increased at constant dilution for unapodised (to row) and apodised (bottom row) cases. The amount of defocus present is indicated underneath each column. The scaling for each row is represented by the plots in the left hand column and is the same as that used in Fig. 4.1.

73
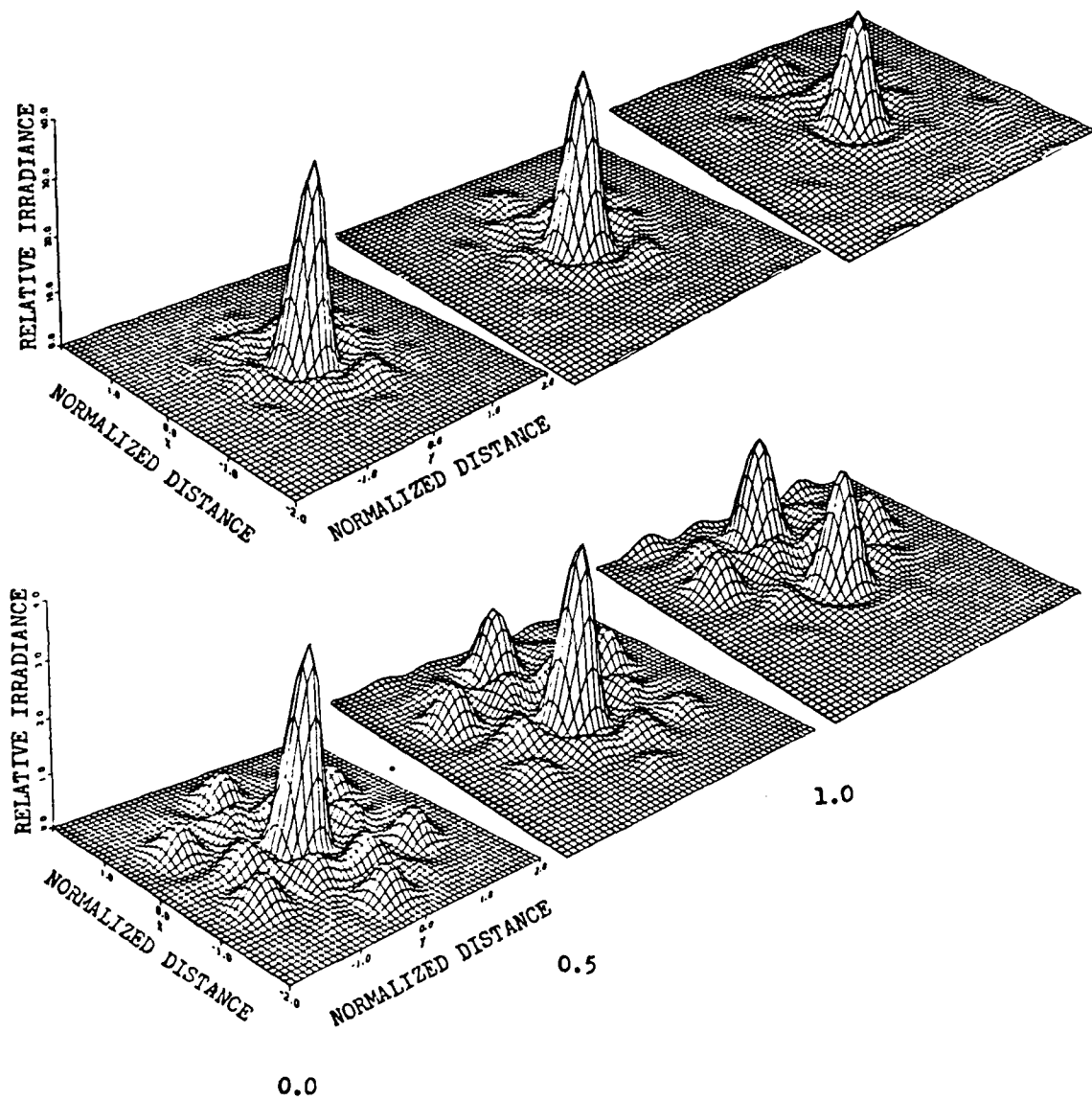
Figure 4.7   Impulse responses as x coma is increased at
            constant dilution for unapodised (top row) and
            apodised (bottom row) cases. The amount of x
            coma present is indicated underneath each
            column. The scaling for each row is
            represented by the plots in the left hand
            column and is the same as that used in Fig. 4.1.

74
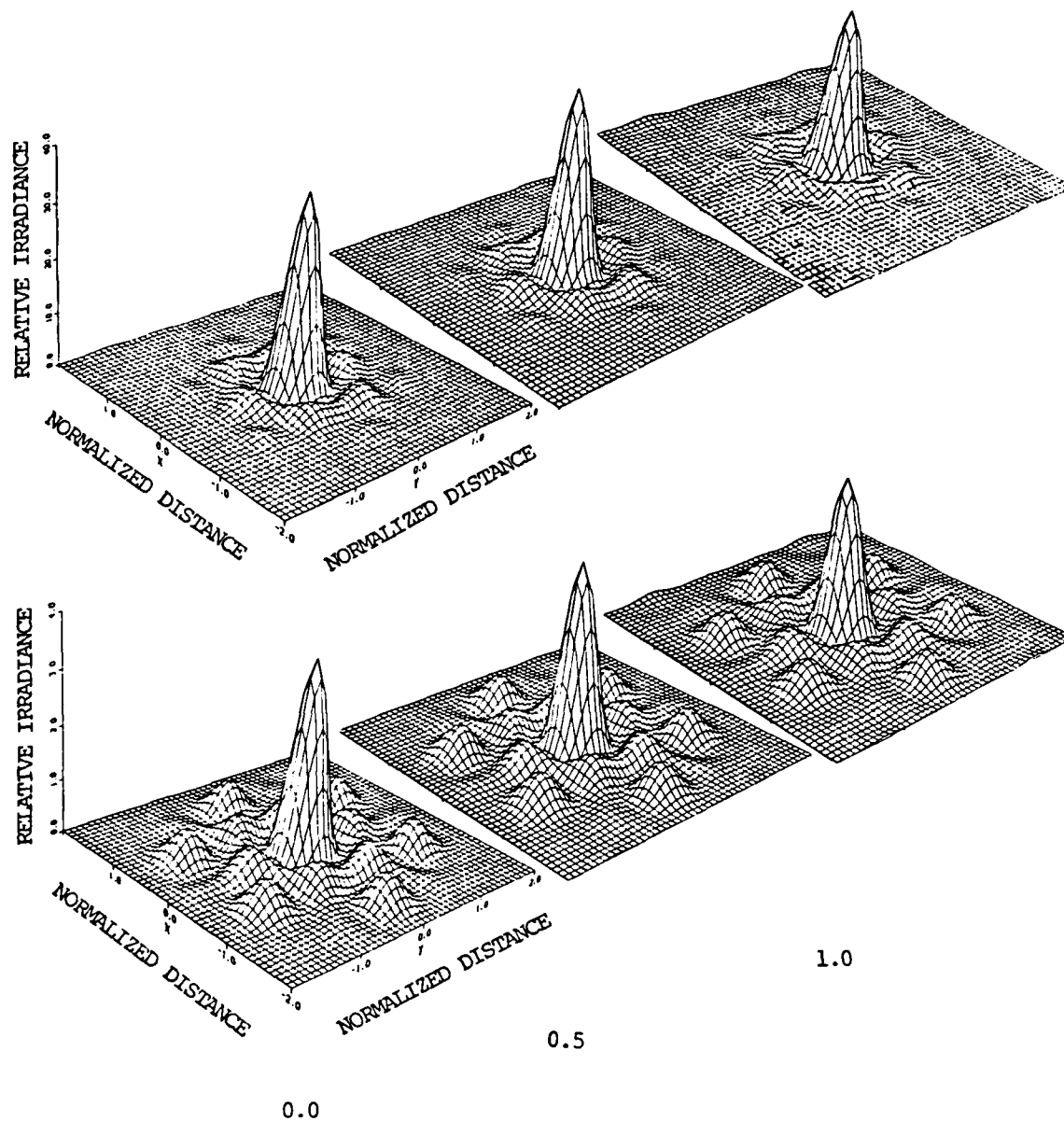
Figure 4.8   Impulse responses as spherical aberration is
             increased at constant dilution for unapodised
             (top row) and apodised (bottom row) cases.
             The amount of spherical aberration present is
             indicated underneath each column. The scaling
             for each row is represented by the plots in
             the left hand column and is the same as that
             used in Fig. 4.1.

75
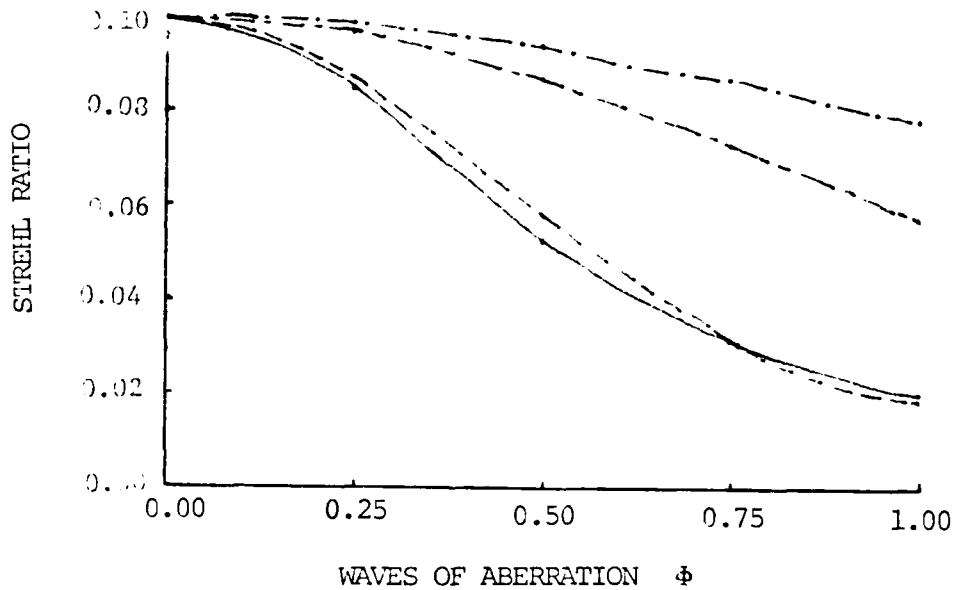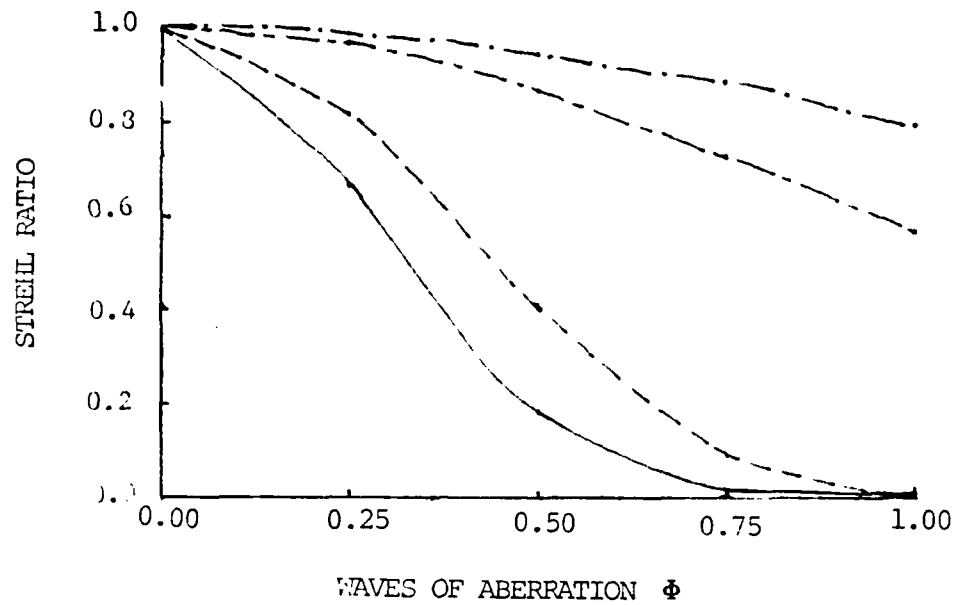
Figure 4.9 Strehl ratio plots as aberrations are increased for the unapodised cases (top) and the apodised cases (bottom). The peak values are normalized to unity for the unapodised, unaberrated systems. The solid line (___) represents 45 astigmatism, the dashed line (---) represents defocus, the broken line (_-_) represents x coma, and the line broken by dots (_._) represents spherical aberration. The symbol Φ along the horizontal axes represent waves of aberrations.

76
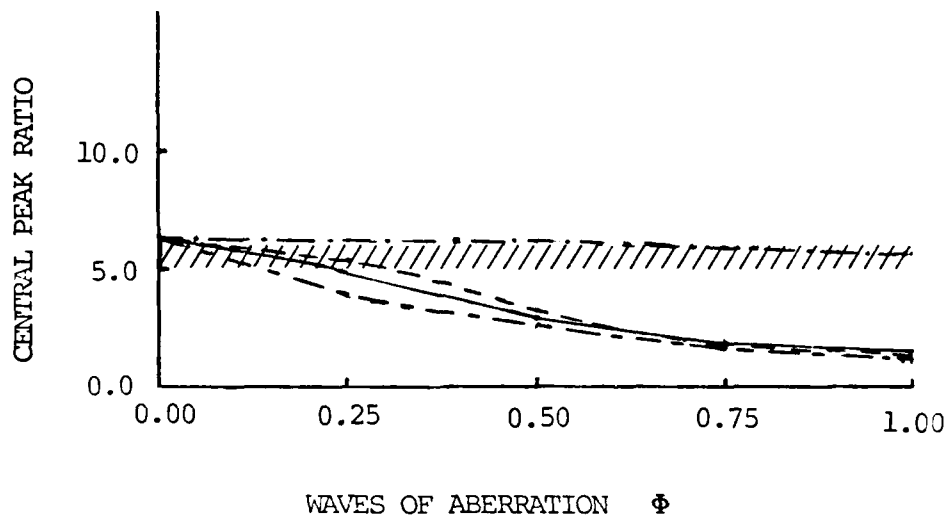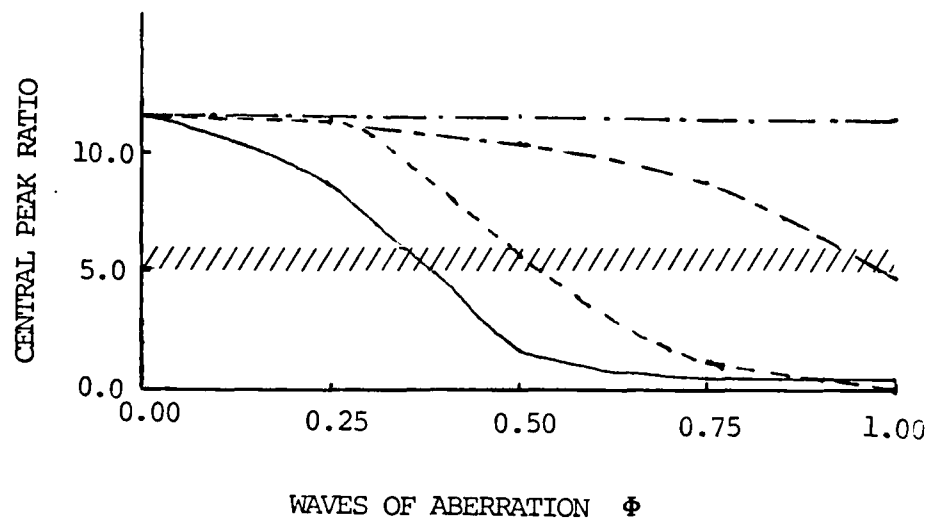
Figure 4.10   Plots of the central peak ratios vs. increasing amounts of aberrations as dilution is held constant for the unapodised cases (top) and apodised cases (bottom). The solid line (___) represents 45° astigmatism, the dashed line (---) represents defocus, the broken line (__-__) represents x coma, and the line broken by dots (__.__) represents spherical aberration, and the wavy line (///) represents the approximate lower limit required for acceptable imaging.

77

When this happened, the central peak was no longer the brightest. Spherical aberration did not pose difficulties even out to a full wave.

When the imaging systems were apodised their tolerance of aberrations dropped. X coma was most affected. The tolerance for it dropped from about 0.90λ to 0.10λ at the most. Spherical aberration was the least affected. A full wave of it could still be present, but there was some loss in image clarity. The apodiser had its most interesting effect on $45°$ astigmatism and defocus. In both cases the tolerance of the imaging system dropped, to 0.20λ from 0.35λ for $45°$ astigmatism, and to 0.25λ from 0.50 for defocus. But for high amounts of the aberrations, 0.35λ to 1.0λ for $45°$ astigmatism, and 0.55λ to 1.0λ for defocus, the presence of the apodiser actually raised the central peak ratio when compared to its unapodised counterpart with the same amount of aberration present. Unfortunately though, the improvement was not nearly enough to yield even marginally acceptable pictures. Hence, the answer to the second main issue of the thesis was clear. Even in the presence of aberrations, apodisers, at least Gaussian ones, did not improve the imaging performance of multiaperture optical imaging systems.

The final approach taken in studying the impulse response verified this result. In this approach the dilution of the imaging system was increased while the

amount of a particular aberration was held constant.
Figs. 4.11-4.14 portray the impulse response when 0.5λ of
each respective aberration was present for both the apodised
and unapodised cases. Since the amount of each aberration
was held constant in this approach the Strehl ratio did not
vary. Thus, the central peak ratio plots of Fig. 4.15 carry
all the useful information which this approach yields. It
can be seen from the unapodised plot that 0.5λ of $45°$
astigmatism even at a dilution of 0.0 was already too much.
A half wave of defocus could be tolerated to a dilution of
about 0.05, 0.5λ of X coma to 0.3, and 0.5λ spherical
aberration to 0.45. In all cases there was a rapid effect
on imaging as the dilution was increased. Looking at the
Gaussian apodised plots it is apparent that the application
of the apodiser immediately drove the central peak ratio
below the level which is required for acceptable imaging for
all the aberrations except spherical. But even it quickly
fell below the threshold as the dilution was increased.
Thus, once again it was clear that the application of an
apodiser does not improve the imaging performance of
multiaperture optical imaging systems.

4.2 Analysis of Edge Imaging

The investigation of edge imaging reaffirmed the
conclusions drawn from the point source imaging study. The
application of a Gaussian apodiser to an aberration free
system did not allow an increase in dilution but rather

79
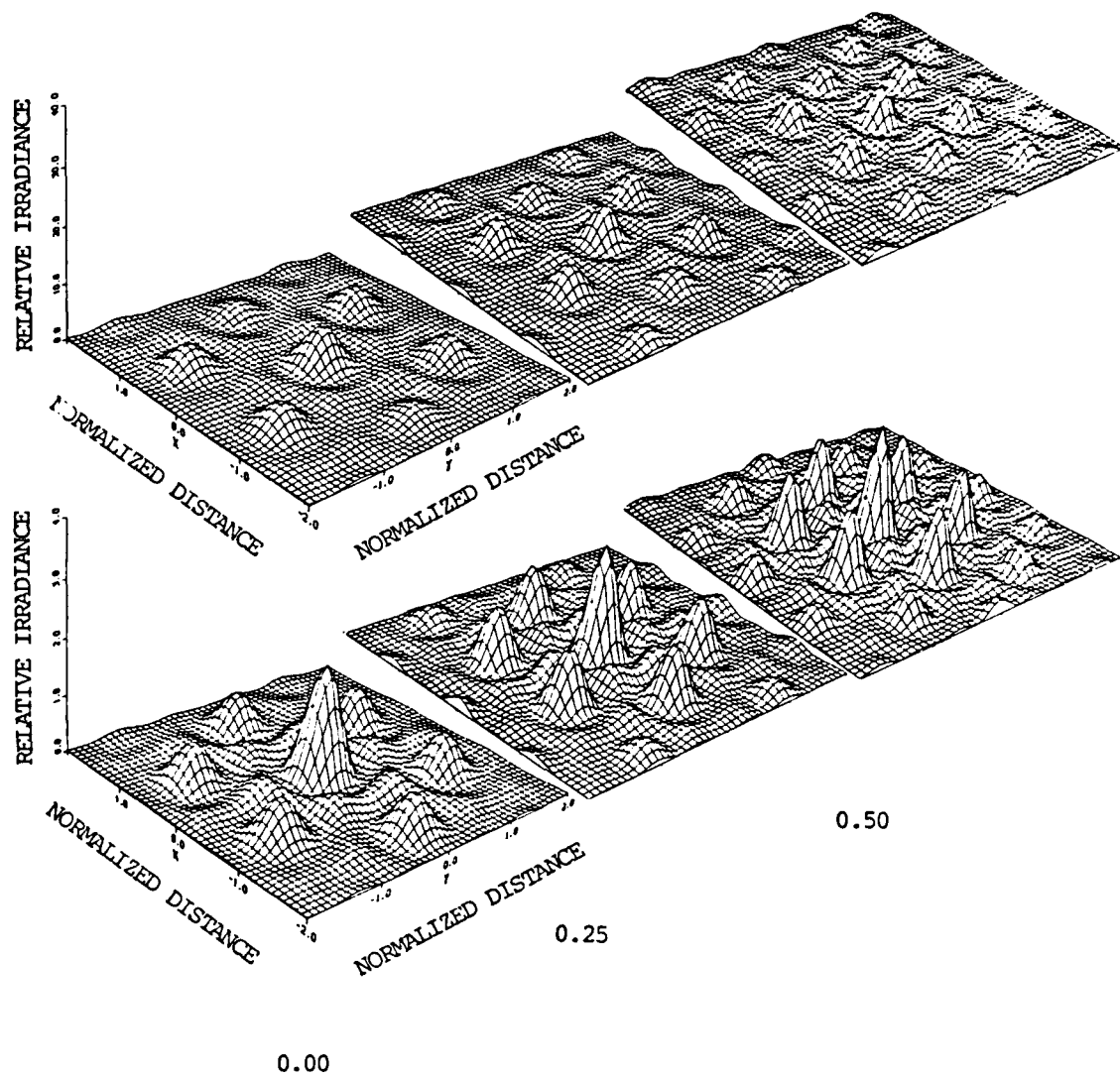
Figure 4.11   Impulse Responses in the presence of 0.5λ of
              45° astigmatism as dilution increases. The
              unapodised plots are along the top row and
              the apodised plots along the bottom row. The
              degree of dilution is indicated underneath
              each column. The scaling for each row is
              represented by the plots in the left hand
              column and is the same as that used in Fig. 4.1.
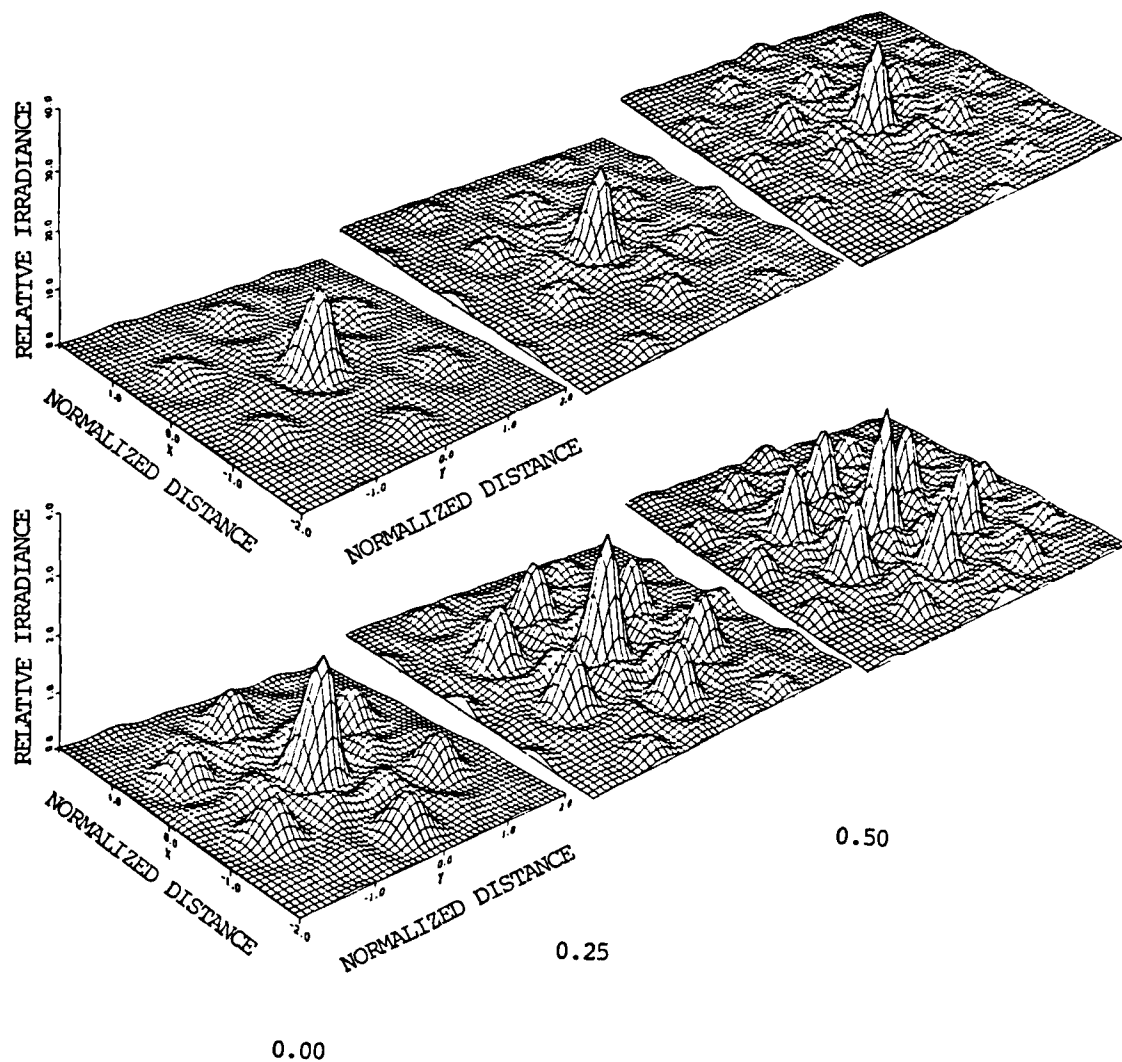
Figure 4.12   Impulse Responses in the presence of 0.5λ of
              defocus as dilution increases. The
              unapodised plots are along the top row and
              the apodised plots along the bottom row. The
              degree of dilution is indicated underneath
              each column. The scaling for each row is
              represented by the plots in the left hand
              column and is the same as that used in
              Fig. 4.1.
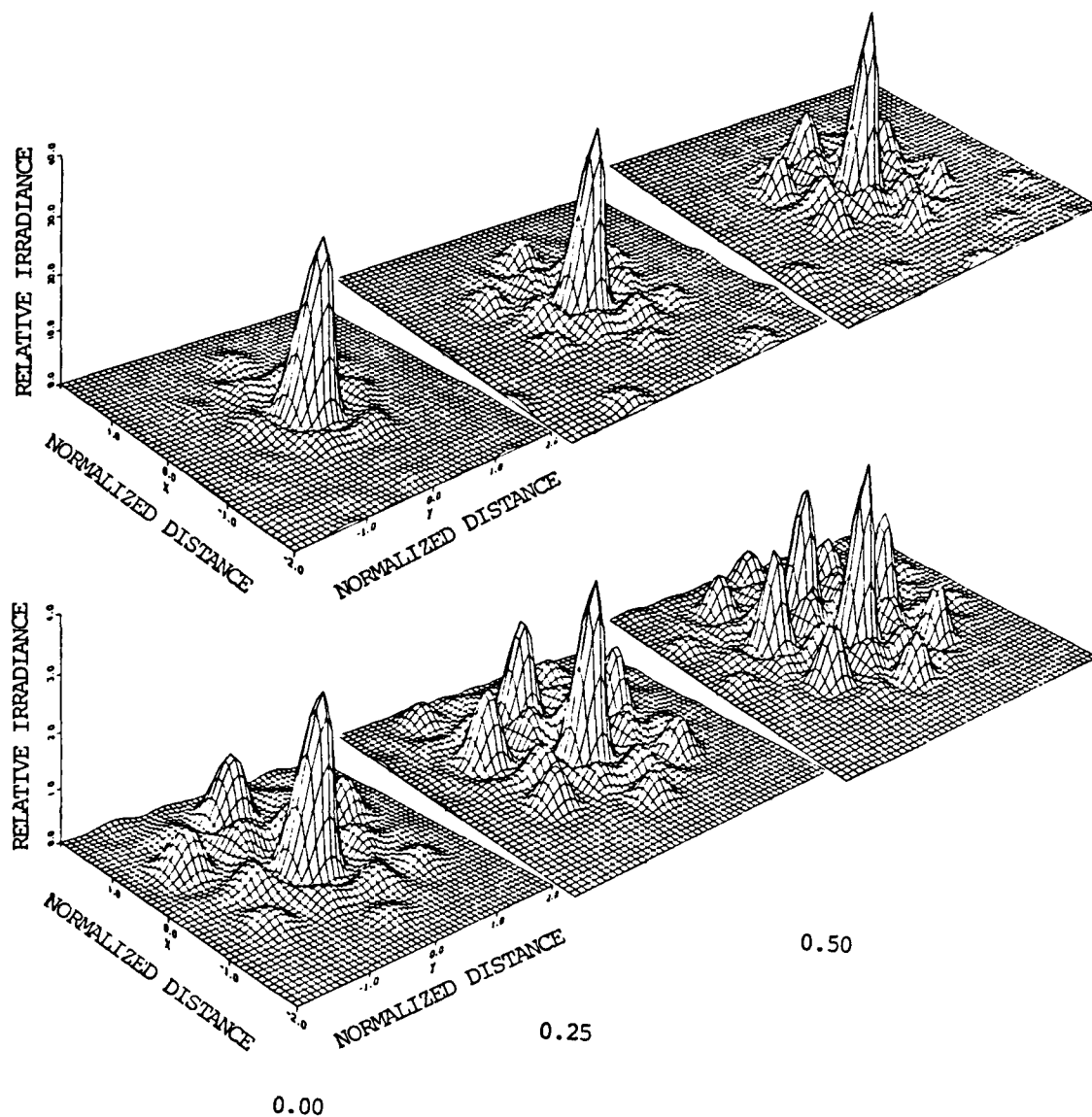
Figure 4.13   Impulse Responses in the presence of 0.5λ of
                x coma as dilution increases. The
                unapodised plots are along the top row and
                the apodised plots along the bottom row. The
                degree of dilution is indicated underneath
                each column. The scaling for each row is
                represented by the plots in the left hand
                column and is the same as that used in Fig. 4.1.
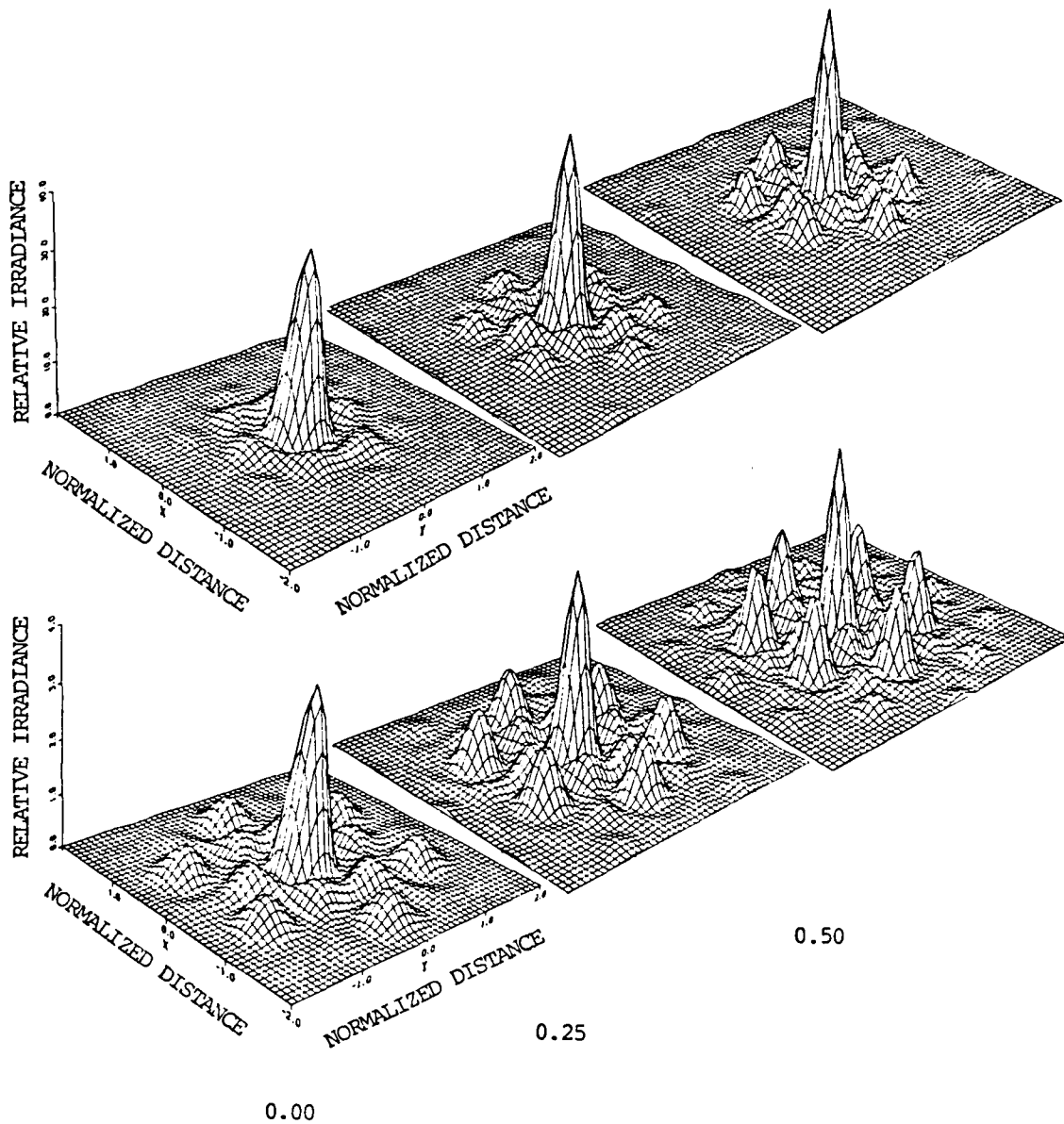
Figure 4.14   Impulse Responses in the presence of 0.5λ of
                spherical aberration as dilution increases. The
                unapodised plots are along the top row and the
                apodised plots along the bottom row. The degree
                of dilution is indicated underneath each column.
                The scaling for each row is represented by the
                plots in the left hand column and is the same as
                that used in Fig. 4.1.
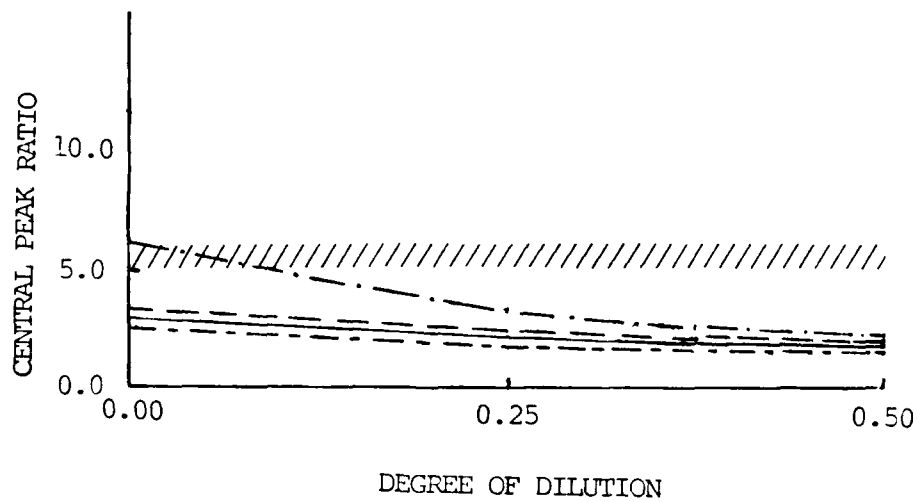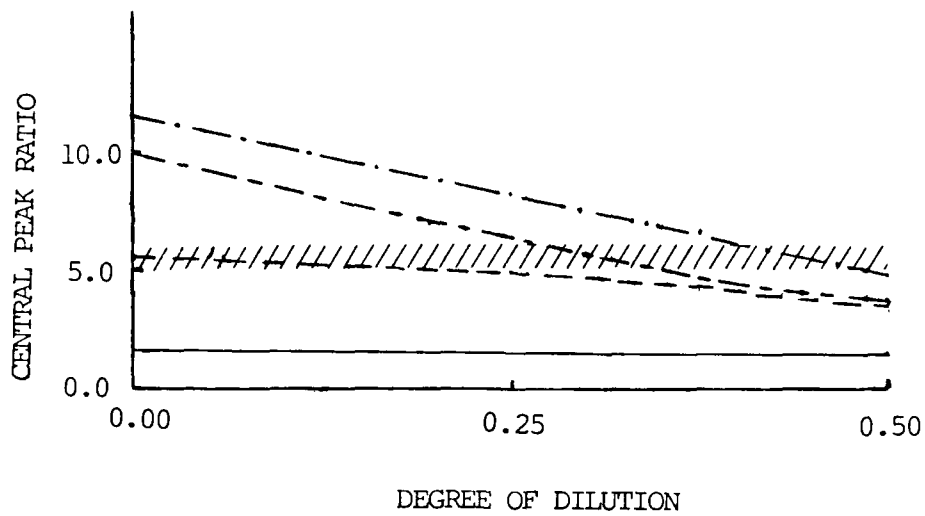
Figure 4.15 Plots for central peak ratio vs. dilution when
            aberrations are held constant. The top plot is
            for the unapodised cases and the bottom plot is
            for the apodised cases. The solid line (___)
            represents 45 astigmatism, the dashed(---)
            represents defocus, the broken line (__-__)
            represents x coma, the line broken by dots (__.__)
            represents spherical aberration, and the wavy line
            (///) represents the approximate lower limit
            required for acceptable imaging.

84
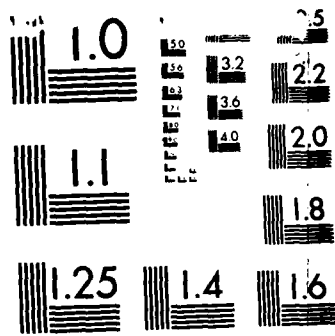
MICROCOPY RESOLUTION TEST CHART

NATIONAL BUREAU OF STANDARDS 1963-A

required a decrease in dilution. Further, once aberrations were present the application of the Gaussian apodiser damaged rather than improved imaging performance. However, three other conclusions became evident from the investigation of edge imaging.

The first one was outlined in the theoretical development of edge imaging through a multiaperture system which was completed in section 2.4.2. In that section it was shown that an annular imaging system was better than a multiaperture system when imaging an edge. The results of this study can be applied without loss of generality to that of an annular system. The second additional conclusion, which will presently be discussed in more detail, was that the decrease in irradiance which occurred when imaging an edge, and which was exacerbated by the addition of a Gaussian apodiser, was severe, and that has serious implications for imaging performance. The last conclusion which was evident from edge imaging was that the introduction of aberrations, especially to only one of the subapertures, caused drastic edge shifting. The application of the Gaussian apodiser neither alleviated nor exacerbated ւ..at problem.

In section 2.4.2 the imaging of an edge through a multiaperture system was seen to be a one-dimensional problem. Hence only two opposite subapertures contribute to imaging. The image of an edge then through such a system

was determined by this thesis to be a series of parallel bars of light. The actual position of the geometric edge was at the central minimum, paralleled on both sides by a pair of matching bars of equal irradiance. Then there was another minimum on each side followed by two more matching bars of lesser intensity. Another pair of minimums followed, then bars and so on. The edge was located halfway in between the two brightest bars. Those results agreed with those found experimentally by an Air Force Institute of Technology team. Fig. 4.16b contains a photograph of the image of an edge obtained from a hexagonal multiaperture exit pupil. For comparison, Fig. 4.16a contains a photograph of the image of an edge obtained through only one of the subapertures. All apertures and subapertures were unaberrated and unapodised. Since a multiaperture system does not produce produce a clear edge, a detection system would be necessary to locate the actual position of the geometric edge. The system would have to be able to identify the two brightest bars and then split the distance between them to determine the position of the edge.

The two parameters which were used by this study to evaluate the image quality of an edge can now be introduced. The first was edge shift. Edge shift is defined as the distance from the geometric edge position that a detection system would place the edge. The other parameter was second central bar ratio. The second central bar ratio
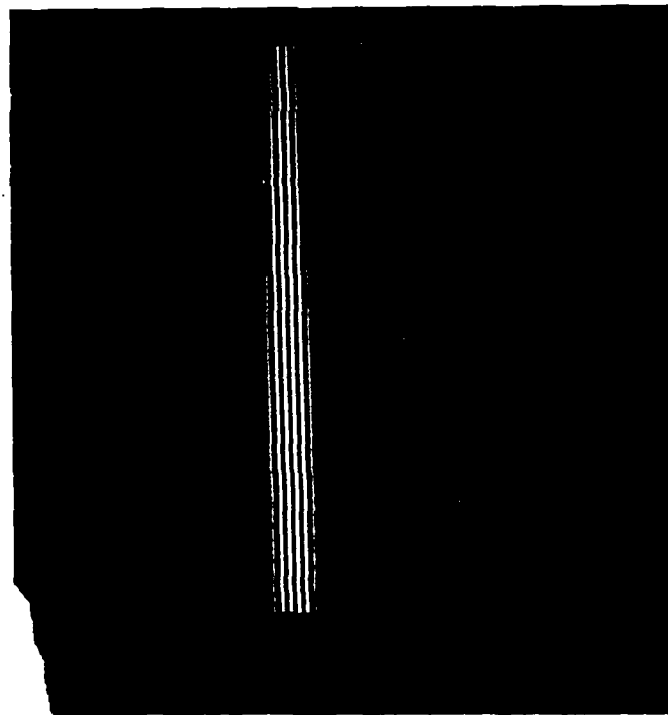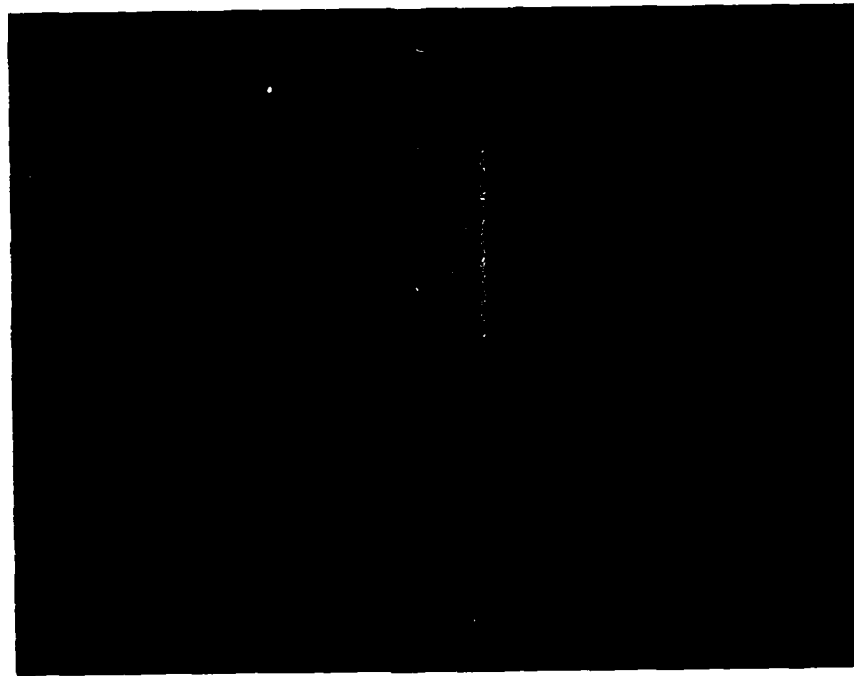
Fig. 4.16   Photographs of the image of an edge
obtained from a single circular exit pupil
(top) and a hexagonal set of circular exit
pupils (bottom) (Bersey and Neidig, 1985).

is defined as the ratio of the peak irradiance of the second brightest central bar to the peak irradiance of the brightest non-central bar. When certain aberrations were introduced and especially when aberrations were added to just one of the subapertures the two central bars no longer had the same irradiance. As the aberrations were increased further, the irradiances of other non-central bars approached and eventually surpassed the irradiance of the dimmer central peak. Since any detection system would have to use the two brightest bars to find the edge, a measure of the changing irradiances was necessary.

Three approaches were taken in evaluating the effect of aposidation on the image of an edge through a hexagonal symmetric multiaperture coherent optical imaging system. In the first approach the dilution between the circular subapertures was increased in the absence of aberrations.

Fig. 4.17 contains cross sections across the edge image as the dilution was increased. The irradiance scale along the vertical axes of the plots is in relative units with a value of 1.0 being the irradiance of the geometric edge. Hence, even the brightest bars were just one tenth the irradiance of the edge. The scale along the horizontal axis is in relative units with the position of the geometric edge always at 2050. When the dilution was 0.0 the two central peak were located at 2038 and 2062. The degree of dilution scale is as before. But it should be

noted that in these cases the same effective aperture was
maintained. Thus as the degree of dilution was increased the
subapertures were also getting smaller which meant less light
passed through. This contributed to a more rapid decline in
the peak irradiance of the central bright fringes than would
have occurred if the dilution had been increased but with the
subapertures kept at the same size. The trend however, if
the latter were the case would have remained the same. Two
other trends exhibited in the plots are growth of the side
lobe peaks and a gradual shift inward in all the peaks as the
dilution was increased. When no aberrations were present
there was no edge shift for either the apodised or unapodised
cases.

A comparison of the Gaussian apodised plot with the
unapodised plot reveals that the apodiser was responsible for
a much larger relative growth in the side lobes. That was
consistent with the Gaussian apodiser's effect on the impulse
response. The effect that the loss in the ratio would have
on the earlier proposed detector's ability to find the
brightest bars would depend on the amount of noise present.
But clearly the signal to noise ratio (SNR) of such a system
would have to be very high. Since the irradiance of the
brightest apodised bars was already only 2.5% when normalized
normalized against the irradiance of the geometric edge, this
is a major concern. If the proposed detector would have a
high SNR it might be assumed that if the second central

89
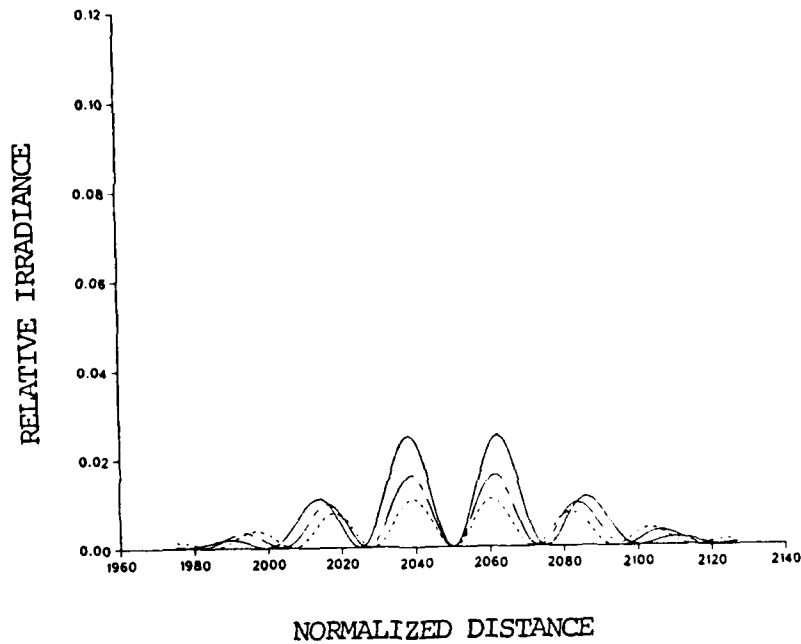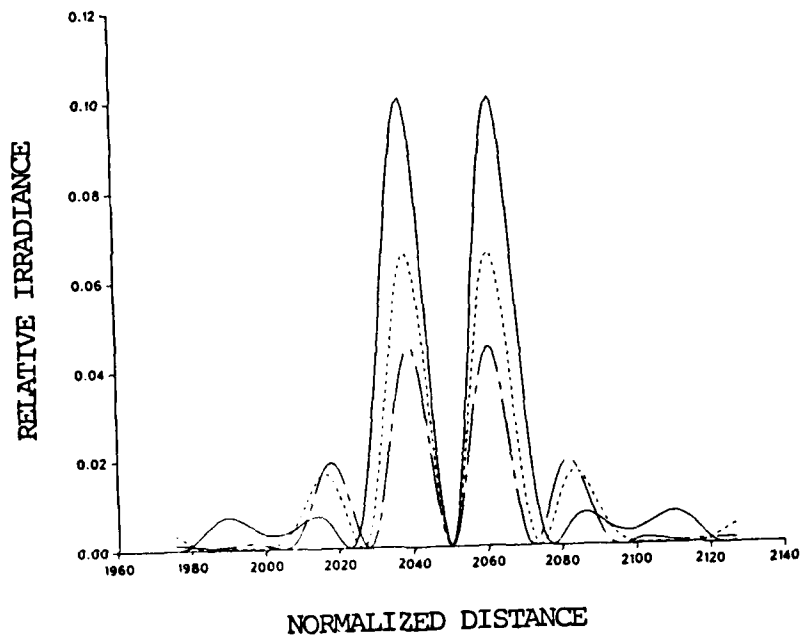
Fig. 4.17 Cross section of the image of an edge as
dilution is increased. The top plot is for the
unapodised cases and the bottom plot is for the
apodised cases. The solid line (___) represents
a dilution of 0.0, the broken line (__-__)
represents a dilution of 0.25 and the dashed
line (---) represents a dilution of 0.50.

90

bar ratio was at least 2:1 the correct "dim" central bar

would always be chosen for edge positioning. That criteria

is of course arbitrary. The reason 2:1 and not some other

ratio is chosen is that at that level the dilution and

various aberration tolerances match almost precisely the

respective tolerances arrived at in the anlaysis of point

source imaging. Fig. 4.18 is a plot of the second central

bar ratio for both the apodised and unapodised cases. The

slashed line represents the approximate limit for acceptable

imaging which corresponds to the arbitrary 2:1 ratio

described above. It can be seen from the plot that

apodisation clearly had a deleterious effect on the imaging

of an edge through an unaberrated multiaperture optical

imaging system.

The next approach taken in evaluating the effect of

apodisation on the imaging of an edge through multiaperture

systems was to apply increasing amounts of various

aberrations to both of the relevant subapertures while

keeping the dilution constant. Cross sections from each of

the cases are plotted in Figs. 4.19-4.20. The dilution of

the six subapertures in all the cases was 0.0. The cross

sections for defocus and $0°$ astigmatism were the same and

hence just defocus is plotted. This was expected as each

has a y squared dependence in one dimension (see Table

1.1). Defocus, $0°$ astigmatism, and spherical aberration

have a symmetric effect on the imaging as they all have a y

91
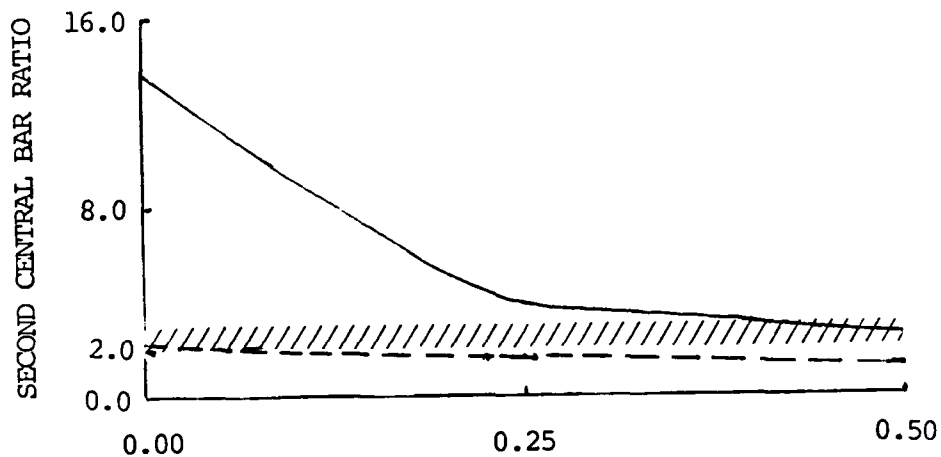
Fig. 4.18 Plot of the second central bar ratio vs.
dilution for the unapodised (___) and apodised
(---) cases as dilution is increased. The wavy
line (////) represents the approximate lower
limit for acceptable imaging.

to an even power dependence in one dimension. Hence there

was no edge shift when these aberrations were present in

equal amounts in both subapertures. y tilt and y coma have

a y dependence to an odd power and thus had a non-symmetric

effect. The amount of edge shifting which occurred for each

of these aberrations is depicted in Fig. 4.21.

y coma did not cause a severe shift in either case, however y tilt had a dramatic effect. When y tilt was first introduced the right central bar declined rapidly while the first bar to the left of the left central bar grew rapidly. Referring to Fig. 4.19 it can be seen that when 0.1λ was present the right central bar was still brighter. When 0.20λ was present the first bar to the left of the left central bar was brighter. At approximately 0.12λ they were equal. When the amount of y tilt exceeded 0.12λ the bar to the left of the original left central bar was brighter and the proposed detector would reposition the edge. Hence there was a jump in the edge shift. Until the jump though, the edge shift was not severe. The next jump occurred at 0.36λ and then another occurred at 0.60λ and so forth. The apodiser appeared to have little effect but in reality actually hurt somewhat as the second central bar ratio was cut and declined sooner. This would add ambiguity as to when the jump might occur.

The second central bar ratio for the cases represented in Figs. 4.19 and 4.20 are depicted in Fig. 4.22. Using the 2:1 imaging criteria ratio described earlier the imaging system was only able to tolerate in the unapodised case 0.08λ of y tilt, 0.40λ of defocus and $0'$ astigmatism, 0.60λ of y coma, and at least a full wave of spherical aberration. The levels for the third order aberrations were thus comparable to the levels which the unapodised impulse

93
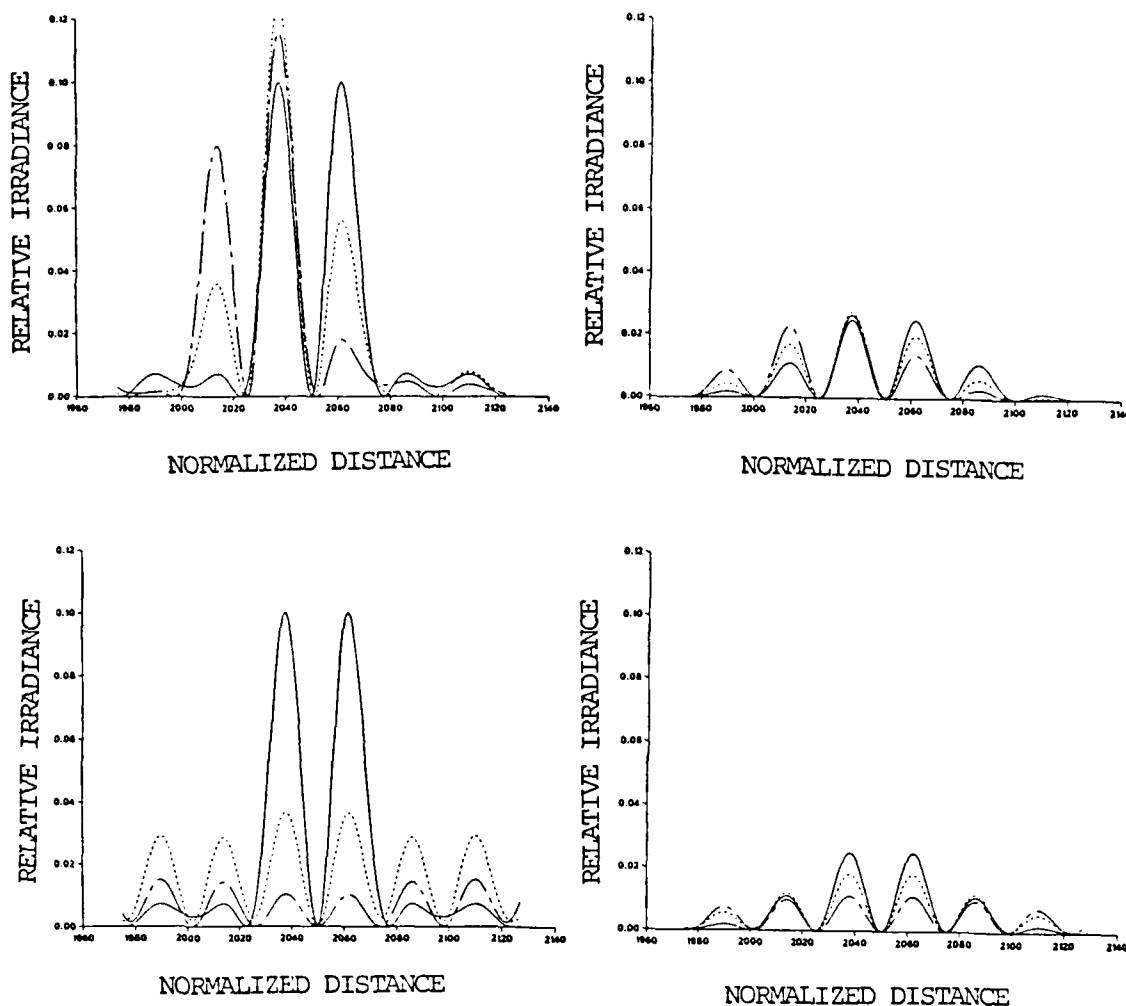
Fig. 4.19 Plots of cross-sections of the image of an edge as y tilt (top row) and defocus (bottom row) are increased across both subapertures. The left column contains the unapodised cases while the right column contains the apodised cases. The solid line (___) represents no aberration,the dashed line (---) represents 0.1λ of y tilt and 0.5λ of defocus, while the broken line (_ - _) represents 0.2 of y tilt and 1.0 of defocus. The scaling is the same as that of Fig. 4.17.

94
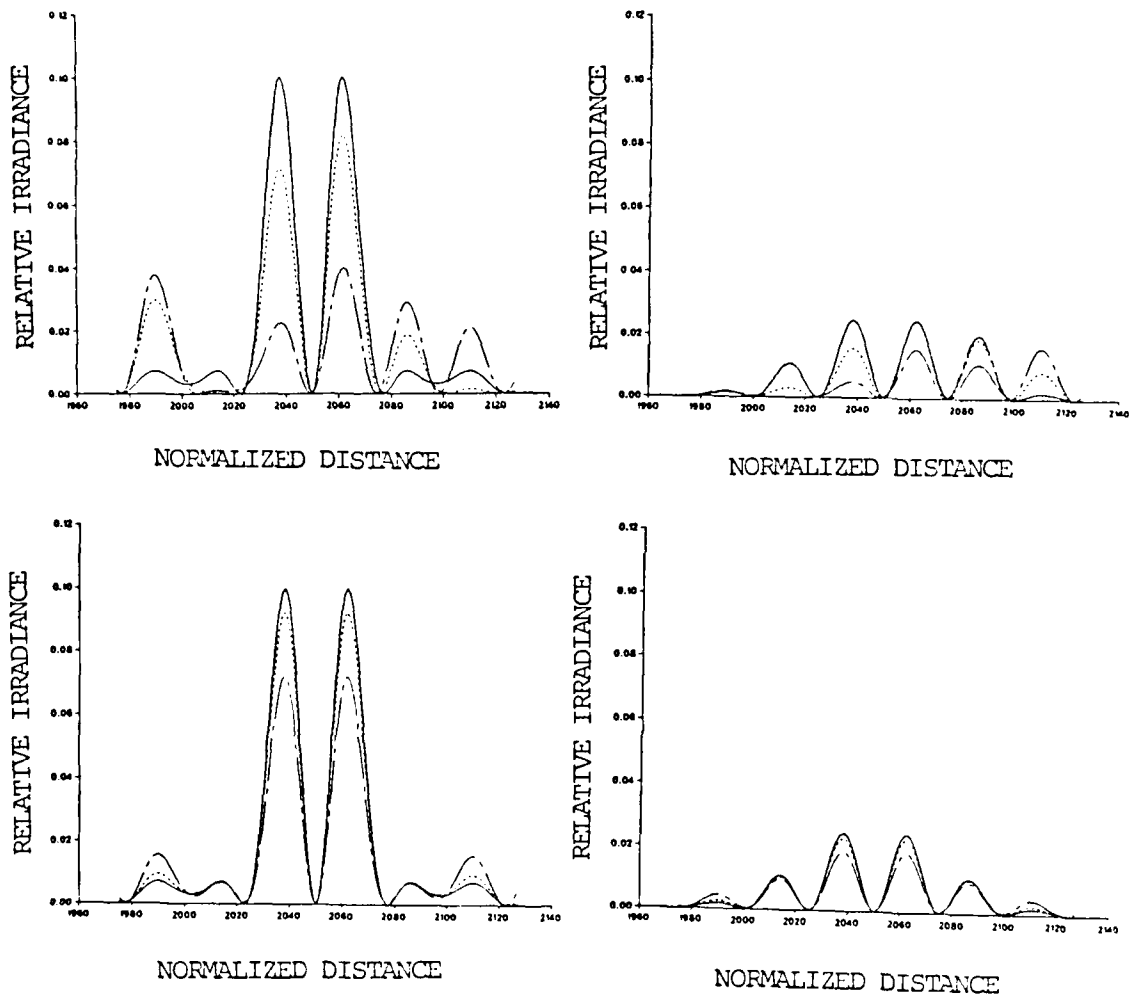
Fig. 4.20   Plots of cross-sections of the image of an edge
            as y coma (top row) and spherical aberration
            (bottom row) are increased across both
            subapertures. The left column contains the
            unapodised cases while the right column contains
            the apodised cases. The solid line (___)
            represents no aberration, the dashed line (---)
            represents 0.5λ of aberration, and the broken
            line (_-_) represents 1.0λ of aberration. The
            scaling is the same as that of Fig. 4.17.

95
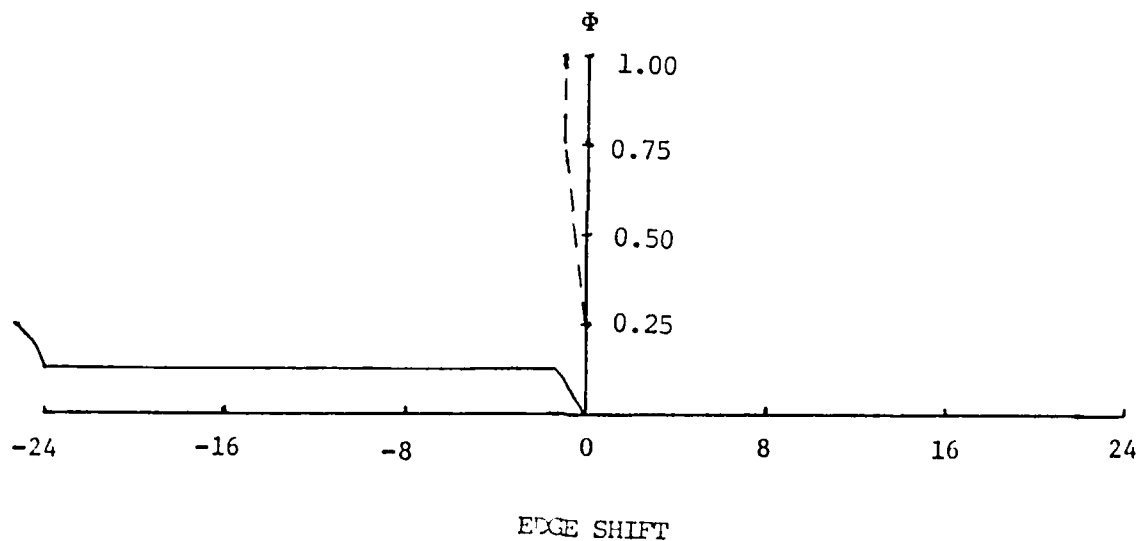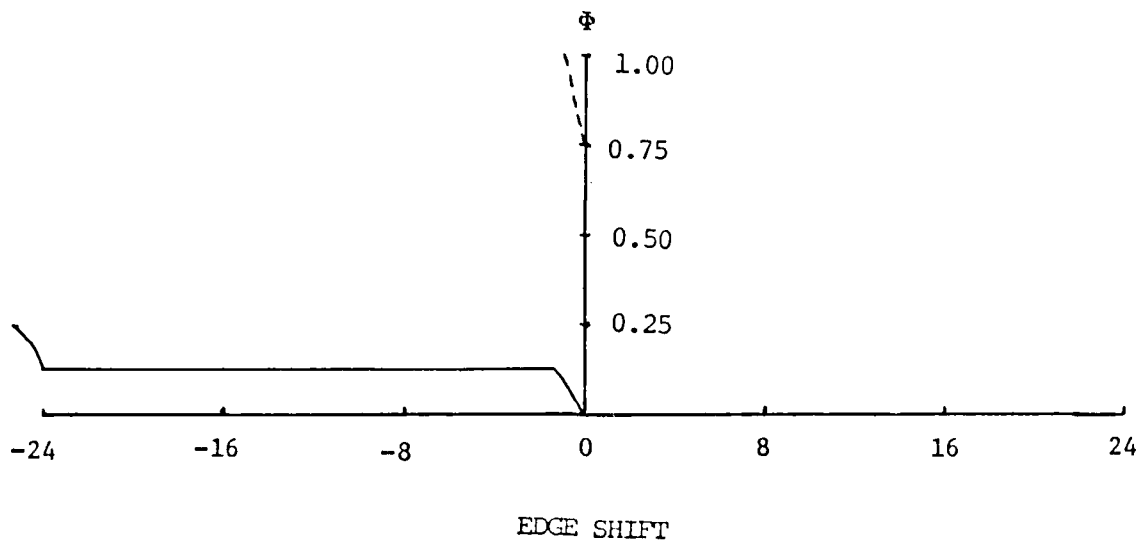
Fig. 4.21 Edge shift as a function of aberration when
simultaneously applied to both subapertures.
The top plot depicts the unapodised cases while
the bottom plot depicts the apodised cases. The
solid line (___) represents y tilt while the
dashed line (---) represents y coma. The
vertical scale is centered upon the geometric
edge position. The vertical axis represents the
waves of aberration present while the horizontal
axis represents relative units of distance.

96

response could tolerate. Upon apodisation,using the same criteria the tolerances fell to 0.02λ of y tilt, 0.25λ of defocus or $0°$ astigmatism, 0.12λ of y coma, and 0.90λ of spherical aberration. It's interesting to note that similar to the impulse response results, the Gaussian apodiser helped slightly for large amounts of defocus and 0 Astigmatism $(0.55\lambda -1.00\lambda)$, but not enough to salvage good imaging performance. Again, the Gaussian apodiser damaged edge imaging and did so to about the same degree as it effected the impulse response. Hence, the Gaussian apodiser did not improve edge imaging performance in multiaperture optical systems even in the presence of aberrations.

The last approach taken in evaluation the utility of apodising multiaperture optical systems involved investigating edge imaging performance when aberrations were applied to only one of the relevant subapertures. Dilution was held constant at 0.0. Figs. 4.23-4.25 portray the slices obtained when this was done.

When aberrations were present in only one of the subapertures the edge shift problem was much more severe than when the same aberrations were present in both of the subapertures. This behavior is plotted in Fig. 4.26. Note that as expected, piston caused no edge shift when a full wave of it was present. The application of the apodiser had only a marginal effect on the edge shifting. The fact that the edge shifting went both ways depending on the

97
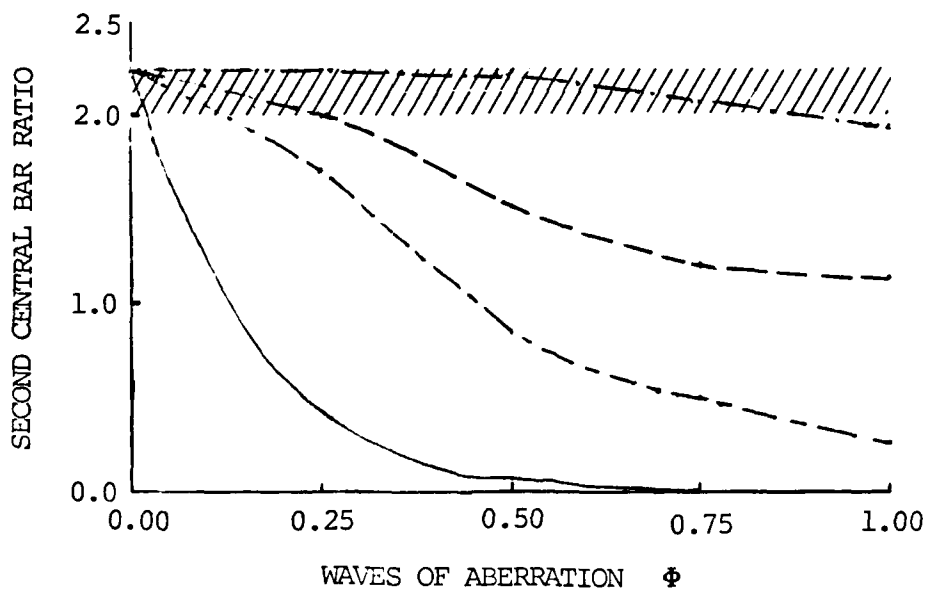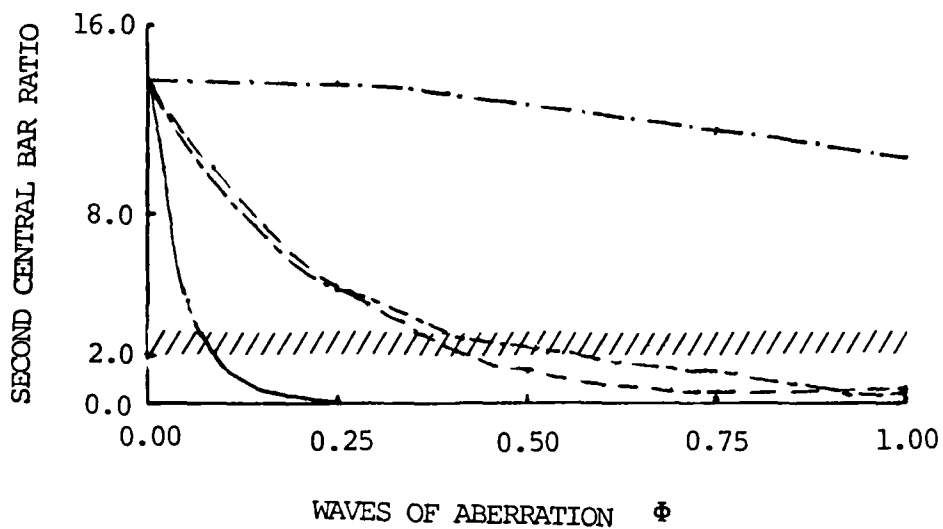
Fig. 4.22 Plots of the second central bar ratio vs.
increasing amounts of aberrations present in both
subapertures. The top plot depicts the unapodised
cases while the bottom depicts the apodised
cases. The solid line (___) represents y tilt,
the dashed line (---) represents defocus and 0
astigmatism, the broken line (_-_) represents y
coma, the line broken by dots (_._) represents
spherical aberration and the wavy line (////)
represents the arbitrary approximate lower limit
for acceptable imaging.

98

aberration present suggests that combinations of some of them may cancel each other out.

The magnitude of the edge shifting made it rival the decline of the second central bar ratio as the primary parameter controlling imaging performance. This was particularly the case with piston, 0 astigmatism, and defocus. Since the unaberrated central bars were located just 12 units away from the geometric edge, a shift of three units in the minimum which used to be at the geometric edge position would be sizable. Using that criteria, from the plots it can be observed that the tolerances were then 0.12λ for piston, 0.35λ for $0°$ astigmatism, and 0.55λ for defocus. But upon Gaussian apodisation edge shifting again became less significant than the second central bar ratio, the behavior of which can be observed in Fig. 4.27. Using the criteria developed earlier, the tolerance for piston dropped to 0.07λ while defocus and $0°$ astigmatism fell to 0.25λ. The tolerances for the other aberrations were 0.12λ of y coma, 1.0λ of spherical aberration and 0.04λ of y tilt. These levels were the same as before, except for a doubling of y tilt. Returning to Figs. 4.23-4.25 it can be seen that in the unapodised cases for all the aberrations except spherical, there was a noticeable and sometimes considerable irradiance reaching where the minimum corresponding to the geometric edge should have been. Apodisation here helped cut down the smearing. But it also cut the second central bar ratio so much that the net effect was deleterious.

99
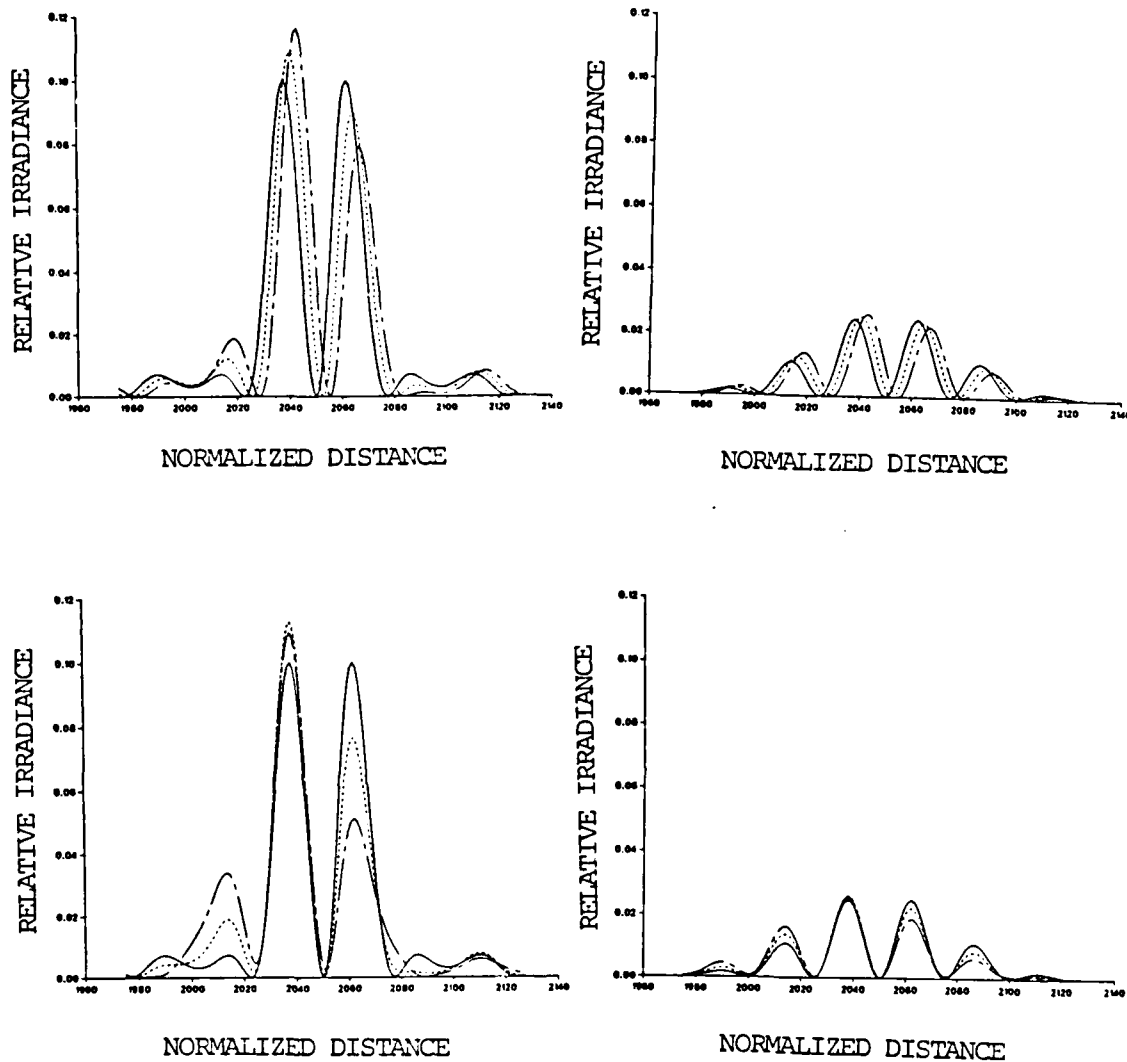
Fig. 4.23   Plots of cross-sections of the image of an edge
            as piston (top row) and y tilt (bottom row) are
            increased across only one of the subapertures.
            The left column contains the unapodised cases
            and the right column contains the apodised
            cases. The solid line (___)represents no
            aberration, the dashed line (---) represents
            0.1λ of aberration, and the broken line (__-__)
            represents 0.2λ of aberration. The scaling is
            the same as that of Fig. 4.17.

100
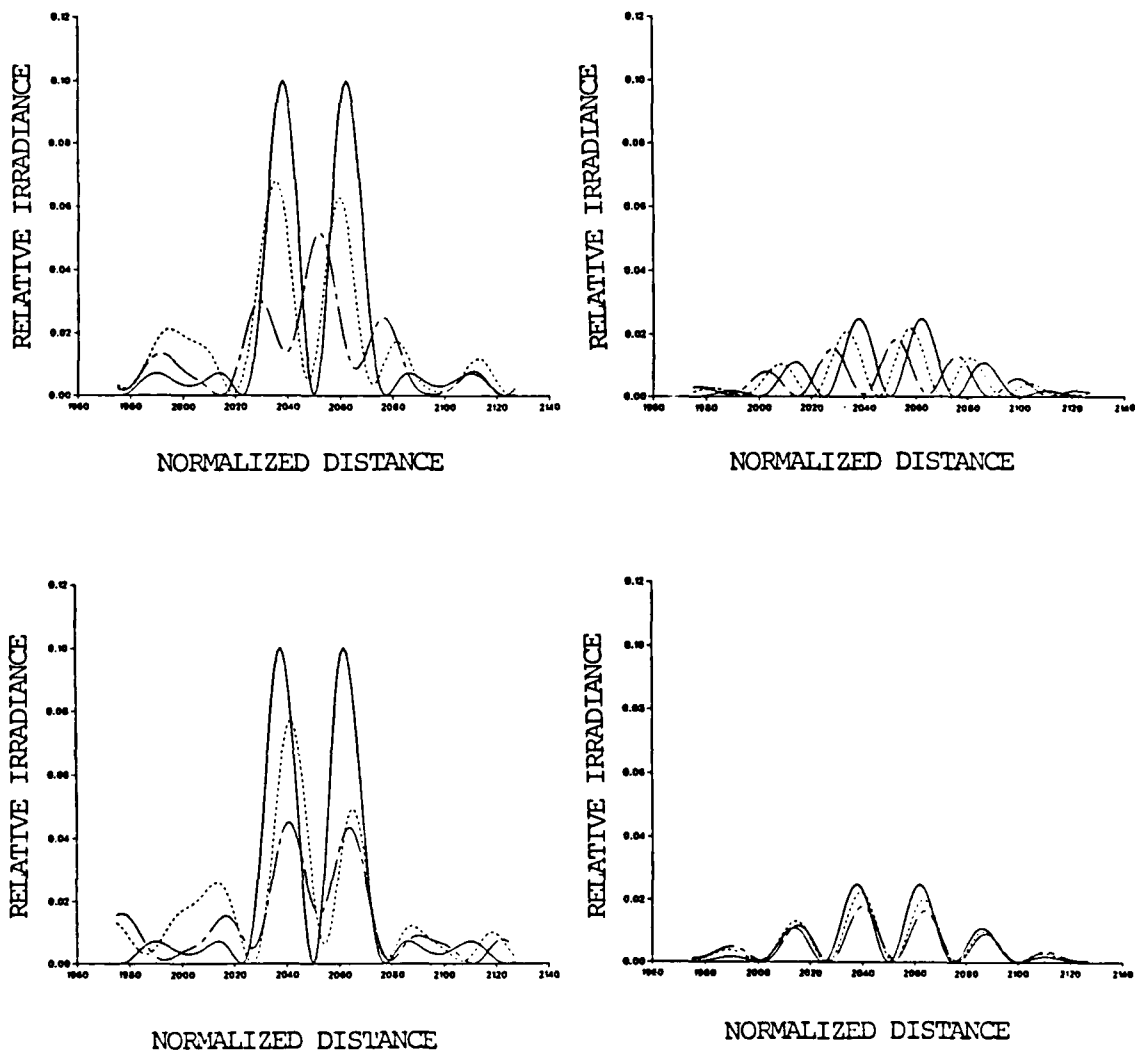
Fig. 4.24   Plots of cross-sections of the image of an edge
            as defocus (top row) and 0ᶜ astigmatism (bottom
            row) are increased across only one of the
            subapertures. The left column contains the
            unapodised cases and the right column contains
            the apodised cases. The solid line (___)
            represents no aberration, the dashed line (---)
            represents 0.5λ of aberration, and the broken
            line (_-_) represents 1.0λ of aberration. The
            scaling is the same as that of Fig. 4.17.

101
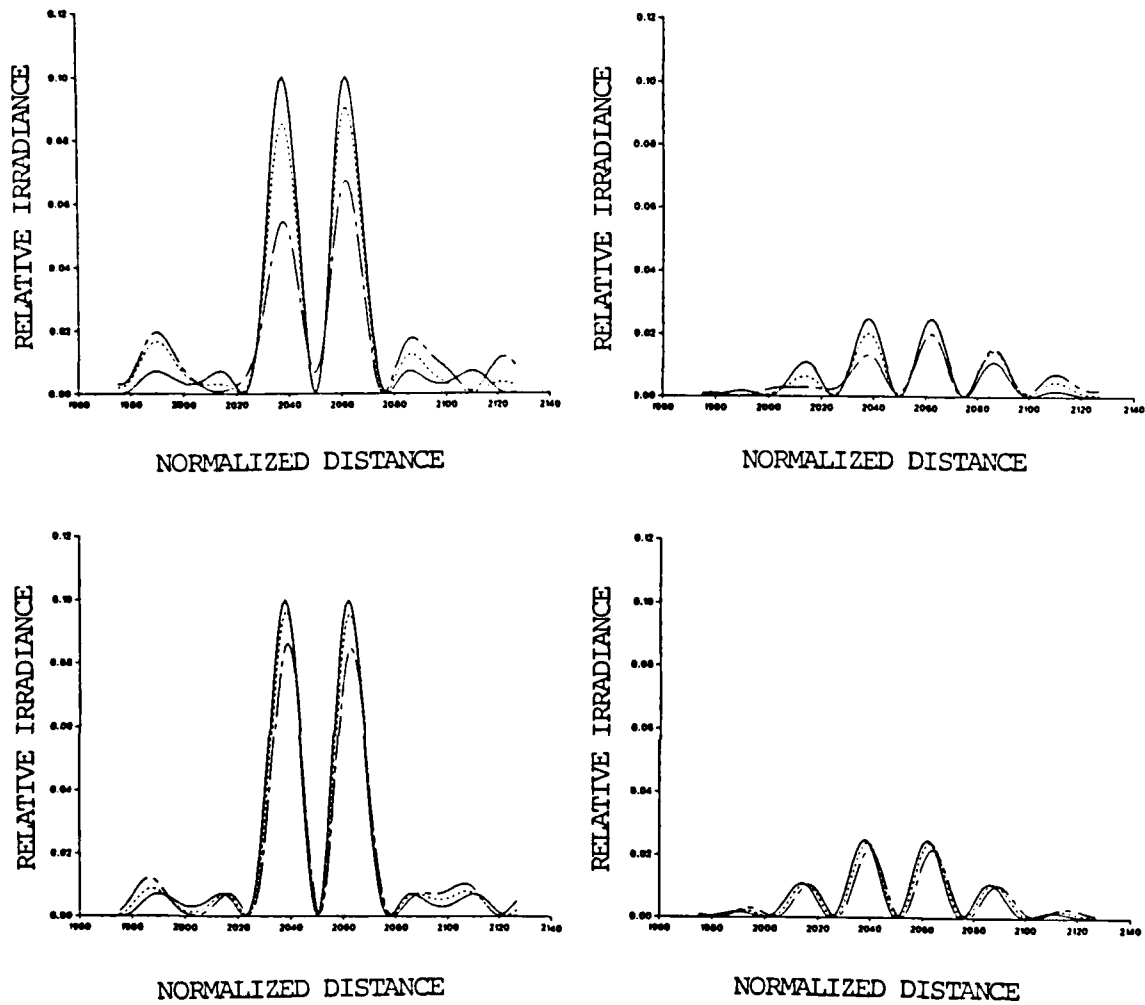
Fig. 4.25   Plots of cross-sections of the image of an edge
as y coma (top row) and spherical aberration
(bottom row) are increased across only one of the
subapertures. The left column contains the
unapodised cases and the right column contains
the apodised cases. The solid line (___)
represents no aberration, the dashed line (---)
represents 0.5λ of aberration, and the broken
line (__-__) represents 1.0λ of aberration. The
scaling is the same as that of Fig. 4.17.

102
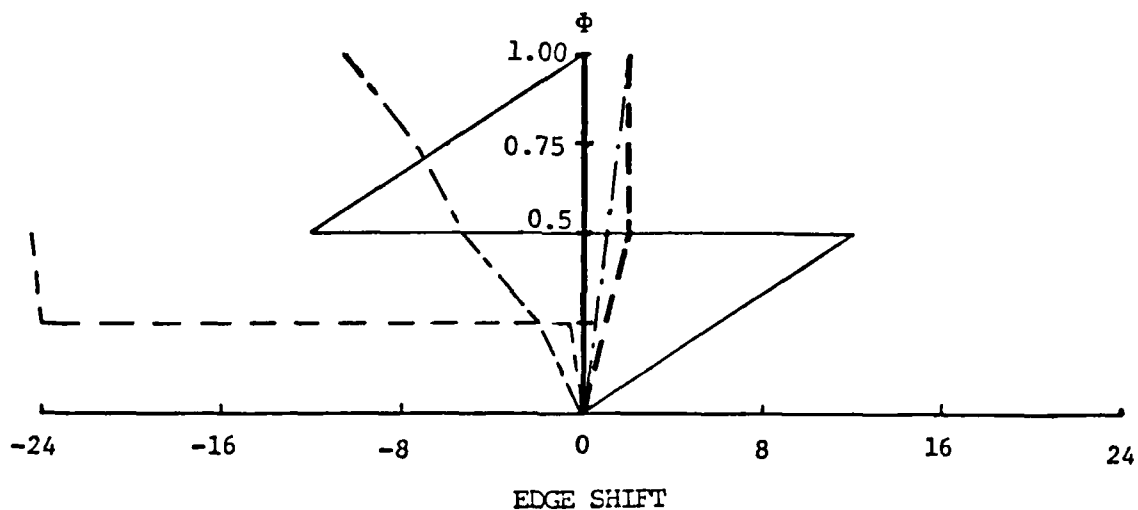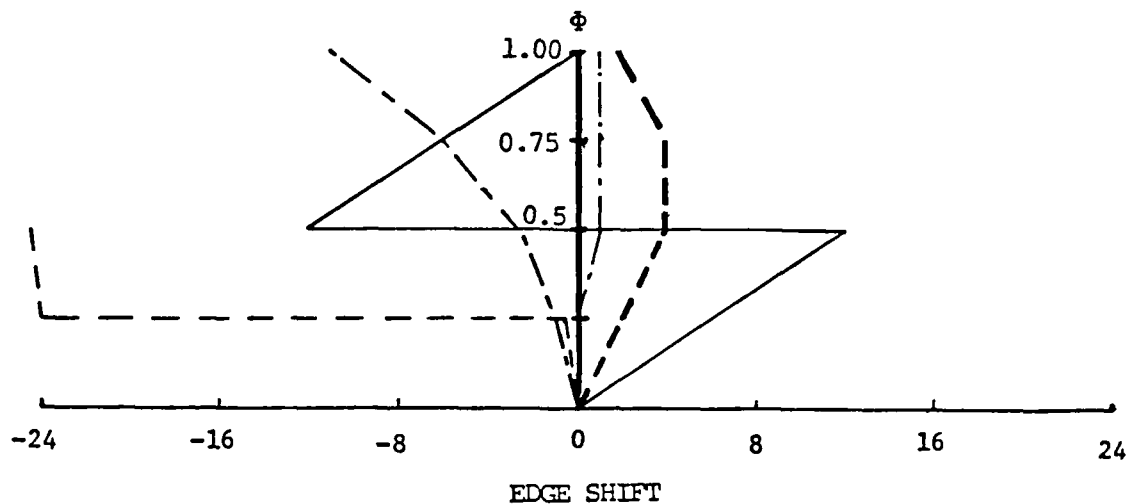
Fig. 4.26 Edge shift as a function of aberration when
applied to only one of the subapertures. The top
plot depicts the unapodised cases while the
bottom plot depicts the apodised cases. The
solid line (___) represents piston, the dashed
line (---) represents y tilt, the broken line
(__-__) represents defocus, the line broken by
dots (__.__) represents spherical aberration, the
heavy line (▬▬) along the vertical axis
represents y coma, and the dashed heavy line' (▬ ▬)
represents 0° astigmatism. The vertical scale is
centered upon the geometric edge position. The
symbol φ represents waves of aberration.

103
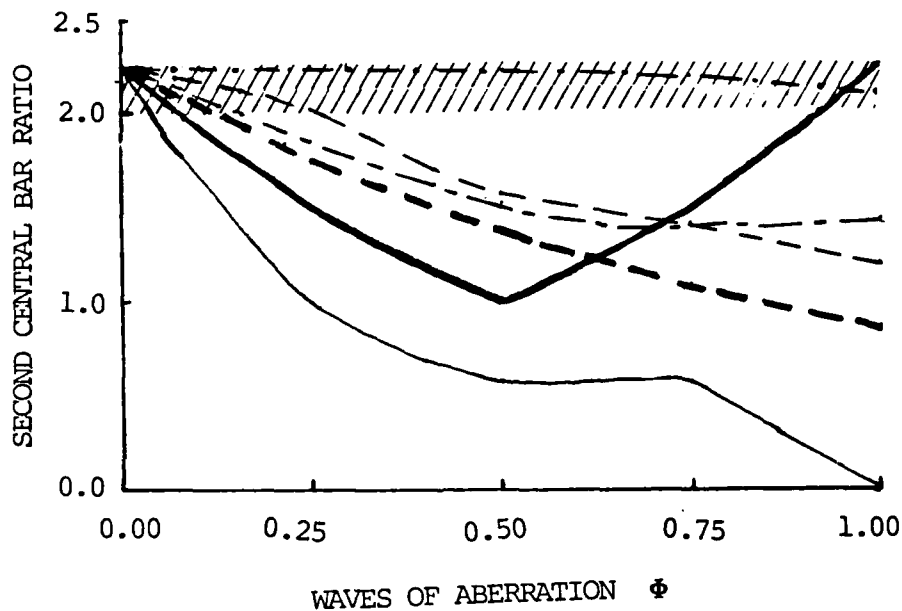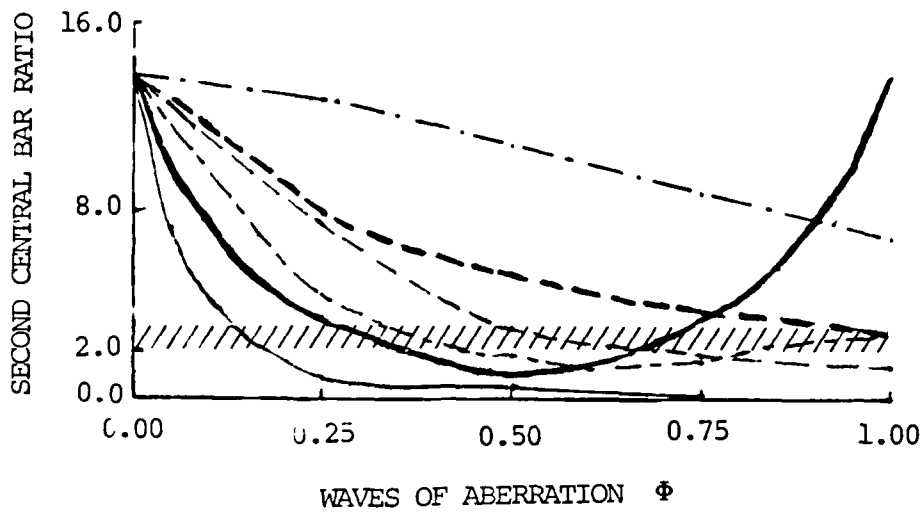
Fig. 4.27 Plots of the second central ratio vs. increasing
amounts of aberrations present in only one
subaperture. The top plot depicts the
unapodised cases while the bottom plot depicts
the apodised cases. The heavy solid line (━━)
represents piston, the solid line (___)
represents y tilt, the dashed line (---)
represents defocus, the broken line (_-_)
represents 0° astigmatism, the heavy dashed
solid line (▪ ▪) represents y coma, the line
broken by dots (_._) represents spherical
aberration and the wavy line (///) represents the
arbitrary approximate lower limit for acceptable
imaging.

104

Thus, the final approach confirms that apodisation does not improve the imaging performance of an edge through a multiaperture optical system.

V. Conclusion

The technique of apodisation has been proven beneficial by several researchers when applied to coherent optical imaging systems. But Gaussian apodisation clearly did not improve the imaging performance through a coherent multiaperture optical imaging system. This was the case whether the object was a point source or an edge, whether the dilution was increased or held constant, or whether aberrations were present or not present.

The decrease in imaging performance occurred mainly due to the height of the secondary sidelobes with respect to the central ??? when a ??? was imaged; and to the relative ??? ??? with respect to the central ??? ??? ??? ??? were measured by ??? ??? ??? and declines in the second central ??? ??? ??? ??? ??? objects.

Specific ??? ??? ??? ??? in which an unaberrated system ??? ??? ??? ??? acceptable imaging fell from ??? ??? the ??? ??? ???, unaberrated case to 0.1 for the Gaussian apodised case. This decline in tolerable dilution was important in at least two respects. First, the effective aperture of the imaging system was cut by about 20%. But even more critically, upon consideration of current engineering constraints, the construction of a Gaussian apodised Multiple Aperture Telescope (MAT) would not be feasible.

106

It is important to note that in the real world almost all imaging systems will have aberrations. That is the group of unaberrated imaging systems compose only a very special subset in the family of imaging systems. Thus in this study the effects of the introduction of aberrations had to be studied in order to yield any practical meaning. When this was done the central peak ratio and second central bar ratio declined as aberrations were increased. When the dilution was increased the decline was exacerbated. The effect was easiest to see when only aberrations were increased while the dilution was held constant. The amounts of aberrations which an unapodised system at a constant dilution of 0.0 could tolerate for imaging purposes were 0.12λ of piston, 0.08λ of y tilt (0.16λ if y tilt was applied to only one subaperture), 0.40λ of defocus, 0.40λ of astigmatism, 0.60λ of coma (over 1.0λ if coma was applied to only one subaperture), and 1.0λ of spherical aberration. It turned out that the application of a Gaussian apodiser to each of the subapertures damaged imaging performances. Upon Gaussian apodisation the amount of the aberrations which could be tolerated for imaging purposes fell to 0.05λ of piston, 0.04λ of y tilt (0.08λ if y tilt was applied to only one subaperture), 0.25λ of defocus, 0.25λ of astigmatism, 0.12λ of coma and 1.0λ spherical aberration.

The application of the Gaussian apodiser also affected the irradiances of the impulse response and edge image. The

peak irradiance of the point source image was cut by a factor of 10. Nevertheless, this peak irradiance was still 3.6 times greater than the peak irradiance which would have resulted if the point source were shined through only one subaperture.

When an edge was imaged through a hexagonal multiaperture imaging system of no dilution the peak irradiance in the image plane was already cut by a factor of 10, even before a Gaussian apodiser was applied. The application of the apodiser cut the peak irradiance by another factor of four, making the edge appear just 1/40 as bright as if it had been shined through a single subaperture. Since a high SNR would be required in edge imaging this great loss in irradiance clearly reduces the capability of imaging dim edges.

The investigation of edge imaging produced two other interesting sidelights. First, when aberrations were present edge shifting was a serious problem, whether a Gaussian apodiser was applied or not. This was especially so when the aberrations were applied to only one of the subapertures.

The second sidelight was that an annular imaging system was determined to better than a multiaperture imaging system when imaging an edge. The edge imaging results of this study can be applied without loss of generality to that of an annular system.

Bibliography

Bersey, Dana J. and David L. Neidig. "Multiaperture
    Imaging," EE6.90 Independent Study. Air Force
    Institute of Technology, Wright-Patterson AFB OH,
    September 1985.

Borrelle, William. "UA announces revolution in mirror
    making," Optics News, 11:8-9 (July 1985).

Born, Max and Emil Wolf. Principles of Optics, (Third
    Edition). New York: Pergamon Press, 1965.

Fender, Janet S. "Synthetic Apertures: An Overview,"
    Proceedings of SPIE. 2-7. SPIE - The International
    Society for Optical Engineering Press, Bellingham WA,
    1974.

Gaskill, Jack D. Linear Systems, Fourier Transforms, and
    Optics. New York: John Wiley & Sons, 1978.

Goodman, Joseph W. "Synthetic Aperture Optics," Progress
    in Optics, Volume VIII, edited by Emil Wolf. New York:
    American Elsevier Publishing Company, Inc., 1970.

Goodman, Joseph W. Introduction to Fourier Optics.
    San Francisco: McGraw-Hill Book Company, 1968.

Hecht, Eugene and Alfred Zajae. Optics. Reading MA:
    Addison-Wesley Publishing Company, 1974.

Hooker, R. Brian. The Effects of Aberrations in Synthetic
    Aperture Systems. PhD Dissertation. University of
    Arizona, Tucson AZ, 1974.

Kervin Paul, Laser Systems Development Physicist. Personal
    correspondence. Air Force Weapons Laboratory, Kirtland
    AFB, Albuquerque, NM, 1 October 1982.

Malacara, Daniel, Optical Shop Testing. New York: John
    Wiley and Sons, 1978.

Meinel, Aden Baker and others. "Multiple Aperture
    Telescope Diffraction Images," Applied Optics and
    Optical Engineering, Vol. 9, edited by Robert R.
    Shannon and James C. Wyant. New York: Academic Press,
    Inc., 1983.

Mills, James Patrick. The Effect of Aberrations and
    Apodisation on the Performance of Coherent Imaging
    Systems. PhD dissertation. University of Rochester,
    Rochester NY, 1984.

Parrent, George B. Jr. and Brian J. Thompson. Physical
    Optics Notebook. Redondo Beach, CA: Society of
    Photo-Optical Instrumentation Engineers Press, 1969.

Sanger, Gregory M. and others. "Some Design Aspects of a
    Multiple-Mirror Telescope," Proceedings of the Society
    of Photo-Optical Instrumentation Engineers, Vol. 28,
    Instrumentation in Astronomy, edited by Lewis Larmore
    and Robert W. Poindexter. Redondo Beach, CA: Society
    of Photo-Optical Instrumentation Engineers, 1972.

Shack, R. V. and others. "Effects of Dilution on a
    Six-Element Synthetic Aperture," Applied Optics,
    10:257-259 (February 1971).

Silver, Samuel. "Microwave Aperture Antennas and
    Diffraction Theory," Journal of the Optical Society of
    America, 52:131 (February, 1962).

Vita

Captain Arley J. Hugghins was born on 6 December 1957 in Brookings, South Dakota. He graduated from high school in Brookings, South Dakota in 1976 and attended South Dakota State University from which he received the degree of Bachelor of Arts in Spanish and the degree of Bachelor of Science in Physics in December 1980. Upon graduation, he received a commission in the USAF through the ROTC program. His initial assingment was with the Air Force Weapons Laboratory at Kirtland AFB, Albuquerque, NM where he was a laser systems development physicist in support of the Airborne Laser Laboratory project. In May 1984 he left Albuquerque to enter the School of Engineering, Air Force Institute of Technology.

Permanent address: 1034 6th Ave.
Brookings, SD 57006

REPORT DOCUMENTATION PAGE

1. REPORT SECURITY CLASSIFICATION	1b. RESTRICTIVE MARKINGS
Unclassified	

2a. SECURITY CLASSIFICATION AUTHORITY	3. DISTRIBUTION/AVAILABILITY OF REPORT
	Approved for public release;
2b. DECLASSIFICATION/DOWNGRADING SCHEDULE	distribution unlimited

4. PERFORMING ORGANIZATION REPORT NUMBER(S)	5. MONITORING ORGANIZATION REPORT NUMBER(S)
AFIT/GEP/ENP/85D-6	

6a. NAME OF PERFORMING ORGANIZATION	6b. OFFICE SYMBOL (If applicable)	7a. NAME OF MONITORING ORGANIZATION
School of Engineering	AFIT/ENP	

6c. ADDRESS (City, State and ZIP Code)	7b. ADDRESS (City, State and ZIP Code)
Air Force Institute of Technology	
Wright-Patterson AFB, Ohio 45433	

8a. NAME OF FUNDING/SPONSORING ORGANIZATION	8b. OFFICE SYMBOL (If applicable)	9. PROCUREMENT INSTRUMENT IDENTIFICATION NUMBER
RADC	OCSE	

8c. ADDRESS (City, State and ZIP Code)	10. SOURCE OF FUNDING NOS.			
Rome Air Development Center	PROGRAM ELEMENT NO.	PROJECT NO.	TASK NO.	WORK UNIT NO.
Grifiss AFB, NY 13441				

11. TITLE (Include Security Classification)
See Box 19

12. PERSONAL AUTHOR(S)

Arley J. Hugghins, B.S., B.A., Captain, USAF

13a. TYPE OF REPORT	13b. TIME COVERED	14. DATE OF REPORT (Yr., Mo., Day)	15. PAGE COUNT
MS Thesis	FROM _____ TO _____	December 1985	111

16. SUPPLEMENTARY NOTATION

17. COSATI CODES			18. SUBJECT TERMS (Continue on reverse if necessary and identify by block number)
FIELD	GROUP	SUB. GR.	Apodisation, Aberrations, Multiaperture Imaging,
20	06		Coherent Imaging, Optical Imaging

19. ABSTRACT (Continue on reverse if necessary and identify by block number)

Title: The Apodisation of Aberrated Coherent Multiaperture Optical Imaging Systems

Thesis Chairman: James P. Mills, Major, USAF
Assistant Professor of Engineering Physics

Approved for public release: IAW AFR 190-1.

LYNN E. WOLAVER   16 JAN 86
Dean for Research and Professional Development
Air Force Institute of Technology (AFC)
Wright-Patterson AFB OH 45433

20. DISTRIBUTION/AVAILABILITY OF ABSTRACT	21. ABSTRACT SECURITY CLASSIFICATION
UNCLASSIFIED/UNLIMITED ☒ SAME AS RPT. ☐ DTIC USERS ☐	

22a. NAME OF RESPONSIBLE INDIVIDUAL	22b. TELEPHONE NUMBER (Include Area Code)	22c. OFFICE SYMBOL
James P. Mills, Major, USAF	513-255-4498	AFIT/ENP

DD FORM 1473, 83 APR EDITION OF 1 JAN 73 IS OBSOLETE.

This investigation determined that the application of a Gaussian apodiser did not improve the imaging performance through a coherent multiaperture optical imaging system. This was the case whether the object was a point source or an edge, whether the dilution was increased or held constant, or whether aberrations were present or not present. Further, the investigation determined that the amount of spacing between the subapertures which either an aberrated or unaberrated optical system could tolerate and still obtain acceptable imaging fell dramatically.

The analysis was accomplished with computer codes which made use of Fourier transform techniques to perform the imaging. The edge imaging results of this study can be applied without loss of generality to that of an imaging system with an annular exit pupil.

END

FILMED

3 -86

DTIC